Strål säkerhets myndigheten
Swedish Radiation Safety Authority

Authors: Peter Segle
Pär Ljustell
Albin Larsson
Johan Kölfors

Research

2017:19

Numerical simulations of headed anchors break in reinforced and non-reinforced concrete structures, Phase 2

Report number: 2017:19 **ISSN:** 2000-0456
Available at www.stralsakerhetsmyndigheten.se

SSM perspective

Background

In the design of anchorage equipment in concrete structures the beneficial effects of reinforcement are, in most cases, not considered. The American ASCI 349-06 code opens up for a more detailed analysis where the beneficial impact of reinforcement on anchor capacity can be taken into account. How this analysis can be done is, however, not explicitly described in the code.

The response of mechanically loaded anchors in reinforced concrete structures can only be understood by a combination of testing and numerical simulations. As concrete is a complex material, interaction between anchors, reinforcement and concrete is consequently also complex. Reported work within this area in the open literature is limited why efforts are needed to fill this gap.

Inspecta Nuclear AB and Scanscot Technology AB have, in a previous work funded by SSM (SSM 2013: 27), studied the possibility to transfer mechanical loads from embedded anchors to the concrete and its reinforcement. The results from that study clearly shown that the reinforcement has a beneficial effect on anchor capacity in both tension and shear.

In the current research project, the response of headed anchors in reinforced and non-reinforced concrete structures is further investigated by means of finite element simulations based on the numerical approach developed in the previous work.

Objectives

The main objective is to get a better understanding of how different type and amount of reinforcement may increase the capacity of anchor plates for a number of new configurations and loading conditions.

Results

Some of the results are as follows

- surface reinforcement has a negligible influence on the failure load level for anchor plates loaded in tension,
- the location of shear reinforcement links is of importance for the tension capacity of anchor plates in shear reinforced structures,
- surface reinforcement has only a small effect on the pry-out failure load level for anchor plates far from concrete edges and loaded in shear,
- the ratio between the tension load and the shear load is of great importance for anchor plates simultaneously loaded in tension and shear, and
- comparisons between numerical simulations and the European CEN/TS 1992-4-2 code show good agreement for investigated non-reinforced structures. This gives confidence in the numerical approach used in this investigation.

The results can be used in safety assessment of concrete structures, as well as in specifying the requirements applicable to the analysis of concrete structures at the Swedish nuclear facilities.

Need for further research

No more research is needed within this area for the moment.

Project information

Contact person SSM: Kostas Xanthopoulos
Reference: SSM2015-847

Strål
säkerhets
myndigheten
Swedish Radiation Safety Authority

Authors: Peter Segle [1], Pär Ljustell [1], Albin Larsson [2], Johan Kölfors [2]
[1] Inspecta Nuclear AB, Stockholm
[2] Scanscot Technology AB, Lund

2017:19

Numerical simulations of headed anchors break in reinforced and non-reinforced concrete structures, Phase 2

Date: May 2017
Report number: 2017:19 **ISSN:** 2000-0456
Available at www.stralsakerhetsmyndigheten.se

This report concerns a study which has been conducted for the Swedish Radiation Safety Authority, SSM. The conclusions and viewpoints presented in the report are those of the author/authors and do not necessarily coincide with those of the SSM.

Summary

In this research project, the response of headed anchors in non-reinforced and reinforced concrete structures is investigated by means of finite element simulations. Based on a previous project [SSM Research report 2013:27], where the numerical approach was developed and available anchor plate tests were simulated, a number of new configurations and loading conditions are investigated. Simulations are conducted with the general purpose finite element program Abaqus.

Investigated configurations are:

- eccentrically tension loaded anchor plates far from concrete edges,
- centrically tension loaded anchor plates close to free concrete edge,
- centrically tension loaded anchor plates in shear reinforced structures far from concrete edges,
- centrically shear loaded anchor plates far from concrete edges,
- centrically shear loaded and eccentrically tension loaded anchor plates far from concrete edges.

For anchor plates located in non-reinforced structures, simulated failure loads agree well with corresponding predictions using CEN/TS 1992-4-2. This result forms basis for reliable simulations of anchor plates loaded in tension and shear in reinforced structures.

For investigated configurations of anchor plates loaded in tension, the surface reinforcement has negligible influence on the concrete cone failure load. Anchor plates in shear reinforced structures are an exception. As the shear reinforcement links enclose the surface reinforcement, load transfer from the links into the concrete structure is further facilitated by the surface reinforcement.

The distance between the anchors and the shear reinforcement links has a strong influence on the failure load of anchor plates in shear reinforced structures loaded in tension. In order to fully utilize the links this distance should not exceed $0.3h_{ef}$.

Edge reinforcement increases the failure load of anchor plates loaded in tension located close to a free edge. The denser the reinforcement the higher the failure load.

For anchor plates in non-reinforced concrete far from concrete edges and loaded in shear, the simulated capacities have been compared with the capacities according to CEN/TS 1992-4-2. For embedment depth 100 mm the simulations show good agreement with CEN/TS both for single anchors and anchor groups. For shorter anchors (50 mm), simulation shows significantly higher load capacity than CEN/TS. The reason is mainly that the factor k_3 used in CEN/TS drops from 2 to 1 for small embedment depths.

For investigated configurations of anchor plates in reinforced concrete far from concrete edges and loaded in shear, the simulations show that the amount of surface reinforcement has only a minor impact on the concrete pry-out failure load capacity.

For investigated configurations of anchor plates in reinforced concrete far from concrete edges and centrically loaded both in tension and shear, the simulations show that surface reinforcement has only a minor impact on the capacity. When an eccentricity of the tension load is introduced, the simulations show a decrease of

capacity when the eccentricity is increased. Furthermore, the simulations show that the combined failure capacity is greatly dependent on the ratio between the tension load and the shear load.

All simulations show that reinforcement makes the failure of anchor plates loaded in tension or shear more ductile.

Finally, recommendations are given for how to perform numerical simulations of anchor plates loaded in tension and shear in non-reinforced and reinforced concrete structures.

Sammanfattning

I detta projekt har simuleringar av brott hos förankringar i oarmerad och armerad betong genomförts med hjälp av finita elementanalyser. Arbetet är baserat på resultaten från föregående projekt [SSM Research report 2013:27] där numeriska simuleringar genomfördes och resultaten jämfördes med olika publicerade resultat från fysiska tester. Syftet med detta projekt är att med numerisk simulering undersöka en rad nya, mer komplexa belastningssituationer. Simuleringarna har genomförts med det generella finita elementprogrammet Abaqus.

De belastningssituationer som undersökts är:

- excentriskt utdragsbelastade förankringar i betong långt från fri kant,
- centriskt utdragsbelastade förankringar nära fri kant,
- centriskt utdragsbelastade förankringar i betong med skjuvarmering,
- centriskt skjuvbelastade förankringar i betong långt från fri kant,
- centriskt skjuvbelastade och excentriskt utdragsbelastade förankringar långt från fri kant.

Simuleringarna av förankringar i oarmerad betong visar generellt god överensstämmelse med de dimensionerande kapaciteter som beräknas enligt CEN/TS 1992-4-2. Detta är en grundförutsättning för att simuleringarna av förankringar i armerad betong ska kunna betraktas som tillförlitliga.

För de olika konfigurationer av utdragsbelastade förankringar som studerats, visar simuleringarna att ytarmeringen har en försumbar påverkan på brottlasten vid ett betongkonbrott.

Simuleringar av förankringar i betong med skjuvarmering i form av byglar som omsluter ytarmeringen visar att armeringen då ger en betydande ökning av brottkapaciteten. Beräkningarna visar att avståndet mellan förankring och skjuvarmeringen är en mycket viktig parameter. För att tillfullo kunna utnyttja skjuvarmeringen för att överföra dragkraft i förankringen bör avståndet mellan förankring och bygel inte överstiga $0.3h_{ef}$.

Vidare visar simuleringarna att kantarmering ger en ökad kapacitet hos utdragsbelastade förankringar nära fri betongkant. Som väntat visar simuleringarna att kapaciteten ökar med ett minskat avstånd mellan kantarmeringsstängerna.

Simuleringarna av skjuvbelastade förankringar långt från fri kant har jämförts med de kapaciteter som ges av CEN/TS 1992-4-2. För förankringar med sättdjup 100 mm visar beräkningsresultaten god överensstämmelse med kapaciteterna enligt CEN/TS 1992-4-2. Denna överensstämmelse är god både för enskilda förankringar och för grupper av förankringar. För kortare förankringar (50 mm) visar dock simuleringarna på en avsevärt högre kapacitet än den som beräknas med CEN/TS 1992-4-2. Huvudorsaken till detta är att den faktor k_3, som används i CEN/TS 1992-4-2 och som normalt har värdet 2, skall minskas till värdet 1 för små sättdjup h_{ef}.

För studerade konfigurationer av skjuvbelastade förankringar i armerad betong långt från fri kant så visar simuleringarna att mängden ytarmering endast har en liten inverkan på brottkapaciteten (pry-out).

Hos förankringar som samtidigt skjuv- och utdragsbelastas och där utdragslasten ges en excentricitet, visar simuleringarna att kapaciteten minskar med ökad excentricitet.

Vidare visar simuleringarna att kapaciteten vid ett kombinerat skjuv- och utdragsbrott är starkt beroende av förhållandet mellan storleken på skjuv- och utdragslasten.

För studerade konfigurationer av samtidigt skjuv- och centriskt utdragbelastade förankringar visar simuleringarna att ytarmering endast har en mycket liten inverkan på brottkapaciteten.

Simuleringarna visar att armering generellt medför att brottförloppet blir mer duktilt.

Slutligen ges i rapporten ett antal rekommendationer för genomförandet av numerisk simulering av skjuv- och utdragsbelastade förankringar i oarmerad och armerad betong.

Content

Nomenclature

a	distance from anchor to closest shear reinforcement link [mm]
$A^0_{c,N}$	projected concrete failure area of single anchor [mm^2]
$A_{c,N}$	projected concrete failure area of anchor group [mm^2]
c_1	edge distance from anchor positioned close to a free concrete edge [mm]
d_t	concrete tension damage [-]
e	eccentricity in numerical simulations [-]
e_N	eccentricity in CEN/TS 1992-4-2 [mm]
E	modulus of elasticity [MPa]
E_0	initial modulus of elasticity used in Abaqus [MPa]
f_c	compressive cylinder strength of concrete [MPa]
f_{ck}	characteristic compressive cylinder strength of concrete [MPa]
f_{cm}	mean value of concrete cylinder compressive strength [MPa]
$f_{c,cube}$	compressive cube strength of concrete [MPa]
$f_{ck,cube}$	characteristic compressive cube strength of concrete [MPa]
$f_{cm,cube}$	mean value of concrete cube compressive strength [MPa]
f_{ct}	tensile strength of concrete [MPa]
f_{ctk}	characteristic tensile strength of concrete [MPa]
f_{ctm}	mean value of tensile strength of concrete [MPa]
G_F	fracture energy [Nm/m^2]
h_{ef}	anchor embedment depth [mm]
k_3	factor used when calculating pry-out resistance [-]
N_{Ed}	design tension force [N]
N_{Rd}	design tension resistance [N]
$N^0_{Rk,c}$	characteristic concrete cone resistance of a single anchor in tension [N]
N_u	failure load of a single anchor or an anchor group in tension [N]
s_1, s_2	distance between anchors [mm]
u_t^{ck}	cracking displacement [m]
u_{t0}^{ck}	cracking displacement at which complete loss of strength takes place [m]
V_{Ed}	design shear force [N]
V_{Rd}	design shear resistance [N]
$V^0_{Rk,c}$	characteristic concrete edge failure resistance of a single anchor [N]
$V_{Rk,cp}$	characteristic concrete pry-out failure resistance of an anchor group [N]
$V^0_{Rm,c}$	mean concrete edge failure resistance of a single anchor [N]
V_u	failure load of a single anchor or an anchor group in shear [N]
β_N	tension utilisation factor [-]
β_V	shear utilisation factor [-]
u	displacement in numerical simulations [mm]
$\dot{u}$	displacement rate in numerical simulations [mm/s]
ϵ	flow potential eccentricity used in Abaqus
ε_c	total strain [-]
ε_{0c}^{el}	elastic strain corresponding to undamaged material [-]
ε_c^{in}	inelastic strain [-]
ε_{max}	maximum strain [-]
ϕ12cc100	surface reinforcement with a rebar diameter of 12 mm and a centre to centre distance between rebars of 100 mm
μ	viscosity parameter or coefficient of friction [-]
ν	Poisson's ratio [-]
ψ	dilation angle [deg]
ρ	density [kg/m^3]
σ_{cu}	ultimate compressive stress used in Abaqus [MPa]
σ_{c0}	uniaxial initial compressive yield stress used in Abaqus [MPa]

σ_{b0}	initial equibiaxial compressive yield stress used in Abaqus [MPa]
σ_{t0}	failure stress in tension used in Abaqus [MPa]

1. Introduction

In ACI 349-13, section D.4.4 and D.4.5, supplementary reinforcement is considered in a simplistic way when calculating the anchor capacity for the failure modes concrete breakout and side-face blowout [ACI 349-13 2013]. Two conditions are defined. Condition A applies where the potential concrete failure surfaces are crossed by supplementary reinforcement proportioned to tie the potential concrete failure prism into the concrete structure. Condition B applies where such supplementary reinforcement is not provided. Depending on condition, type of load and type of anchor, different strength-reduction factors ϕ are given. According to ACI 349-13, section D.4.4 and D.4.5, the concrete breakout and side-face blowout strength is between 7 and 15 % higher with supplementary reinforcement than without.

According to ACI 349-13, section D.4.2.1, the effect of supplementary reinforcement provided to confine or restrain the concrete breakout, or both, shall be permitted to be included in the design models used for determining the anchor capacity. The ACI code thus opens up for a more detailed analysis where the beneficial impact of reinforcement on anchor capacity can be taken into account. How this analysis can be done is, however, not explicitly described in the code.

In CEN/TS 1992-4-2, section 6.2 and 6.3, supplementary reinforcement is considered by means of replacing the concrete cone and/or concrete edge failure mode verification in tension and shear respectively with two reinforcement related failure modes [CEN/TS 1992-4-2 2009]. This approach means that the supplementary reinforcement should be designed to resist the total load. Requirements such as distance between anchor and reinforcing bar, diameter of reinforcement, type of reinforcement and anchorage lengths in the concrete failure prism and the concrete member has to be fulfilled. The rebars should also be organised as a wire mesh, enabling adequate transmission of the load (strut and tie).

In addition, CEN/TS 1992-4-2 section 6.3.5.2.7, provides a simplistic way of enumerate the capacity for the concrete edge failure mode if sufficient supplementary reinforcement is present. The uprating factor is either 1.2 or 1.4 depending on the position of the fastening.

Guidelines for how to explicitly consider reinforcement in structural verification of anchorage equipment in concrete structures is of interest. In a previous project with the acronym ANKARM [SSM Research report 2013:27], numerical simulations of single anchors and anchor groups in non-reinforced and reinforced concrete were performed. Headed anchors loaded in tension far from concrete edges and headed anchors loaded in shear close to a free concrete edge were investigated. The concrete constitutive model and the numerical approach were validated against available experimental results from testing of single cast-in headed anchors loaded in tension and shear. The general purpose finite element program Abaqus [Dassault Systémes, 2014] was used for the numerical simulations. In summary, results from the ANKARM project revealed that:

- The concrete damaged plasticity material model in Abaqus showed to be well suited for simulation of headed anchors loaded in tension and shear in non-reinforced and reinforced concrete.

- Available experimental results from testing of single cast-in headed anchors could rather well be simulated.

- Global stiffness of the concrete structure determined if splitting failure, concrete cone failure or a combination of both controlled failure of anchors loaded in tension.

- Simulations showed that reinforcement in the direction of the applied load led to a distinct increase of the concrete edge failure capacity if the reinforcement bar location in the breakout body was sufficiently close to the anchors.

- In general, reinforcement made the failure of anchors more ductile.

- For anchors in non-reinforced concrete, results from numerical simulations agreed rather well with corresponding predictions with CEN/TS 1992-4-2.

In the present project, additional configurations and loading scenarios are investigated. The same numerical approach and constitutive model for the concrete material is used as in the ANKARM project [SSM Research Report 2013:27]. Both single anchors and anchor groups are studied for tension load and shear load and combinations thereof. Analyses are performed with the finite element program solver Abaqus/Explicit version 6.14 [Dassault Systémes 2014] which is a well-known and thoroughly tested general purpose finite element program. The total scope of the project is divided into different tasks as described in Table 1-1. Far from concrete edges here means that the distance between the closest edge and the anchor bolts is far enough not influencing the results.

Table 1-1 Description of tasks within the project.

Task	Description
1	Anchor plate far from concrete edges loaded in tension. The concrete member is shear reinforced. Effect of longitudinal reinforcement and its absence is studied.
2	Anchor plate close to a free concrete edge loaded in tension. Non-reinforced and reinforced concrete is studied.
3	Anchor plate far from concrete edges eccentrically loaded in tension. Non-reinforced and reinforced concrete is studied.
4	Anchor plate far from concrete edges loaded in shear. Non-reinforced and reinforced concrete is studied.
5	Anchor plate far from concrete edges simultaneously loaded in tension and shear. Effect of eccentricity of the tension load is investigated. Non-reinforced and reinforced concrete is studied.

Focus for all tasks is to study the effect of different reinforcement setups on the structural response. Together with results from the previous ANKARM project, the aim is to better understand how structural verification of cast-in headed anchors in

concrete structures can be performed taking reinforcement into account. Issues of interest are such as the interaction of local stress field in the vicinity of the anchor with global stress field in the concrete structure, the possibility to transmit mechanical loads from the embedded anchors to the concrete and its reinforcement and how to perform rational modelling and analysis of mechanically loaded anchors in concrete structures. One important outcome of this project is an enhanced understanding for how structural verification of in-cast headed anchors in reinforced concrete can be performed in accordance with CEN/TS 1992-4-2.

2. Constitutive models and general analysis prerequisites

2.1. General

All numerical simulations conducted within current project are performed with Abaqus version 6.14, which is a well-known and thoroughly tested general purpose finite element program [Dassault Systémes 2014]. The physical problem is numerically studied quasi-statically and simulated with the explicit solver.

The concrete material is in the numerical simulations modelled with the Abaqus material model "concrete damaged plasticity" (CDP). A presentation of the constitutive model is given in section 2.2. Section 2.3 reflects general implementation of values necessary for defining the CDP material model.

Elastic response (if not otherwise stated) is assumed for the steel material, i.e. reinforcement, anchors and steel plates, whilst the concrete is modelled with non-linear behaviour. Material strength values and properties used in the numerical simulations are presented in section 2.4.

Other general analysis input data utilized in the numerical simulations presented within this report are presented in section 2.5.

2.2. Concrete damaged plasticity model in Abaqus

The concrete damaged plasticity model (CDP) is based on work carried out by [Lee et al. 1998] and [Lubliner et al. 1989] and is available in both the implicit and the explicit integration solver (Abaqus/Standard and Abaqus/Explicit). The CDP model uses the concept of isotropic damaged elasticity in combination with isotropic tensile and compressive plasticity to represent the inelastic behaviour of concrete. The model consists of the combination of non-associated multi-hardening plasticity and scalar (isotropic) damaged elasticity to describe the irreversible damage that occurs during the fracturing process. The model allows the definition of strain hardening in compression and can be defined to be sensitive to the straining rate, which resembles the behaviour of concrete more realistically.

The CDP model is applicable for applications in which concrete is subject to monotonic loading, cyclic loading with alternating tension/compression loading, and/or dynamic loading. The model allows stiffness recovery during cyclic loading reversals. Under uniaxial tension the stress-strain response follows a linear elastic relationship until the value of the failure stress is reached. Beyond the failure stress the formation of micro-cracks is represented macroscopically with a softening stress-strain response, which induces strain localization in the concrete structure. Under uniaxial compression the response is linear until the value of initial yield. In the plastic regime the response is typically characterized by stress hardening followed by strain softening beyond the ultimate stress. Figure 2-1 illustrates the proceeding of a loading cycle starting in tension passing to compression.

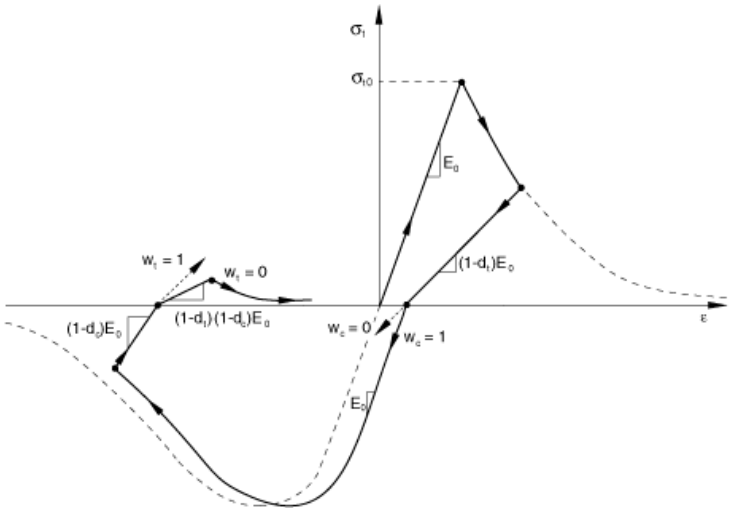

Figure 2-1 Uniaxial load cycle of the concrete damaged plasticity model [Dassault Systémes 2014].

When the concrete specimen is unloaded from any point on the strain softening branch of the stress-strain curve, the unloading response is weakened, i.e. the elastic stiffness of the material appears to be damaged (or degraded).

The CDP model provides a general capability for modelling concrete materials in all types of structure elements, e.g. beams, trusses, shells, and solids.

2.3. Determination of constants in CDP-model

The different parameters that need to be specified when using the CDP model are stated in Table 2-1.

Table 2-1 Concrete damaged plasticity parameters.

Parameter	Description	Default value
ψ	Dilation angle	User defined
ϵ	Flow potential eccentricity	0.1
σ_{b0}/σ_{c0}	Ratio of initial equibiaxial compressive yield stress to initial uniaxial compressive yield stress	1.16
K_c	Ratio of the second stress invariant on the tensile meridian to that on the compressive meridian at initial yield for any given value of the pressure invariant such that the maximum principal stress is negative	0.6667
μ	Viscosity parameter	0.0 in Abaqus/Standard N/A in Abaqus/Explicit

The CDP model assumes non-associated potential plastic flow in which the Drucker-Prager hyperbolic function describes the flow potential *G* [Dassault Systémes 2014].

$$G = \sqrt{(\in \cdot \sigma_{t0} \cdot \tan\psi)^2 + \bar{q}^2} - \bar{p} \cdot tan\psi \quad \text{(Eq. 2-1)}$$

In equation 2-1, $\bar{q}$ denotes effective Mises stress and $\bar{p}$ the effective stress caused by hydrostatic pressure. The dilation angle ψ is measured in the *p*-*q* plane at high confining pressure and indicates the ratio between the volume change and the shear strain. The dilation angle value for concrete is commonly specified in the range of 30° to 40°. The flow potential eccentricity ϵ defines the rate at which the function approaches the asymptote. With the default value of $\epsilon = 0.1$ the dilation angle is almost the same over a wide range of confining pressure stress values. The uniaxial failure tensile stress σ_{t0} is via the tension stiffening definition specified by the user [Dassault Systémes 2014].

The third and fourth parameter stated in Table 2-1 is included in the yield function used in the CDP model, which in terms of effective stresses has the form:

$$F = \frac{1}{1-\alpha}(\bar{q} - 3\alpha\bar{p} + \beta(\tilde{\varepsilon}^{pl})\langle\hat{\bar{\sigma}}_{max}\rangle - \gamma\langle-\hat{\bar{\sigma}}_{max}\rangle) - \bar{\sigma}_c(\tilde{\varepsilon}_c^{pl}) = 0 \quad \text{(Eq. 2-2)}$$

with

$$\alpha = \frac{(\sigma_{b0}/\sigma_{c0}) - 1}{2(\sigma_{b0}/\sigma_{c0}) - 1} \quad \text{(Eq. 2-3)}$$

$$\beta = \frac{\bar{\sigma}_c(\tilde{\varepsilon}_c^{pl})}{\bar{\sigma}_t(\tilde{\varepsilon}_t^{pl})}(1-\alpha) - (1+\alpha) \quad \text{(Eq. 2-4)}$$

$$\gamma = \frac{3(1-K_c)}{2K_c - 1} \quad \text{(Eq. 2-5)}$$

2.3.1. Concrete behaviour in compression

The concrete material behaviour in compression outside the elastic regime is defined by the relation of yield stress σ_{c0} and inelastic strain $\tilde{\varepsilon}_c^{in}$. The inelastic strain is defined as the total strain minus the elastic strain corresponding to the undamaged material, see equation 2-6 and Figure 2-2 [Dassault Systémes 2014].

$$\tilde{\varepsilon}_c^{in} = \varepsilon_c - \varepsilon_{0c}^{el} \quad \text{(Eq. 2-6)}$$

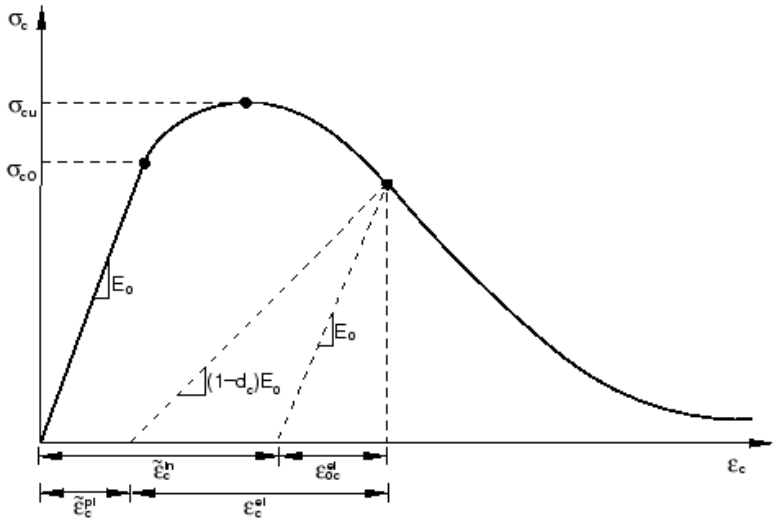

Figure 2-2 Definition of the compressive inelastic strain.

The uniaxial initial yield stress value σ_{c0} is according to [Boverket 2004] defined as 60 % of the ultimate compressive stress σ_{cu}. Corresponding strain is then calculated according to Hookes law, i.e. $\varepsilon_{0c}^{el} = \frac{\sigma_{c0}}{E_0}$ and the maximum strain is taken as $\varepsilon_{max} = \varepsilon_{0c}^{el} \cdot 20$. The inelastic stress curve is thenceforth defined according to [Lubliner et al. 1989] in the following manner:

$$\sigma_c = \sigma_{c0}\left[(1+a)\cdot e^{-b\cdot\tilde{\varepsilon}_c^{pl}} - a\cdot e^{-2\cdot b\cdot\tilde{\varepsilon}_c^{pl}}\right] \qquad \text{(Eq. 2-7)}$$

with

$$a = 2\cdot\frac{f_{cm}}{\sigma_{c0}} - 1 + 2\sqrt{\left(\frac{f_{cm}}{\sigma_{c0}}\right)^2 - \frac{f_{cm}}{\sigma_{c0}}} \qquad \text{(Eq. 2-8)}$$

$$b = \frac{\left(\frac{d\sigma}{d\tilde{\varepsilon}_c^{pl}}\right)}{\sigma_{c0}(a-1)} \qquad \text{(Eq. 2-9)}$$

The numerator in equation 2-9 describes the inclination of the curve at the initial yield stress value.

2.3.2. Concrete behaviour in tension

In general when using the CDP material model, the concrete behaviour in tension is defined as the relation between post failure stress and either of cracking strain $\tilde{\varepsilon}_t^{ck}$, cracking displacement u_t^{ck} or fracture energy G_f. In the work carried out within current project the tension behaviour is given as the relation between post failure stress and cracking displacement as seen in Figure 2-3. This is due to the fact that non-reinforced structures are unreasonable mesh sensitive when using the cracking strain definition.

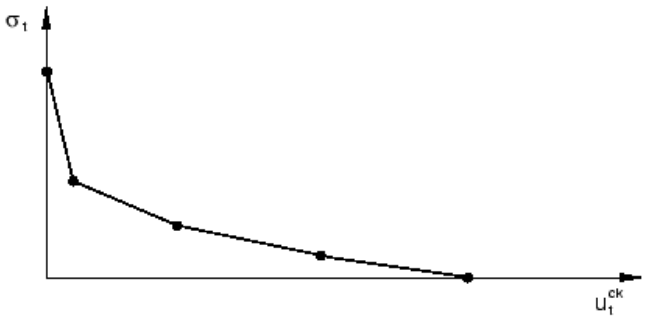

Figure 2-3 Stress displacement relation after tensile failure [Dassault Systémes 2014].

The relation between post failure stress and cracking displacement is calculated according to [Cornelissen et al. 1986] in the following manner:

$$\frac{\sigma_t}{f_{ctm}} = f(u_t^{ck}) - \frac{u_t^{ck}}{u_{t0}^{ck}} \cdot f(u_t^{ck} = u_{t0}^{ck}) \qquad \text{(Eq. 2-10)}$$

where

$$f(u_t^{ck}) = \left(1 + \left(\frac{C_1 \cdot u_t^{ck}}{u_{t0}^{ck}}\right)^3\right) \cdot e^{-C_2 \cdot u_t^{ck}/u_{t0}^{ck}} \qquad \text{(Eq. 2-11)}$$

For a normal weight concrete the constants C_1 and C_2 given in equation 2-11 are 3 and 6.93 respectively. The concrete fracture energy is defined as the area underneath the graph seen in Figure 2-3. The cracking displacement at which complete loss of strength takes place u_{t0}^{ck}, may be determined by first establish a reasonable concrete fracture energy G_F and then integrate the combined expression of equation 2-10 and 2-11. For a normal weight concrete this gives following relation:

$$u_{t0}^{ck} = \frac{G_F}{0.195 \cdot f_{ctm}} \qquad \text{(Eq. 2-12)}$$

When using the CDP material model, the damage caused by strains is measured with a damage tension parameter denoted “concrete tension damage” d_t. The parameter may be visualized during post processing and indicates the status of the concrete after cracking has occurred, i.e. grade of impaired stiffness. In the work carried out within current project the concrete tension damage is linearly defined with a maximum of 0.9. This means that an element gets inactive when the cracking displacement u_{t0}^{ck} is reached and at this point the damage tension parameter has the value of 0.9.

2.4. Material data in numerical simulations

2.4.1. Concrete

In the numerical simulations conducted within current project the default values presented in Table 2-1 are used. Also, the value of the dilation angle is set to 35 degrees and since the analyses are performed with the Abaqus/Explicit solver the viscosity parameter μ is not used.

Besides the parameters stated in Table 2-1, the fundamental material parameters need to be defined. That is, modulus of elasticity E, density ρ and Poisson's ratio υ. Values of concrete material parameters that are used in the analyses are presented in Table 2-2. The concrete behaviour is specified in compression and tension according to Figure 2-4 and Figure 2-5, respectively.

Table 2-2 Concrete material values used in analyses.

Parameter	Description	Value (20°C)
E	Modulus of elasticity	31 GPa
σ_{cu}	Ultimate compressive stress	25.0 MPa
σ_{t0}	Failure tensile stress	2.46 MPa
υ	Poissons ratio	0.2
ρ	Density	2400 kg/m^3

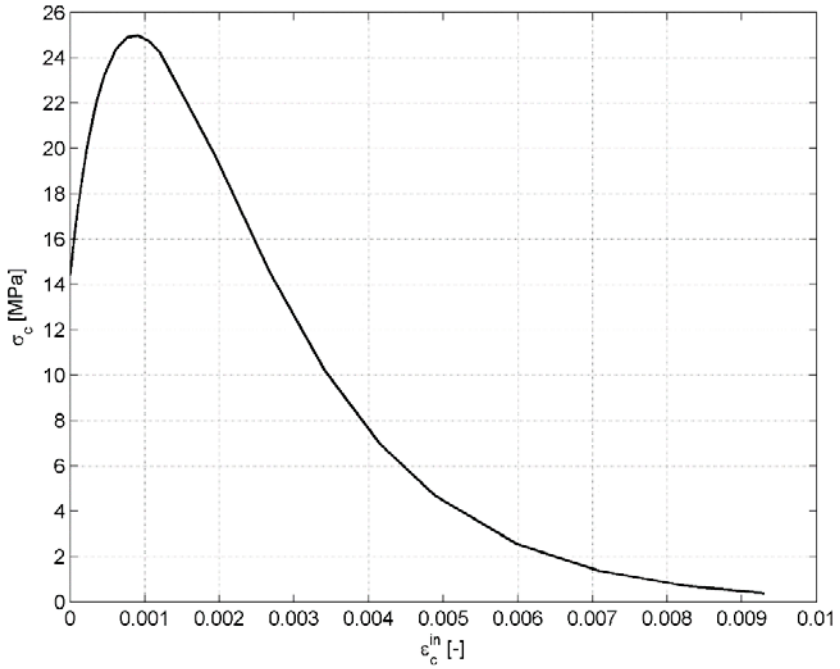

Figure 2-4 Concrete behaviour in compression.

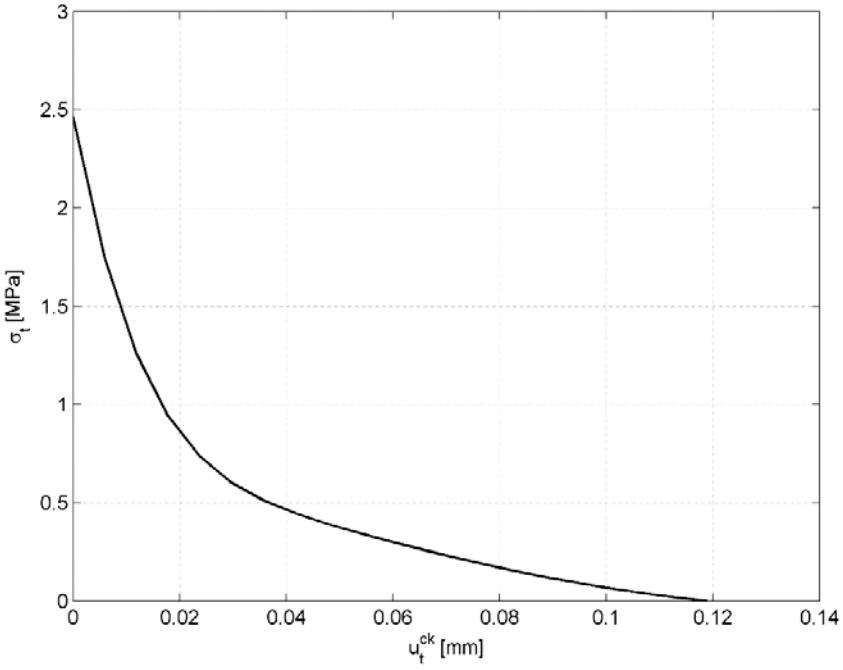

Figure 2-5 Concrete behaviour in tension.

2.4.2. Steel

The steel constituting the anchors, steel plates and reinforcement is modelled elastically (if not otherwise stated) with material values according to Table 2-3.

Table 2-3 Steel material values used in analyses.

Parameter	Description	Value (20°C)
E	Modulus of elasticity	210 GPa
υ	Poissons ratio	0.3
ρ	Density	7800 kg/m^3

2.5. General analysis prerequisites

The analyses simulate a static loading scenario but are in Abaqus/Explicit performed dynamically. The displacement rate is 50 mm/s in all numerical simulations, unless otherwise stated. This rate keeps the analysis times to a minimum without adding dynamic effects.

The concrete, anchors and steel plates are modelled with 8-node continuum elements with one integration point in each element. These elements are in Abaqus denominated as C3D8R. The reinforcement is modelled with beam elements that are denominated as B31 in Abaqus [Dassault Systémes 2014].

The general contact algorithm provided in Abaqus is used with default settings to model the contact behaviour between the anchors, steel plate and the concrete. The interaction is defined as a pure master-slave contact with the concrete as the slave surface and the anchor plate as the master surface. The penalty formulation is used in the tangential direction, generally with an assumed constant friction coefficient of $\mu = 0.4$ as interaction property. Overclosure in the normal direction is handled with the "hard" contact formulation [Dassault Systémes 2014]. Separation of the surfaces after contact is allowed.

The interaction between the explicitly modelled reinforcement and the concrete is defined using option "embedded region" in Abaqus. The interaction is then defined by constraint equations between the translational degrees of freedom of the nodes in beam elements, representing the reinforcement, and the nodes of the solid elements, representing the concrete. Only the nodes of the solid elements enclosing the beam nodes are constrained to the beam nodes [Dassault Systémes 2014].

3. Anchor plates loaded in tension

3.1. General

For an anchor in tension, the concrete in the vicinity of the anchor is subjected to both a global stress field as a result of global deformation of the structure and a local stress field caused by interaction between the anchor and the concrete. The global stress field caused by the transverse tension load is for most concrete structures dominated by global bending stresses. These bending stresses are tensile at the face where the anchor is located. As the concrete strength is strongly limited in tension, the global stress field in the vicinity of the anchor can be detrimental for the tension breakout capacity.

Global bending of a concrete structure caused by a transverse load is influenced by a number of different parameters. In general, the curvature of the concrete structure increases linearly with load level, decreases with the square of the thickness, increases with the square of the structure width, decreases with stiffness in boundary conditions of the structure and decreases with the amount of reinforcement. Corresponding global bending stresses in the concrete are directly related to the curvature of the concrete structure.

Presence of reinforcement in the vicinity of the anchor also has a local impact on the anchor behaviour and anchor capacity. If potential concrete failure surfaces are crossed by reinforcement, the potential concrete failure prism can be tied to the concrete structure and the concrete breakout strength can increase. If the reinforcement loaded in tension starts to yield in the anchor region, however, increased concrete cracking can result in reduced anchor capacity.

As the character of the concrete material is strongly nonlinear, determination of the concrete breakout capacity is best done either by testing or numerical simulation. The presence of reinforcement complicates the response of the anchor in tension even more and necessitates one of these two methods in determining its capacity.

3.2. Previous ANKARM project

In the previous ANKARM project, centrically loaded anchor groups far from concrete edges in non-reinforced and reinforced concrete were investigated [SSM Research Report 2013:27].

Table 3-1 shows investigated configurations and corresponding simulated tension failure loads for reinforced structures. The embedment depth of the anchors was $h_{ef} = 220$ mm and the compressive cylinder strength was $f_c = 25$ MPa.

Table 3-1 Investigated configurations of anchor groups in reinforced concrete slabs in the ANKARM project [SSM Research Report 2013:27]. N_u is the tension failure load of the group.

Slab	Slab dimension [m]	Top rein-Forcement	Support	Anchor Group	Cross-section of profile [mm]	N_u [kN]
1	2.2x2.2x0.3	ø12cc300	Ring	2x2	120x120	341
2	2.2x2.2x0.3	ø12cc150	Ring	2x2	120x120	464
3	2.2x2.2x0.3	ø12cc100	Ring	2x2	120x120	492
4	2.2x2.2x0.3	ø12cc150	Ring	2x2	220x220	461
5	2.2x2.2x0.3	ø12cc300	Ring	2x3	120x120	340
6	2.2x2.2x0.3	ø12cc150	Ring	2x3	120x120	443
7	2.2x2.2x0.3	ø12cc100	Ring	2x3	120x120	502
8	2.2x2.2x0.6	ø12cc150	Ring	2x2	120x120	612
9	2.2x2.2x0.6	ø12cc150	Ring	2x2	220x220	622
10	3x3x0.6	ø12cc300	Simply Supported	2x2	220x220	600
11	3x3x0.6	ø12cc300	Clamped	2x2	220x220	618

In summary, the results showed the importance of global stiffness of the structure. As seen in in Table 3-1, thickness of the concrete structure, the amount of reinforcement and the boundary conditions have an influence on the tension failure load. The more flexible the structure gets, the more vulnerable the concrete is to splitting failure which reduces the failure load. The reason for failure load to increase for slab 1, 2 and 3, as the amount of reinforcement increases, is essentially that the global stiffness of the structure increases. The local effect of surface reinforcement crossing the breakout concrete prism has a minor influence. Increase of the concrete structure thickness from 0.3 to 0.6 m has the largest impact on the tension failure load. The main reason is that splitting failure is avoided and that concrete cone failure thus limits the capacity.

3.3. Initial conditions

In order to investigate, in a controllable way, how reinforcement locally interacts with an anchor group breakout prism, the failure modes splitting and concrete cone breakout need to be separated. The splitting failure mode is essentially controlled by the global bending stiffness of the structure. The stiffer the structure is, the lesser splitting will contribute to failure of an anchor group loaded in tension. Thickness of concrete structure, reinforcement density and boundary conditions of the structure all influence the global bending stiffness.

In order to suppress splitting and promote concrete cone failure to occur for an anchor group loaded in tension, the global bending stiffness of the concrete structure is exaggerated. This is done by choosing a concrete block thickness of 0.6 m. Furthermore, the bottom of the concrete block is constrained to move in the direction of the tension load. With these conditions, the local impact of reinforcement density on the evolution of the concrete cone breakout can be studied for different configurations of anchor groups loaded in tension. A comparison with the concrete cone failure load determined with CEN/TS 1992-4-2 is also facilitated with these conditions.

3.4. Eccentrically loaded far from concrete edges

3.4.1. General

Eccentrically loaded anchor plates in non-reinforced and reinforced concrete structures are investigated numerically. The anchor plates are located far from concrete edges. In order to avoid the impact of global bending stresses and thereby promoting concrete cone failure to occur, the anchor plates are located in a 0.6 m thick concrete structure. In addition, the bottom of the structure is constrained to move in the direction of the tension load.

3.4.2. Definition of eccentricity

The loading situation of an anchor plate that is eccentrically loaded in tension corresponds to an anchor plate that is centrically loaded by a tension force *N* and a bending moment *M*. Figure 3-1 shows a side view of this loading condition for an anchor plate with four anchors assuming a rigid plate.

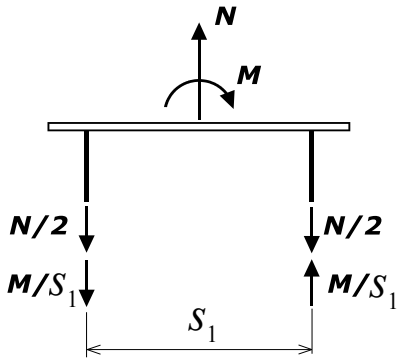

Figure 3-1 Side view of an anchor plate with four anchors subjected to a tension load *N* and a bending moment *M* applied in the centre of the plate.

In this investigation, eccentricity (non-dimensional) of the tension load is defined as

$$e = \frac{M/s_1}{N/2} \qquad \text{(Eq. 3-1)}$$

An eccentricity $e = 0$ means that the anchor plate is centrically loaded with no bending moment. An eccentricity $e = 1$ corresponds to an eccentrically loaded anchor plate where the tension load is located $s_1/2$ from the centre of the plate. In CEN/TS 1992-4-2, eccentricity e_N is defined as the distance between the applied tension load and the centre of the anchor plate.

3.4.3. Analysed configurations

The influence of eccentricity in one direction and density of reinforcement is investigated for a tension loaded anchor plate far from concrete edges.

Investigated amount of surface reinforcement (in two orthogonal directions) is

- No reinforcement
- ϕ12cc300
- ϕ12cc200
- ϕ12cc100
- ϕ16cc300
- ϕ16cc200
- ϕ16cc100

Investigated eccentricities are

e = 0, 1, 2, 5 and 10

Eccentricity $e = 10$ is only investigated for ϕ12 reinforcement.

3.4.4. Finite element geometry and boundary conditions

The geometry of the anchor plate is given in Figure 3-2. The anchor plate is embedded in the concrete and the embedment depth h_{ef} of the anchors is 195 mm. The distance 150 mm between the anchors is chosen to suit the different reinforcement configurations. The overall concrete structure measures 2.2x2.2x0.6 m.

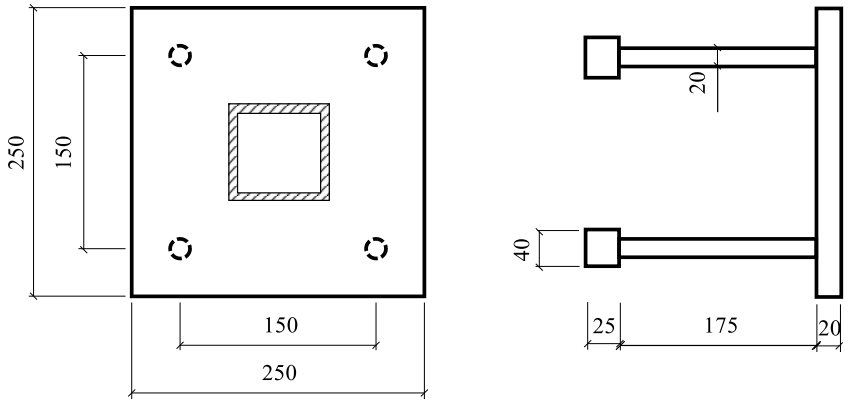

Figure 3-2 Anchor plate geometry in mm.

Since the tension load is eccentrically applied, half of the structure needs to be modelled. Figure 3-3 shows the finite element model. The size of the elements in the region where the concrete cone is developed is 5 mm. Table 3-2 shows corresponding size of the model.

The bottom plane of the concrete structure is constrained to move in the direction of the tension load. Symmetry boundary condition is applied on the surface with normal opposite to the positive Y-axis.

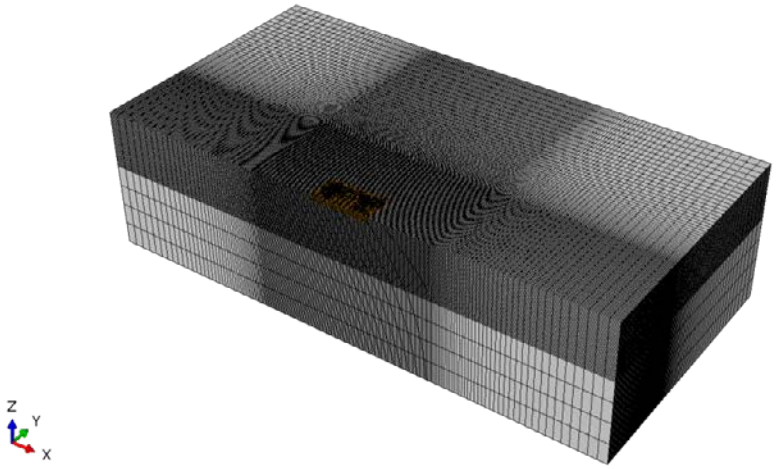

Figure 3-3 Example of a finite element model with an anchor plate coloured in orange. The element side length in the dense meshed region is 5 mm.

Table 3-2 Approximate size of a FEA-model constituting a group of four anchors and reinforcement.

Number of nodes	Number of elements	Number of degrees of freedom
~1 530 000	~1 470 000	~4 570 000

Figure 3-4 shows an example of the reinforcement in the concrete structure. Irrespective of reinforcement dimension, the concrete cover is set to 30 mm. The reinforcement in the different directions is separated into different planes on the upper and lower surfaces, however still abutting each other. The reinforcement along the Y-axis is enclosing the reinforcement along the X-axis. The radius of curvature for the reinforcement is 120 mm.

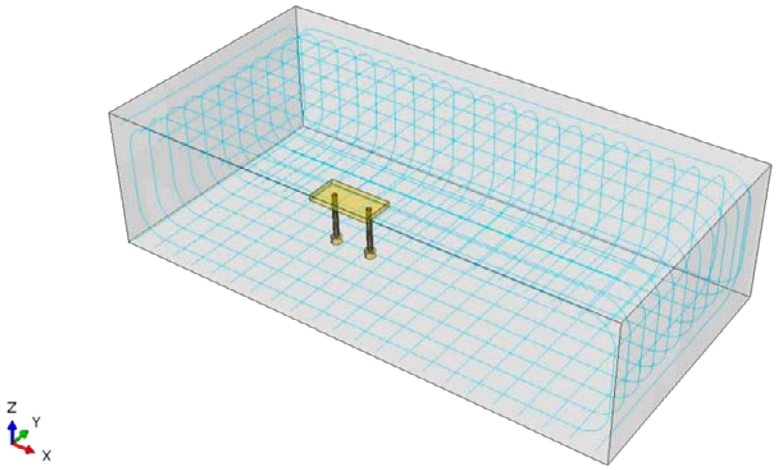

Figure 3-4 Transparent view of model with reinforcement density $\boldsymbol{\phi 12cc100}$. The rigid beam along the X-axis for application of tension load is not shown.

The eccentric tension load is applied by use of a rigid beam that, in one of its ends, is rigidly attached (by kinematic coupling) to the nodes configuring the support

beam cross section at the top surface of the anchor plate, see Figure 3-5. In the free end of the rigid beam, the tension load is applied through displacement control. A displacement rate is applied perpendicular to the anchor plate. The length of the rigid beam directly corresponds to the tension load eccentricity.

Information about Abaqus elements used in the finite element model is given in chapter 2.

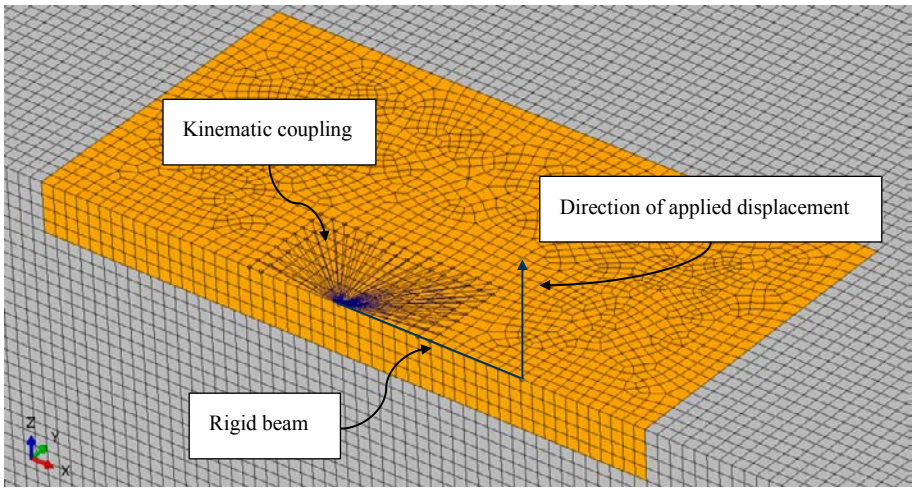

Figure 3-5 Configuration with eccentricity *e* = 1. Anchor plate in orange and concrete in grey.

3.4.5. Finite element analysis

The finite element analyses are conducted in Abaqus version 6.14 using double precision, small deformations and the explicit solver. A constant displacement rate of 50 mm/s is applied to the free end of the rigid beam and the displacement is evaluated at the node rigidly attached to the support beam cross section (centre of anchor plate), see Figure 3-5.

3.4.6. Results for non-reinforced concrete

For comparison reasons, the concrete cone failure load as a function of eccentricity is calculated for non-reinforced concrete by use of CEN/TS 1992-4-2. According to the code, the characteristic resistance of this group of fasteners in non-cracked concrete is written as

$$N_{Rk,c} = N^0_{Rk,c} \cdot \frac{A_{c,N}}{A^0_{c,N}} \cdot \psi_{s,N} \cdot \psi_{re,N} \cdot \psi_{ec,N} \qquad \text{(Eq. 3-2)}$$

where

$$N^0_{Rk,c} = 11.9 \cdot \sqrt{f_{ck,cube}} \cdot h_{ef}^{1.5} \quad \text{(non-cracked)} \qquad \text{(Eq. 3-3)}$$

$$A^0_{c,N} = 9 \cdot h_{ef}^2 \qquad \text{(Eq. 3-4)}$$

$$A_{c,N} = \left(3 \cdot h_{ef} + s_1\right)^2 \qquad \text{(Eq. 3-5)}$$

$$\psi_{ec,N} = \frac{1}{1+2\cdot e_N/s_{cr,N}} \leq 1 \quad \text{(Eq. 3-6)}$$

$$s_{cr,N} = 3 \cdot h_{ef} \quad \text{(Eq. 3-7)}$$

$$\psi_{s,N} = \psi_{re,N} = 1 \quad \text{(Eq. 3-8)}$$

In equation 3-6 the eccentricity e_N is given as the distance between the centre of the anchor plate and the applied tension load. Equation 3-1 gives that $e_N = e \cdot s_1/2$.

Correct value of $f_{ck,cube}$ has to be inserted into equation 3-3 when comparing the CEN/TS 1992-4-2 with numerical results. In performed numerical analyses, an ultimate compressive stress $\sigma_{cu} = 25$ MPa is used. This value corresponds to a compressive cylinder strength $f_c = 25$ MPa. The relation between cylinder and cube compressive strength value is given by [Betonghandbok- Material 2008] as $f_c = 0.76 \cdot f_{c,cube}$. The value used for $f_{ck,cube}$ in equation 3-3 is hence given as

$$f_{c,cube} = \frac{25}{0.76} = 32.9 \text{ MPa} \quad \text{(Eq. 3-9)}$$

Finally, the characteristic resistance $N_{Rk,c}$ is multiplied by 1.33 in order to get the mean tension failure load, i.e.

$$N_{u,CEN/TS} = 1.33 \cdot N_{Rk,c} \quad \text{(Eq. 3-10)}$$

Table 3-3 shows a comparison between simulated failure loads and failure loads determined by use of CEN/TS 1992-4-2, section 6.2.5. The results show that simulations predict similar tension failure loads as CEN/TS 1992-4-2 does for smaller eccentricities. As the eccentricity increases beyond $e = 2$, the deviation increases with increasing eccentricity. One explanation for this difference might be that CEN/TS 1992-4-2, with equation 3-6, cannot capture the dependence of eccentricity accurately enough when the eccentricity gets larger.

Table 3-3 Tension failure load in non-reinforced concrete as a function of eccentricity determined by simulation and by CEN/TS 1992-4-2.

e *(Eq. 3-1)* [-]	$N_{u,simulation}$ [kN]	$N_{u,CEN/TS}$ [kN]	$\frac{N_{u,simulation}}{N_{u,CEN/TS}}$
0	364	390	0.93
1	322	311	1.04
2	219	205	1.07
5	111	136	0.82
10	60	87	0.69

An increase in eccentricity reduces the concrete cone failure load. Figure 3-6 and Figure 3-7 show contour plots of the damage tension parameter at failure load for no eccentricity $e = 0$ and an eccentricity $e = 10$ in non-reinforced structures. Both figures clearly show a developed concrete cone. It is also seen that the concrete cone moves from the centre of the anchor plate towards the most tensioned anchor pair as eccentricity increases. As the eccentricity gets large, corresponding bending moment *M* shown in Figure 3-1 completely will control the loading scenario and the level of failure load.

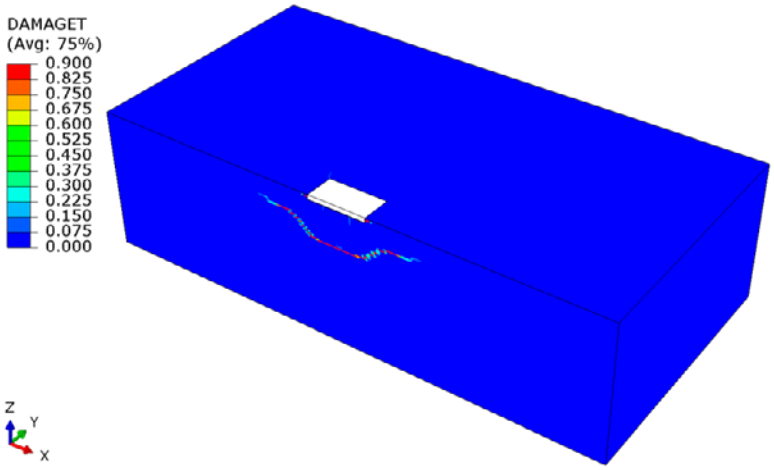

Figure 3-6 Damage tension parameter (DAMAGET) at failure load for eccentricity *e* = 0. No reinforcement.

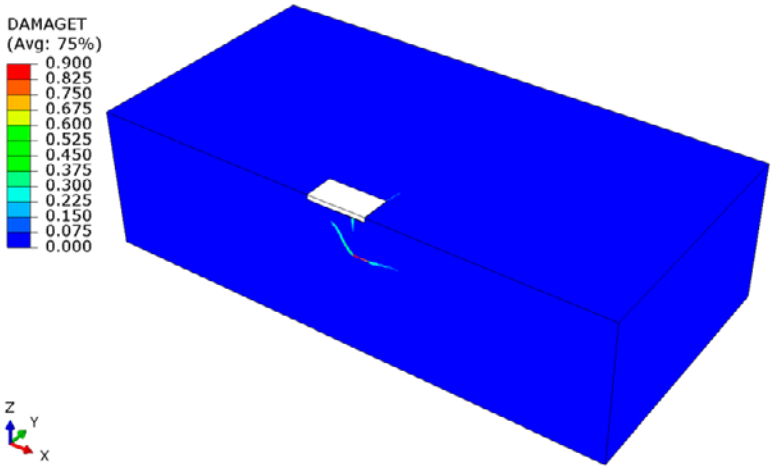

Figure 3-7 Damage tension parameter (DAMAGET) at failure load for eccentricity *e* = 10. No reinforcement.

3.4.7. Results for reinforced concrete

The numerical simulations show that the amount of surface reinforcement has a very small impact on the concrete cone failure load. This result is independent of eccentricity. Figure 3-8 shows force-displacement curves as a function of amount of Ø12 surface reinforcement and eccentricity of the tension load. As seen, also the shape of the force-displacement curves is almost independent of the amount of reinforcement. Eccentricity, on the other hand, has an influence on the failure load as already discussed above for the non-reinforced structure.

The reason why there is no effect of reinforcement on the concrete cone failure load is that the plane of the surface reinforcement is oriented perpendicular the tension load. This orientation makes it difficult to transfer the tension load into the reinforcement bars. In the previous ANKARM project [SSM Research Report 2013:27], the amount of reinforcement had an impact on the failure load for anchor groups loaded in tension, see

Table 3-1. In those simulations, however, failure was controlled by the splitting failure mode. The thickness of investigated concrete blocks was 0.3 m and the global bending stiffness was dependent of the amount of reinforcement. In the present investigation, the bottom of the concrete structure is constrained in the direction of the tension load in order to avoid splitting failure and instead promote concrete cone failure to occur.

Figure 3-9 shows force-displacement curves as a function of the amount of Ø16 surface reinforcement and eccentricity of the tension load. The results are almost identical with those for the Ø12 surface reinforcement. It is thus concluded that surface reinforcement has a very small influence on the concrete cone failure load for eccentrically loaded anchor plates loaded in tension if splitting can be avoided.

The effect of eccentricity on the concrete cone failure load is almost the same for reinforced as non-reinforced concrete. This can be seen both in Figure 3-8 and Figure 3-9.

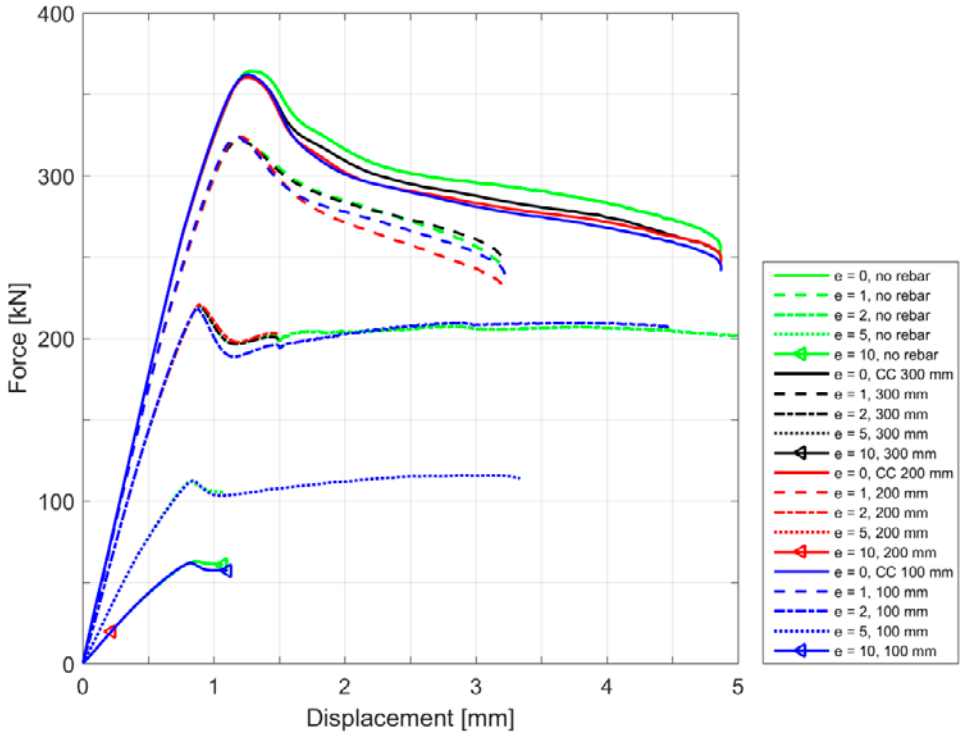

Figure 3-8 Force-displacement curves as a function of amount of Φ12 reinforcement and tension load eccentricity *e* (see Eq. 3-1). Displacement is measured at the centre of the anchor plate.

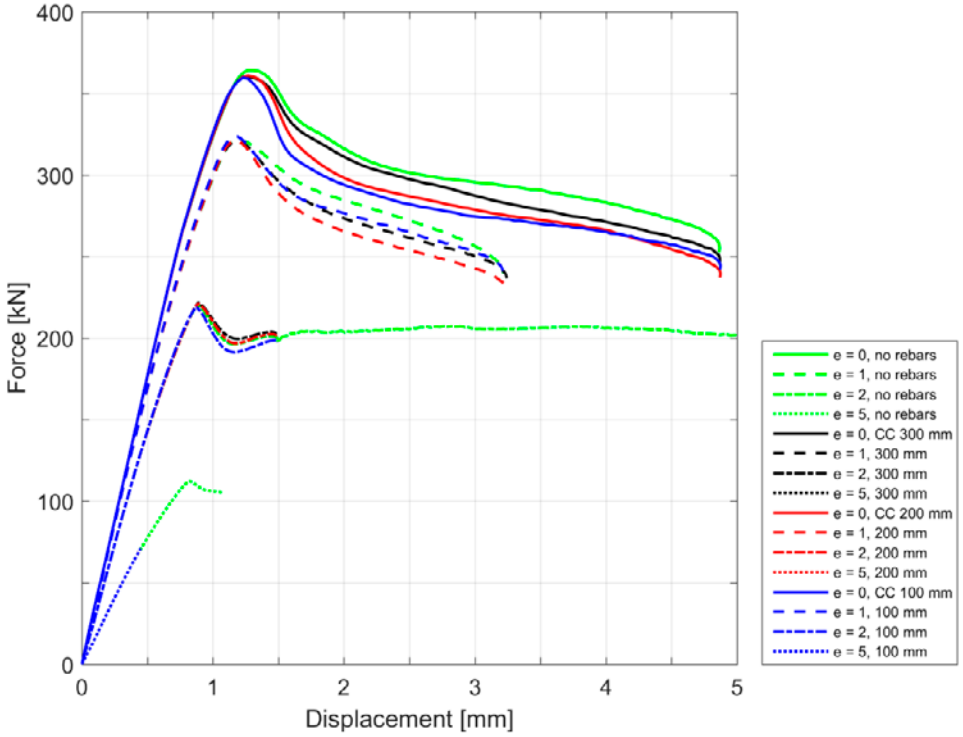

Figure 3-9 Force-displacement curves as a function of amount of Φ16 reinforcement and tension load eccentricity *e* (see Eq. 3-1). Displacement is measured at the centre of the anchor plate.

3.5. Centrically loaded close to a free concrete edge

3.5.1. General

Centrically loaded anchor plates close to a free concrete edge in non-reinforced and reinforced concrete structures are investigated numerically. In order to avoid the impact of global stresses and thereby promoting concrete cone failure to occur, the anchor plates are located in a 0.6 m thick concrete structure. In addition, the bottom of the structure is constrained to move in the direction of the tension load.

3.5.2. Analysed configurations

The influence of the distance to a free concrete edge and the density of reinforcement is investigated for anchor plates centrically loaded in tension.

Investigated edge distances are

$c_1 = 75$, 150 and 200 mm

Investigated amount of surface reinforcement (in two orthogonal directions) is

- No reinforcement
- ϕ12cc300
- ϕ12cc200
- ϕ12cc100

Corresponding surface reinforcement at the free concrete edge, here designated edge reinforcement, is considered.

3.5.3. Finite element geometry and boundary conditions

The geometry of the anchor plate is given in Figure 3-10. The anchor plate is embedded in the concrete and the anchor embedment depth $h_{ef} = 195$ mm. A distance $s_1 = 150$ mm between the anchors is chosen to suit the different reinforcement configurations. The whole concrete structure model measures 2.2x1.1x0.6 m.

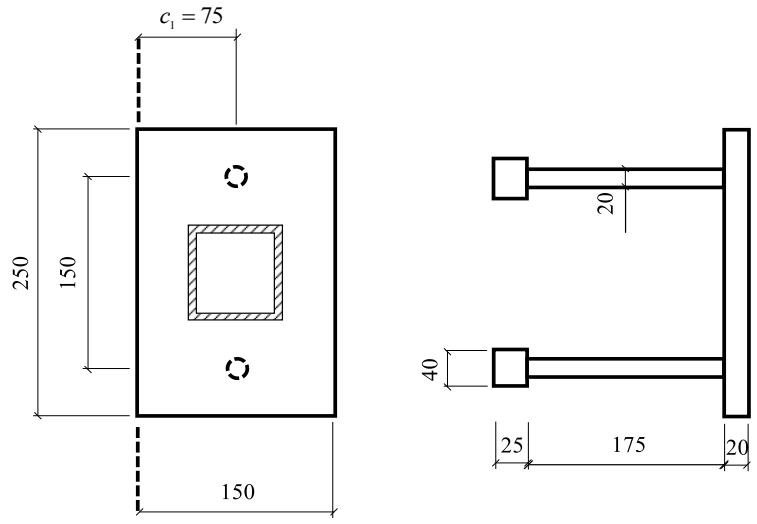

Figure 3-10 Anchor plate geometry with edge distance $c_1 = 75$ mm.

Since the tension load is centrically applied, only half of the structure needs to be modelled. Figure 3-11 shows an example of a finite element model where the distance from the anchors to the free edge is 75 mm. The size of the elements in the region where the concrete cone is developed is 5 mm. Table 3-4 shows the average model size.

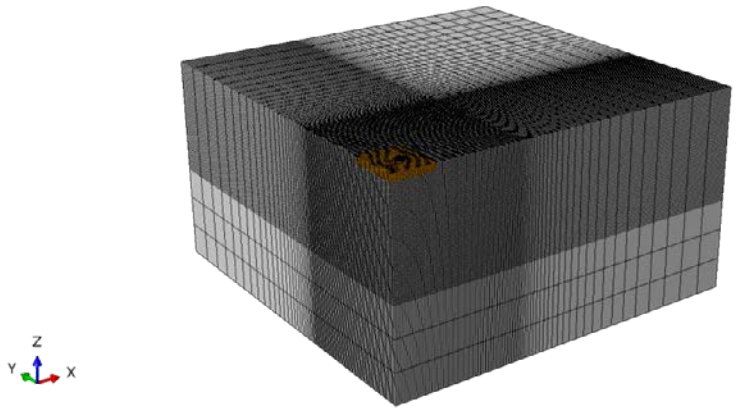

Figure 3-11 Finite element model of a centrically loaded anchor plate close to a free concrete edge. The figure shows the case with edge distance $c_1 = 75$ mm. Element side length in the dense meshed region is 5 mm. Y-Z plane to the left is a symmetry plane.

Table 3-4 Average size of FEA-model constituting a group of two anchors and reinforcement.

Number of nodes	Number of elements	Number of degrees of freedom
~743 000	~712 000	~2 220 000

The bottom plane of the concrete structure is constrained in the Z-direction. The surface with normal opposite to the positive X-axis is the symmetry surface. All other surfaces are free.

Figure 3-12 shows an example of the reinforcement in the concrete structure. The same reinforcement configurations are used as for the model with an eccentrically applied load far from concrete edges. The concrete cover is set to 30 mm, the radius of curvature for the reinforcement is 120 mm, reinforcement is separated into different planes and the reinforcement along the Y-axis is enclosing the reinforcement along the X-axis.

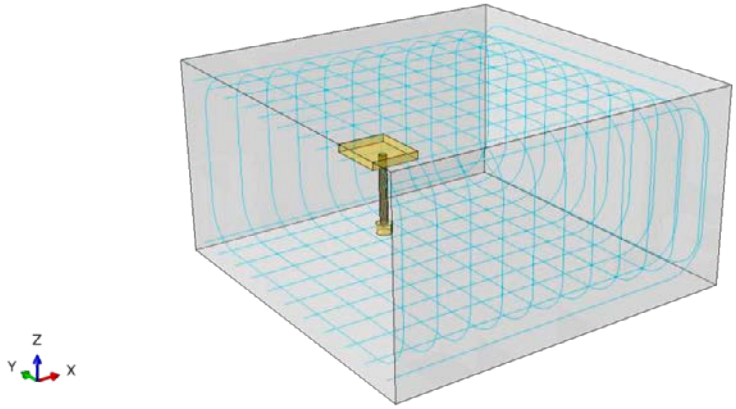

Figure 3-12 Transparent view of model with a centrically loaded anchor plate close to a free concrete edge. Reinforcement density is $\Phi 12cc100$ and the edge distance $\boldsymbol{c_1}$ = **75** mm.

The tension load is applied where the support beam (75x75x5 mm) is attached to the anchor. A master node is used with a kinematic constraint controlling the displacement of the nodes on the cross section area in the Z-direction. The displacement and corresponding reaction force is evaluated at the master node.

Information about Abaqus elements used in the finite element model is given in chapter 2.

3.5.4. Finite element analysis

The finite element analyses are conducted in Abaqus version 6.14 using double precision, small deformations and the explicit solver. A constant displacement rate of 50 mm/s is applied to the master node controlling the displacement of the support beam cross section area.

3.5.5. Results for non-reinforced concrete

For comparison reasons, the concrete cone failure load as a function of distance to the concrete edge is calculated for non-reinforced concrete by use of CEN/TS 1992-4-2. According to the code, the characteristic resistance of a group of fasteners in non-cracked concrete close to a free concrete edge is written as

$$N_{Rk,c} = N^0_{Rk,c} \cdot \frac{A_{c,N}}{A^0_{c,N}} \cdot \psi_{s,N} \cdot \psi_{re,N} \cdot \psi_{ec,N} \qquad \text{(Eq. 3-11)}$$

where

$$N^0_{Rk,c} = 11.9 \cdot \sqrt{f_{ck,cube}} \cdot h_{ef}^{1.5} \quad \text{(non-cracked)} \qquad \text{(Eq. 3-12)}$$

$$A^0_{c,N} = 9 \cdot h_{ef}^2 \qquad \text{(Eq. 3-13)}$$

$$A_{c,N} = \left(c_1 + 1.5 \cdot h_{ef}\right) \cdot \left(s_1 + 3 \cdot h_{ef}\right) \qquad \text{(Eq. 3-14)}$$

$$\psi_{s,N} = 0.7 + 0.3 \cdot \frac{c_1}{c_{cr,N}} \leq 1 \qquad \text{(Eq. 3-15)}$$

$$c_{cr,N} = 1.5 \cdot h_{ef} \qquad \text{(Eq. 3-16)}$$

$$\psi_{re,N} = \psi_{ec,N} = 1 \qquad \text{(Eq. 3-17)}$$

The characteristic compression cube strength $f_{ck,cube}$ used in equation 3-12 and the tension failure load N_u are given by equations 3-9 and 3-10, respectively.

Table 3-5 shows a comparison between simulated failure loads and concrete cone failure loads determined by use of CEN/TS 1992-4-2, section 6.2.5. The results reveal that simulated failure loads and failure loads predicted with CEN/TS 1992-4-2 correspond rather well.

Table 3-5 Tension failure load in non-reinforced concrete as a function of edge distance c_1 determined by simulation and by CEN/TS 1992-4-2.

c_1 [mm]	$N_{u,simulation}$ [kN]	$N_{u,CEN/TS}$ [kN]	$\frac{N_{u,simulation}}{N_{u,CEN/TS}}$
75	152	152	1.00
150	219	201	1.09
200	262	237	1.11

According to CEN/TS 1992-4-2, section 6.2.7, blow-out failure should be checked if $c_1 \leq 0.5 \cdot h_{ef}$. For $c_1 = 75$ mm the blow-out failure load is determined as 356 kN which is clearly higher than corresponding concrete cone failure load.

Figure 3-13, Figure 3-14 and Figure 3-15 show contour plots of the damage tension parameter at failure load for non-reinforced concrete and an edge distance $c_1 = 75$, 150 and 200 mm, respectively. For an edge distance $c_1 = 75$ mm, a concrete cone is clearly indicated in Figure 3-13. As seen, the cone is cut by the free edge. The failure load increases with the distance to the edge according to Table 3-5. This increase in failure load with distance to the free edge results in a combination of concrete cone failure and local splitting at the X-Y symmetry plane, see Figure 3-14. The splitting failure mode is further accentuated as the edge distance increases to $c_1 = 200$ mm, see Figure 3-15. When splitting failure starts, the bending stress in the beam prism results in damage accumulation in the symmetry plane just below the anchor plate, see Figure 3-14 and Figure 3-15.

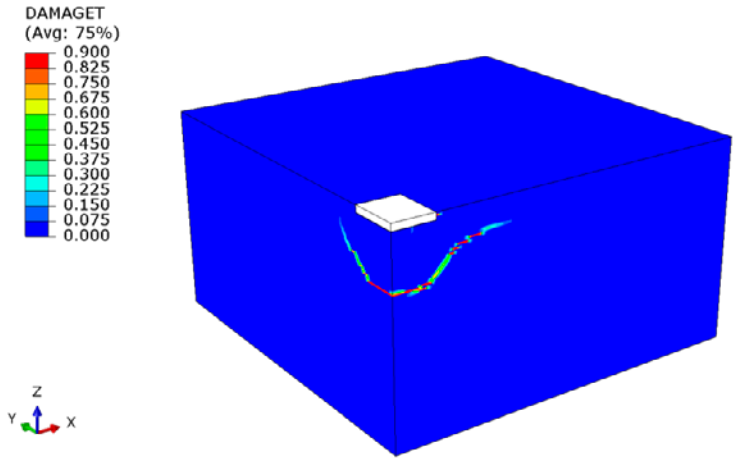

Figure 3-13 Damage tension parameter (DAMAGET) at failure load for an edge distance $c_1 = 75$ mm. No reinforcement. Y-Z plane to the left is a symmetry plane.

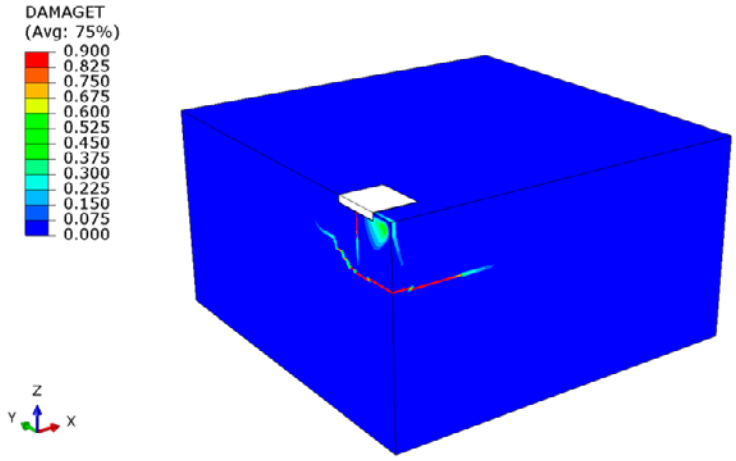

Figure 3-14 Damage tension parameter (DAMAGET) at failure load for an edge distance $c_1 =$ **150 mm**. No reinforcement. Y-Z plane to the left is a symmetry plane.

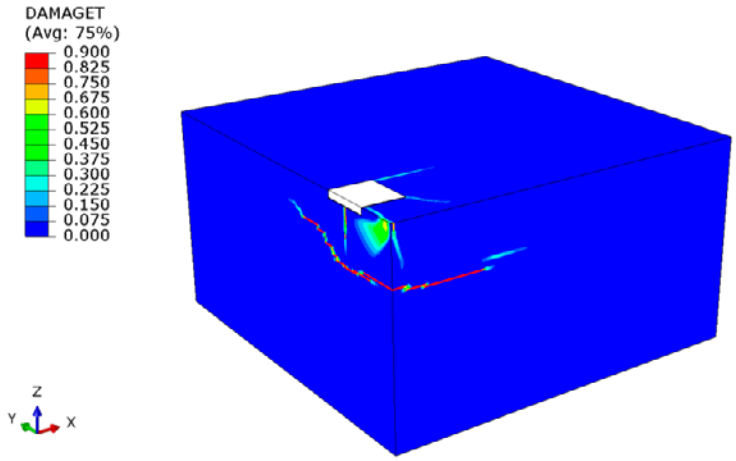

Figure 3-15 Damage tension parameter (DAMAGET) at failure load for an edge distance $c_1 =$ **200 mm**. No reinforcement. Y-Z plane to the left is a symmetry plane.

3.5.6. Results for reinforced concrete

The numerical simulations show that both the amount of reinforcement and the distance to the free concrete edge influence the failure load and the force-displacement curve. Figure 3-16 shows force-displacement curves as a function of these two parameters. As expected, and contrary to the anchor plate far from concrete edges, the failure load increases with the amount of reinforcement. The reason is that the tension load applied on the anchor plate can be transferred from the anchors through the concrete and into the edge reinforcement. For the anchor plate with the largest edge distance $c_1 = 200$ mm, the amount of reinforcement has least impact on the failure load. For a further increase of the edge distance, it is expected that the effect of reinforcement would vanish.

The effect of the edge distance on the failure load is clearly seen in Figure 3-16. For the edge distances investigated and independent of reinforcement density, the biggest change is when going from $c_1 = 75$ to $c_1 = 150$ mm. The explanation for this result is that the size of the concrete cone increases with the edge distance c_1.

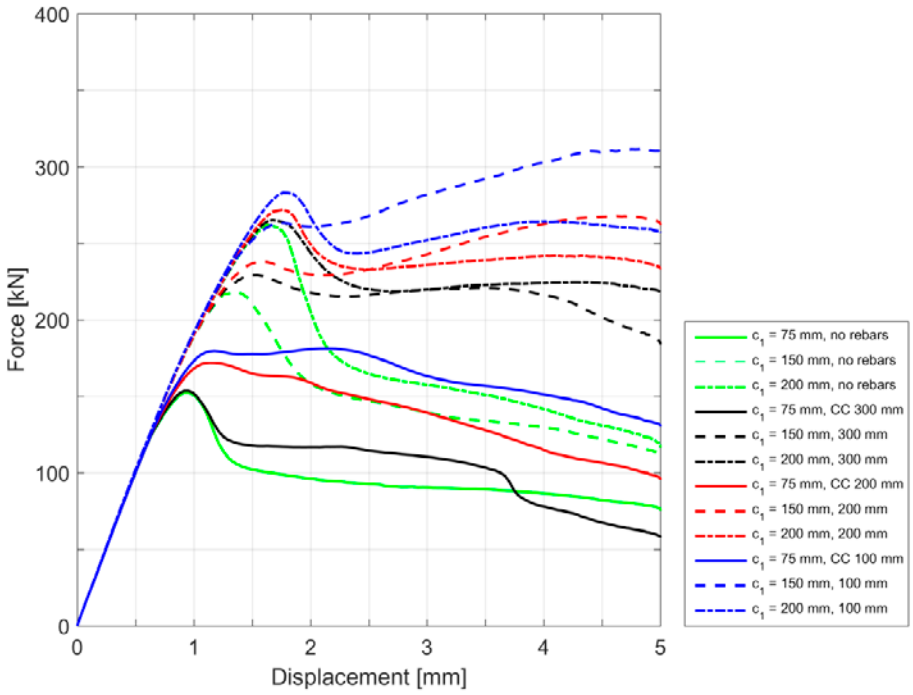

Figure 3-16 Force-displacement curves as a function of distance to free concrete edge $\boldsymbol{c_1}$ and amount of $\boldsymbol{\phi 12}$ reinforcement.

Figure 3-17, Figure 3-18 and Figure 3-19 show contour plots of the damage tension parameter at failure load for a reinforcement density ϕ12cc100 and an edge distance $c_1 = 75$, 150 and 200 mm, respectively. A comparison with the non-reinforced cases (Figure 3-13, Figure 3-14 and Figure 3-15) reveals that the tendency of combined concrete cone and splitting failure mode now is less pronounced.

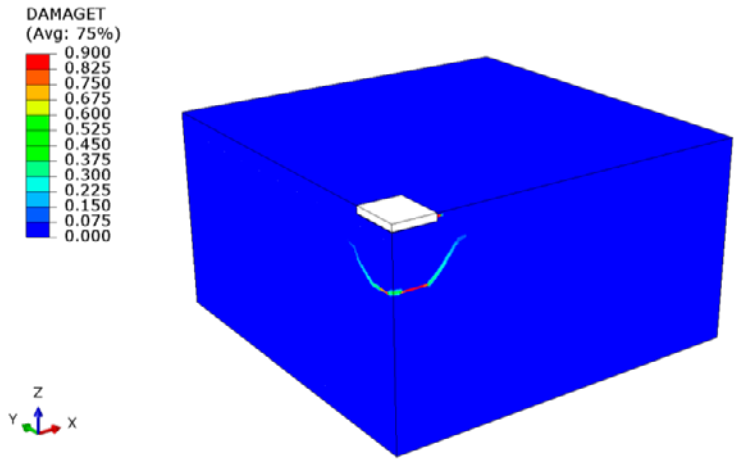

Figure 3-17 Damage tension parameter (DAMAGET) at failure load for an edge distance $\boldsymbol{c_1 = 75\ mm}$. Reinforcement density $\boldsymbol{\phi 12cc100}$. Y-Z plane to the left is a symmetry plane.

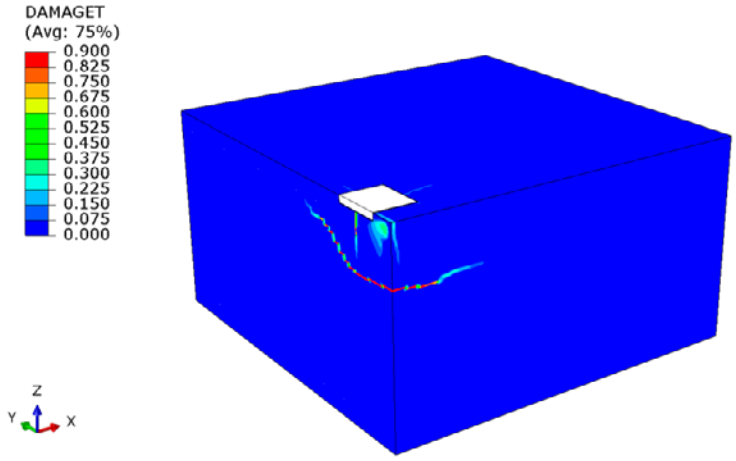

Figure 3-18 Damage tension parameter (DAMAGET) at failure load for an edge distance $c_1 =$ **150 mm**. Reinforcement density **ϕ12cc100**. Y-Z plane to the left is a symmetry plane.

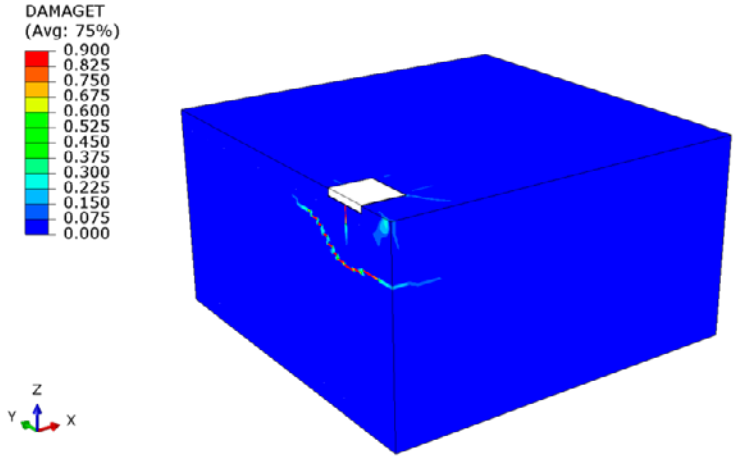

Figure 3-19 Damage tension parameter (DAMAGET) at failure load for an edge distance $c_1 =$ **200 mm**. Reinforcement density **ϕ12cc100**. Y-Z plane to the left is a symmetry plane.

For anchor plates located in reinforced concrete at an edge distance $c_1 = 75$ mm, a blow-out concrete breakout body is developed at the end of the simulations. As an example, Figure 3-20 shows the damage tension parameter at the end of the simulation for the case ϕ12cc100. The concrete breakout body is indicated at the Y-Z symmetry plane. The reason why blow-out occurs in reinforced but not in non-reinforced concrete is that tensioned edge reinforcement close to the anchor plate promotes the blow-out failure mode. Regarding the non-reinforced concrete, concrete cone failure happens before the blow-out failure mode has been initiated. This corresponds well with above calculated failure loads for concrete cone and blow-out failure for $c_1 = 75$ mm and non-reinforced concrete, i.e. 152 and 356 kN, respectively.

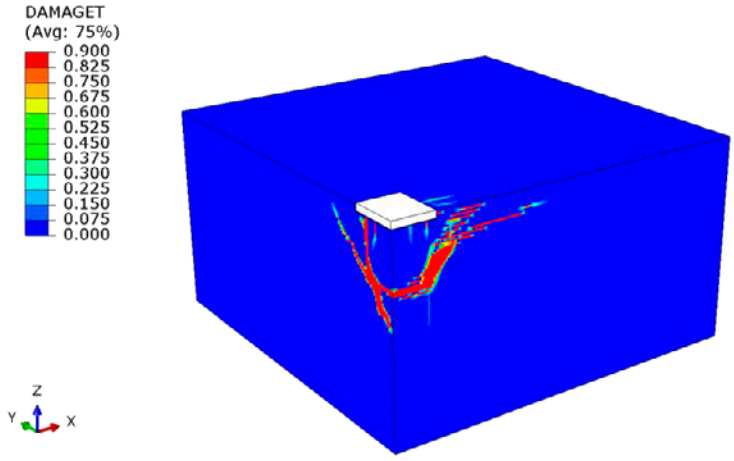

Figure 3-20 Damage tension parameter (DAMAGET) at end of simulation for an edge distance $c_1 = 75$ mm. Reinforcement density $\phi 12cc100$. Y-Z plane to the left is a symmetry plane.

The failure load increases with the amount of reinforcement. Table 3-6 gives the stress in the edge reinforcement bars that cross the concrete breakout cone at failure load for different edge distances and amount of reinforcement. The results show that the stress in the bar closest to the cone centre increases with reinforcement density independent of distance to edge. Furthermore, with a reinforcement density of $\phi 12cc100$, stress in the bar closest to the cone centre increases with distance to the edge. This result is somewhat unexpected. However, as the failure load increases with distance to edge (see Figure 3-16), more tension load is transferred from the anchor plate into the concrete and the reinforcement bars. The stress in the second closest bar is considerably lower than that in corresponding closest bar, particularly for the concrete structures with low reinforcement density. With a reinforcement density of $\phi 12cc300$, the second closest bar does not cross the concrete breakout cone which Table 3-6 indicates.

Table 3-6 Stress at failure load in edge reinforcement bars crossing concrete breakout cone.

c_1 [mm]	Reinforcement	Bar closest to concrete cone centre [MPa]	Bar second closest to concrete cone centre [MPa]
75	$\phi 12cc300$	133	1
	$\phi 12cc200$	164	4
	$\phi 12cc100$	185	43
150	$\phi 12cc300$	76	2
	$\phi 12cc200$	88	5
	$\phi 12cc100$	206	123
200	$\phi 12cc300$	100	3
	$\phi 12cc200$	131	25
	$\phi 12cc100$	236	68

3.6. Centrically loaded with shear reinforcement far from concrete edges

3.6.1. General

In order to increase the concrete cone tension capacity (as well as the pry-out capacity), the concrete structure in the vicinity of the anchor plate can be shear reinforced, see schematic sketch in Figure 3-21. The purpose of the shear reinforcement is to transfer tension load from the anchor plate, via the concrete breakout prism, into the concrete structure. As seen in Figure 3-21, the shear reinforcement links enclose the surface reinforcement.

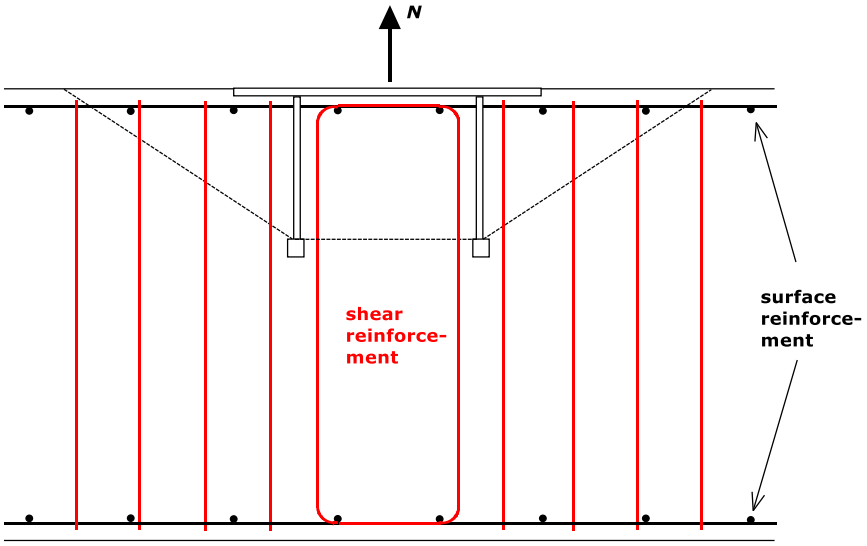

Figure 3-21 Concrete structure with shear reinforcement (in red) in the vicinity of the anchor plate.

The following configuration is used in the shear reinforcement simulations:

- Headed anchors and anchor plate; measures are given in Figure 3-2, elastic properties are used.
- Surface reinforcement; ϕ12cc100, elastic perfectly plastic material properties are used with a yield stress of 500 MPa.
- Shear reinforcement links; ϕ16, width of link is 148 mm, radius of link curvature is 24 mm, distance between links is $0.35h_{ef} = 68.3$ mm, elastic perfectly plastic material properties are used with a yield stress of 500 MPa.
- Thickness of concrete structure is 600 mm.
- Concrete cover is 30 mm.
- Anchor plate is centrically loaded in tension and located far from concrete edges.
- Tension load is deformation controlled (50 mm/s) and applied where the support beam (75x75x5 mm) is attached to the anchor plate.

Since the tension load is centrically applied and the anchor plate is located far from concrete edges, only one fourth of the structure needs to be modelled. Figure 3-22 shows the finite element model used in the numerical simulations. The size of the

elements in the region where major concrete damage is developed is 5 mm. Table 3-7 shows the model size.

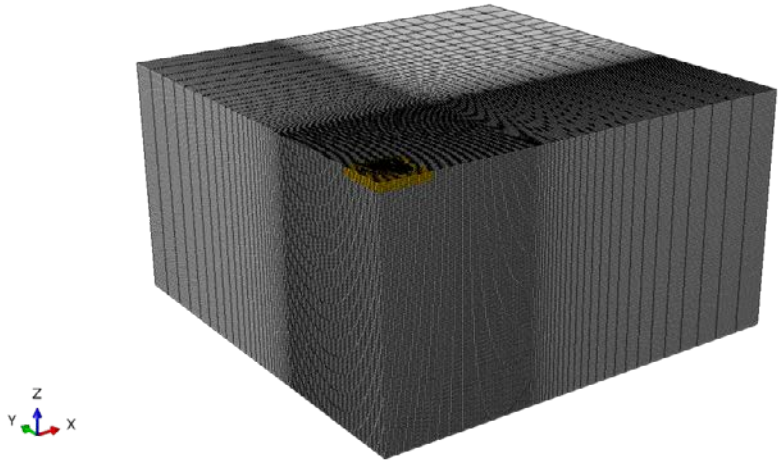

Figure 3-22 Finite element model of a centrically loaded anchor plate far from concrete edges. Due to symmetry, only one fourth of the structure is modelled. Element side length in the dense meshed region is 5 mm.

Table 3-7 Size of FEA-model constituting a group of four anchors, surface reinforcement and shear reinforcement.

Number of nodes	Number of elements	Number of degrees of freedom
~790999	~741063	~2338791

The bottom plane of the concrete structure is constrained in the Z-direction. The surfaces with normal opposite to the positive X-axis and the positive Y-axis are symmetry surfaces. All other surfaces are free.

Figure 3-23 shows the reinforcement in the concrete structure. The radius of curvature for the surface reinforcement is 120 mm, surface reinforcement is separated into different planes and the surface reinforcement along the Y-axis is enclosing the surface reinforcement along the X-axis. The concrete structure is shear reinforced with 16 shear reinforcement links in the vicinity of the anchor plate. Due to symmetry, only eight half links are modelled. All links are constrained to move in the Z-direction at the bottom of the concrete structure.

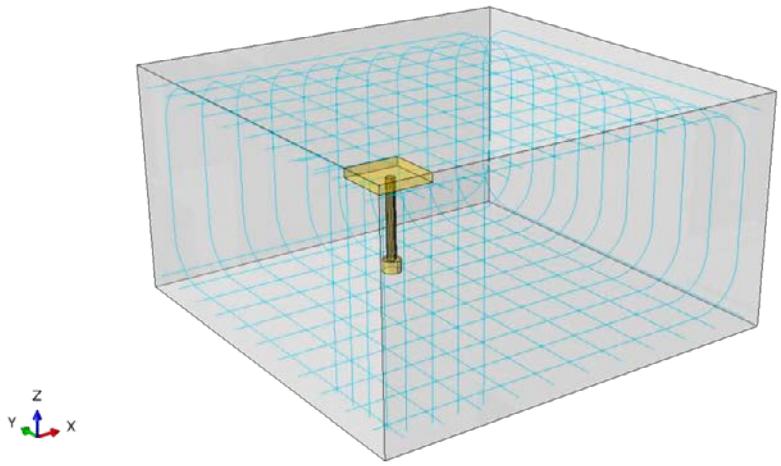

Figure 3-23 Transparent view of surface reinforcement and eight half shear reinforcement links. Due to symmetry, only one fourth of the structure is modelled.

3.6.2. Effect of distance between shear reinforcement links and anchors

The effect of four shear reinforcement links (one in each horizontal direction) located a distance a from the closest anchors is investigated, see Figure 3-24. It is of interest to determine how close to the edge of the concrete breakout prism the shear reinforcement links can be located without losing the possibility to transfer tension load from the anchor plate, via the breakout prisms and the links, into the concrete structure.

Analysed distances are given as multiples of h_{ef} as

$$\frac{a}{h_{ef}} = \{0.15, 0.3, 0.4, 0.5, 0.625, 0.75, 1, 1.25\} \qquad \text{(Eq. 3-18)}$$

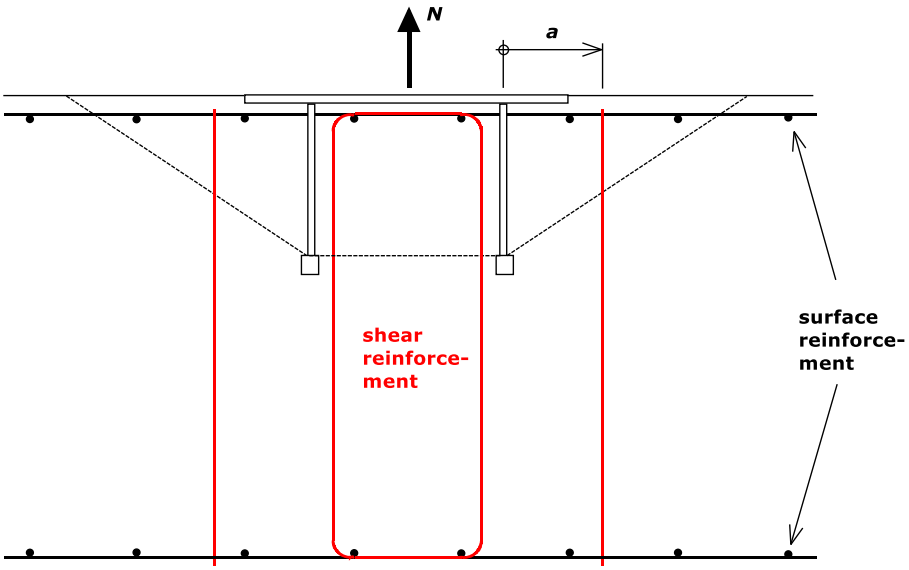

Figure 3-24 Concrete structure with one shear reinforcement link in each horizontal direction. Four links are used in total.

Figure 3-25 shows force-displacement curves for centrically tension loaded anchor plates with four shear reinforcement links located at different distance a from the anchors. As expected, the larger the distance a, the lower the tension capacity. The displacement at which failure load (maximum load) is reached is increased with reduced distance a. This means that not only the capacity but also the ductility increases as the shear reinforcement links are located closer to the anchor plate.

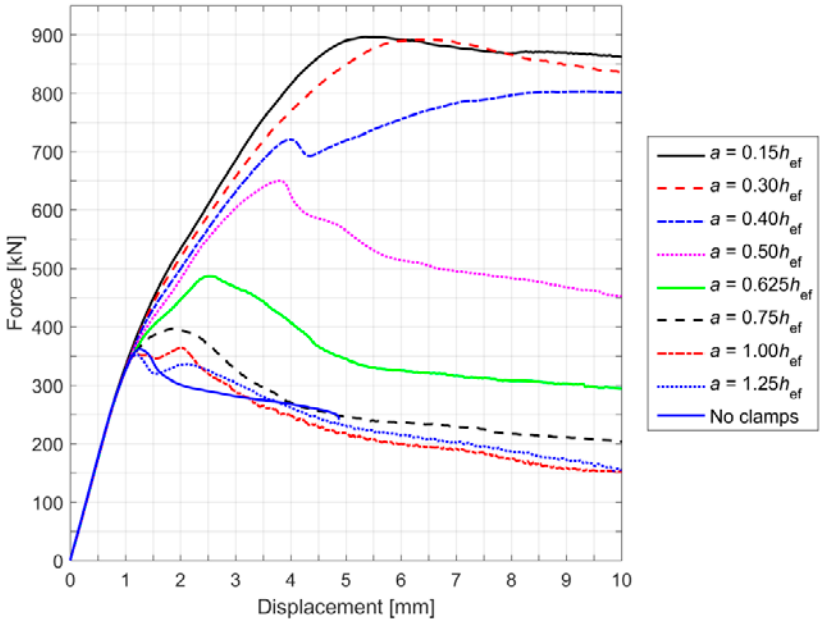

Figure 3-25 Force-displacement curves for anchor plates with four shear reinforcement links located at distance $\boldsymbol{a} = \{\mathbf{0.15}, \mathbf{0.3}, \mathbf{0.4}, \mathbf{0.5}, \mathbf{0.625}, \mathbf{0.75}, \mathbf{1.0}, \mathbf{1.25}\}\boldsymbol{h_{ef}}$. The case with no links is shown for comparison reasons.

Figure 3-26 shows failure load as a function of distance a for the simulated cases. The shear reinforcement links contribute the most if the links are located at distances $a \leq 0.3h_{ef}$. At distances $0.3h_{ef} < a \leq 0.75h_{ef}$, the failure load is gradually reduced as a increases. Beyond a distance of $a = 0.75h_{ef}$, the shear reinforcement links do not contribute to the tension load capacity.

With a yield stress of 500 MPa, one ϕ16 rebar has a tension capacity of about $\pi \cdot 8^2 \cdot 500 = 100$ kN. Hence, at most the capacity of four shear reinforcement links is about 800 kN. Figure 3-27 shows total normal force in the respective shear reinforcement link group. The maximum force 800 kN is reached for the cases $a = 0.15, 0.3$ and $0.4h_{ef}$. This means that these links are fully utilized, i.e. the whole cross section of the links is yielding. For the cases $a \geq 0.5h_{ef}$, 800 kN is not reached, see Figure 3-27. Local yielding occurs in the links as a result of bending in the link curvature.

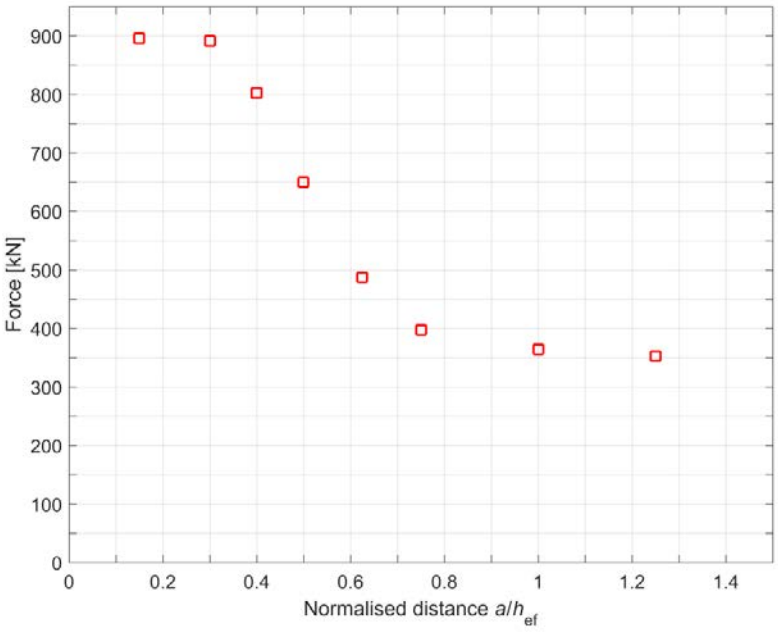

Figure 3-26 Failure load as a function of distance *a* for an anchor plate with four shear reinforcement links. Distance *a* is given as multiples of $\boldsymbol{h_{ef}}$.

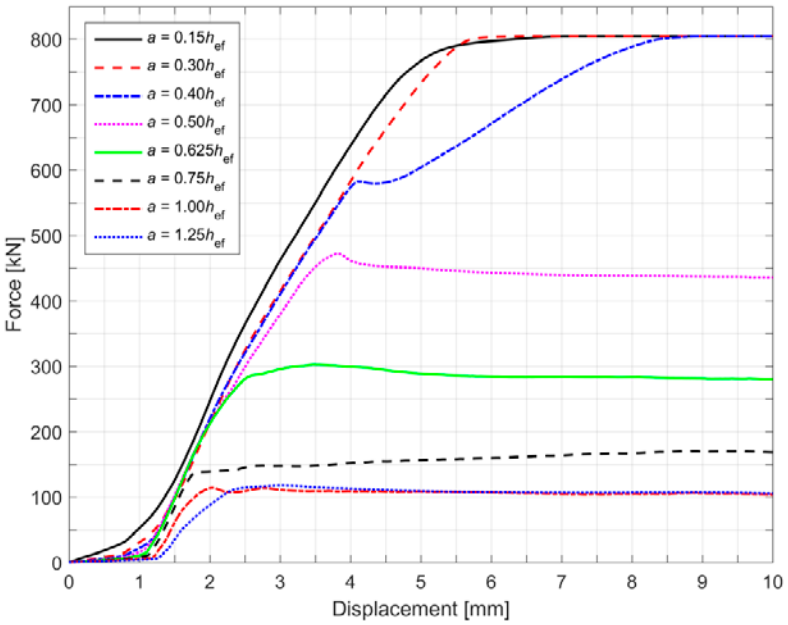

Figure 3-27 Total normal force in the respective shear reinforcement link group, i.e. $\boldsymbol{a/h_{ef}} = \{\mathbf{0.15}, \mathbf{0.3}, \mathbf{0.4}, \mathbf{0.5}, \mathbf{0.625}, \mathbf{0.75}, \mathbf{1.0}, \mathbf{1.25}\}$, as a function of displacement in centre of anchor plate.

Without shear reinforcement, failure load is reached at a displacement of about 1.25 mm, see solid blue curve in Figure 3-25. With shear reinforcement, the normal force in the links has just started to develop at this displacement, see Figure 3-27. Thus, before the links are activated and can take load, the concrete cone has to be developed. The load mechanisms and the force flow in the concrete structure differ with distance a. For $a = 0.15h_{ef}$ and $0.3h_{ef}$, plastic deformation in the shear reinforcement links starts where the concrete cone separates from the concrete structure. As a is increased, initial plastic deformation in the links starts closer to the link curvature at the top of the structure.

Figure 3-28 shows the damage tension parameter for the case $a = 0.15h_{ef}$ at failure load. As the shear reinforcement links are located close to the anchors and thereby also close to the base of the concrete cone breakout prism, yielding of the links determines the tension load capacity of the anchor plate. The same scenario holds for $a = 0.3h_{ef}$.

For an intermediate distance $0.3h_{ef} < a < 0.75h_{ef}$, a local concrete breakout prism emanates from the concrete cone just before the failure load of the anchor plate has been reached. Figure 3-29 shows the damage tension parameter for the case $a = 0.4h_{ef}$ at failure load. The local breakout prism is clearly seen in the figure. Force-displacement curves in Figure 3-25 for the cases $a = 0.4, 0.5$ and $0.625h_{ef}$ show a local drop in force at a displacement of about 2-5 mm. This drop corresponds with initiation of the local breakout prism. The deviating force-displacement curve shape in Figure 3-27 for the case $a = 0.4h_{ef}$, and to some extent for the case $a = 0.5h_{ef}$, also reflects this phenomenon. The shape of the local breakout prism is determined by the location of the shear reinforcement links. For $a \leq 0.3h_{ef}$, the thickness of the concrete cone is too large and the angle too steep for the local breakout prism to develop before the shear reinforcement links yield. For $a > 0.75h_{ef}$, the tension load in the links never reach a level such that a local breakout prism can develop before the edge of the concrete cone breaks. Figure 3-30 confirms this for the case $a = 0.75h_{ef}$ where no local breakout prism is developed at failure load.

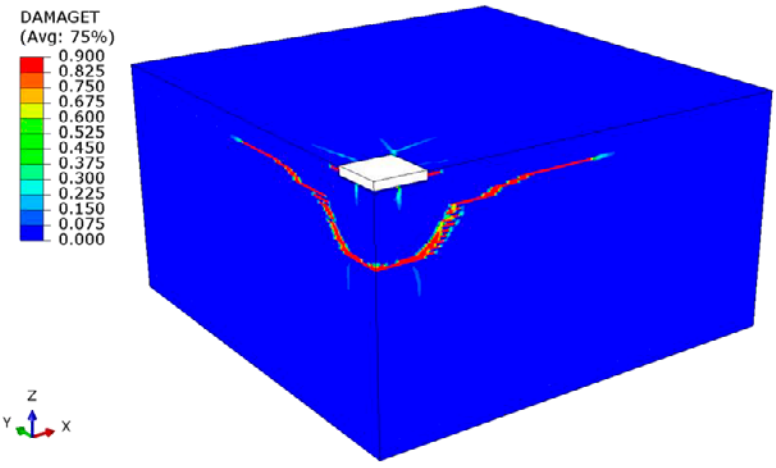

Figure 3-28 Damage tension parameter (DAMAGET) at failure load for an anchor plate with four shear reinforcement links. Distance $\boldsymbol{a = 0.15h_{ef}}$.

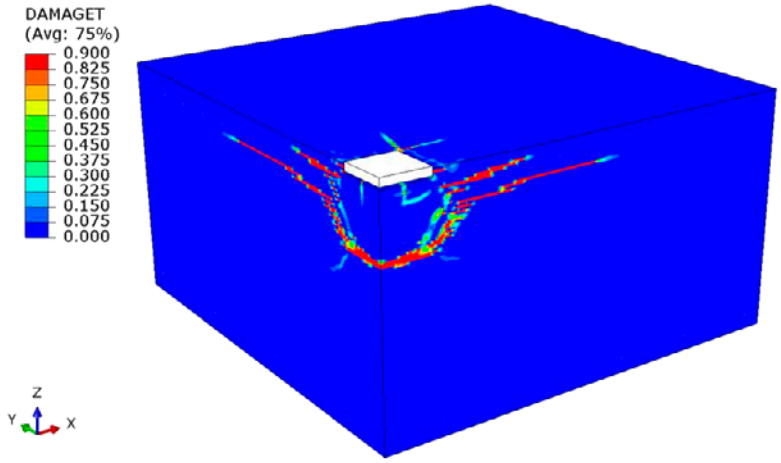

Figure 3-29 Damage tension parameter (DAMAGET) at failure load for an anchor plate with four shear reinforcement links. Distance $\boldsymbol{a = 0.4h_{ef}}$.

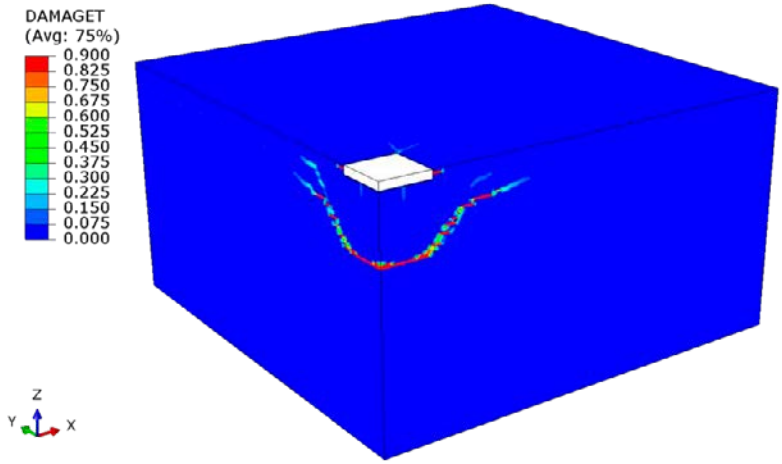

Figure 3-30 Damage tension parameter (DAMAGET) at failure load for an anchor plate with four shear reinforcement links. Distance $\boldsymbol{a = 0.75h_{ef}}$.

3.6.3. Effect of shear reinforcement on tension capacity

Shear reinforcement of the concrete structure contributes to the anchor plate tension capacity. In this simulation, 16 shear reinforcement links are used, see Figure 3-21 and Figure 3-23. The location of the links are given as a function of a (defined in Figure 3-24) as

$$\frac{a}{h_{ef}} = \{0.15, 0.5, 0.85, 1.2\} \qquad \text{(Eq. 3-19)}$$

where the distance between the links is $0.35h_{ef} = 68.3$ mm.

Figure 3-31 shows the force-displacement curve (red) for the anchor plate with 16 shear reinforcement links. Compared to the case with four links and $a = 0.15h_{ef}$ where the failure load was 900 kN (see Figure 3-25), addition of another twelve links increases the failure load to 1300 kN. It is obvious that the added links cannot be utilised up to full yielding before the concrete cone breaks. Deformation of the

concrete cone explains why the tension load applied on the anchor plate cannot be equally transferred to the links. The black curves in Figure 3-31 show total normal force in the respective shear reinforcement link group, i.e. $a/h_{ef} = \{0.15,0.5,0.85,1.2\}$. As expected, the links at $a = 0.15h_{ef}$ contribute most to the tension capacity with about 800 kN. Only these links fully yield. The links at $a = 0.5h_{ef}$ reach a normal force of about 400 kN. Due to bending, these links yield locally at the link curvature. The remaining links stay essentially elastic. The total sum of the normal forces in the shear reinforcement links somewhat exceeds the total reaction force (red curve). Prying effects between the concrete cone and the adjacent concrete structure explain this deviation.

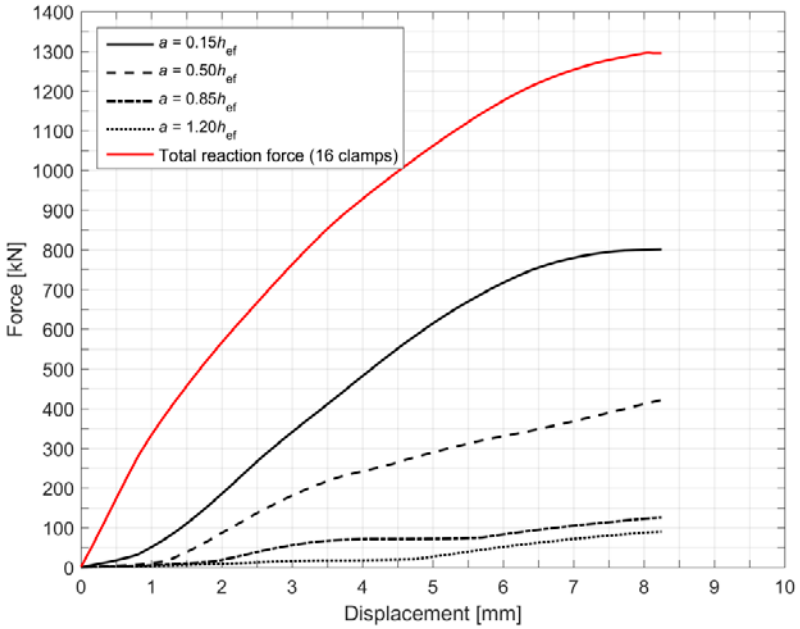

Figure 3-31 Force-displacement curve (red) for an anchor plate loaded in tension with 16 shear reinforcement links as a function of displacement of anchor plate. Black curves show total normal force in the respective shear reinforcement link group, i.e. $\boldsymbol{a/h_{ef} = \{0.15, 0.5, 0.85, 1.2\}}$.

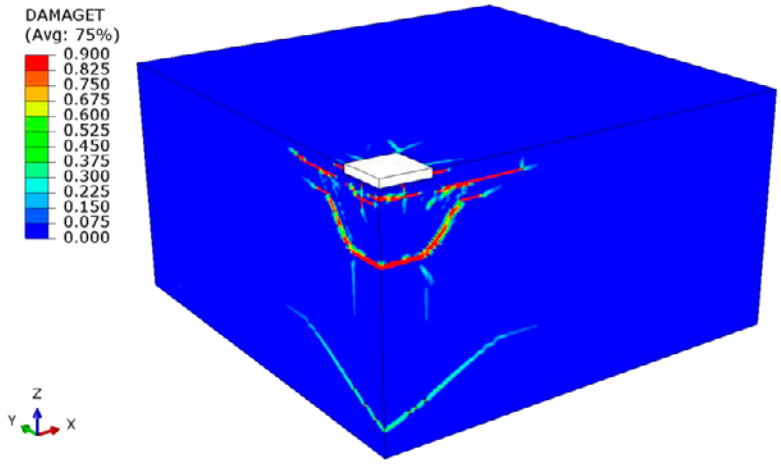

Figure 3-32 Damage tension parameter (DAMAGET) at failure load for an anchor plate with 16 shear reinforcement links.

The damage tension parameter at failure load is shown for the anchor plate in the shear reinforced structure in Figure 3-32. The shape of the concrete breakout cone is influenced by the shear reinforcement. Furthermore is damage developed where the surface reinforcement cross the concrete structure. This happens at a later stage of the simulation. The damage at the bottom of the concrete structure is an artefact of the way the modelling is done. It is developed at the end of the simulation and does not influence the results.

4. Anchor plates loaded in shear

4.1. General

In general design of anchorage to concrete according to codes and regulations such as the European CEN/TS, several failure mode capacities are determined and the governing capacity sets the load carrying limit of the anchor plate. Failure modes in tension and shear are studied separately. The shear failure modes are:

- Steel failure of anchor
- Concrete edge failure
- Concrete pry-out failure

In case of supplementary reinforcement, CEN/TS allows for replacing the concrete edge failure mode with two reinforcement related failure modes [CEN/TS 1992-4-2 2009]. This approach means that the supplementary reinforcement should be designed to resist the total load.

Within chapter 4, the response of headed anchors loaded in shear in non-reinforced and reinforced concrete structures is investigated by means of numerical simulations.

In the previous ANKARM project, concrete edge failure was investigated for anchors in non-reinforced and reinforced concrete [SSM Research Report 2013:27]. A summary is given in section 4.2. The capacity of anchor plates far from concrete edges and loaded in shear may be governed by the concrete pry-out failure mode. Numerical simulations of mentioned failure mode are conducted within the scope of current project and presented in section 4.3.

4.2. Previous ANKARM project

Within the scope of the predecessor to current project, the concrete edge failure mode was numerically simulated with focus on anchors in reinforced concrete structures [SSM Research Report 2013:27]. Table 4-1 shows investigated configurations and corresponding simulated shear failure loads. The embedment depth of the anchors was h_{ef} = 100 mm.

Table 4-1 Investigated configurations regarding studies of the concrete edge failure mode in the ANKARM project [SSM Research Report 2013:27].

Anchor configuration	Reinforcement		$V_{u,simulation}$
	Longitudinal *	Shear	[kN]
Single anchor	-	-	45.0
	ϕ12cc150	-	42.6
	ϕ12cc150	ϕ12cc150	52.6
	ϕ12cc150	ϕ12cc100	66.3
Group of two anchors	-	-	52.4
	ϕ12cc150	-	52.4
	ϕ12cc150	ϕ12cc150	79.4
	ϕ12cc150	ϕ12cc100	87.9

* Bending surface reinforcement arranged parallel to the concrete edge

In summary, the simulations showed good agreement with results from physical tests and that reinforcement in the direction of the applied load led to a distinct increase of the concrete edge failure load. The normal stress in the reinforcement bars close to the anchors was considerably higher than in the rest of the bars that tied the breakout body to the concrete member. The shear reinforcement close to the anchors was able to transfer the load from the anchor into the concrete structure and thereby increase the simulated failure load substantially. Longitudinal reinforcement arranged parallel to the concrete edge did not increase the simulated failure load. However, the numerical simulations showed that longitudinal reinforcement made the failure more ductile.

4.3. Centrically loaded far from concrete edges

4.3.1. General

Within section 4.3, anchor plates far from concrete edges are studied by means of numerical simulations. The geometry setup thus eliminates the concrete edge failure mode.

Three different anchor plate configurations are investigated, including headed stud anchors with embedment depths h_{ef} = 50 mm and h_{ef} = 100 mm. The study comprises both single anchors and a group of four anchors in non-reinforced and reinforced concrete. For comparison with a design code, the concrete pry-out failure load is predicted for non-cracked concrete based on [CEN/TS 1992-4-2 2009]. The main objective is to study the effect of surface reinforcement on the concrete pry-out capacity.

The pry-out mechanism is schematically shown in Figure 4-1. The shear force V gives rise to crushing of the concrete which leads to a lowering of the centroid of resistance V_b. The eccentricity between V and V_b is balanced by a pressure force C between the steel plate and the concrete surface as well as a tensile force N in the anchor stud. If the tensile anchor force exceeds corresponding force associated with the maximum concrete fracture surface, a crater of concrete behind the anchor will break out.

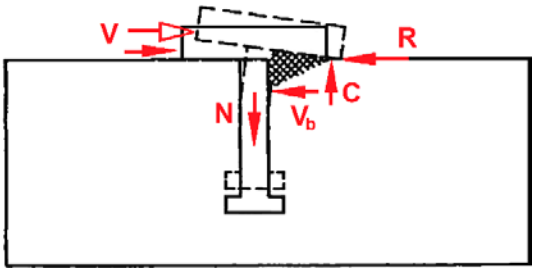

Figure 4-1 Concrete pry-out failure mode [Eligehausen et al. 1992]

4.3.2. Concrete pry-out resistance according to CEN/TS

According to CEN/TS 1992-4-2, section 6.3.4 [CEN/TS 1992-4-2 2009], the characteristic concrete pry-out resistance $V_{Rk,cp}$ given in [N] is calculated as:

$$V_{Rk,cp} = k_3 \cdot N_{Rk,c} \quad \text{(Eq. 4-1)}$$

where

$k_3 = k_{cp} = 1$	for $h_{ef} < 63.5\ mm$	[ACI 349-13]
$k_3 = k_{cp} = 2$	for $h_{ef} \geq 63.5\ mm$	[ACI 349-13]
$N_{Rk,c}$	Characteristic concrete cone failure resistance	

The factor k_3 shall according to CEN/TS be taken from the relevant European Technical Specification, valid for applications without supplementary reinforcement. In case of supplementary reinforcement, k_3 shall be multiplied with 0.75 [CEN/TS 1992-4-2 2009]. According to ACI 349-13, section D.6 [ACI 349-13], corresponding factor denominated as k_{cp} is either 1.0 or 2.0 depending on the anchor embedment depth. Further on, the characteristic concrete cone failure resistance is calculated as:

$$N_{Rk,c} = N^0_{Rk,c} \cdot \frac{A_{c,N}}{A^0_{c,N}} \cdot \psi_{s,N} \cdot \psi_{re,N} \cdot \psi_{ec,N} \quad \text{(Eq. 4-2)}$$

where

$$N^0_{Rk,c} = 11.9 \cdot \sqrt{f_{ck,cube}} \cdot h_{ef}^{1.5} \quad \text{(Eq. 4-3)}$$

$A_{c,N}$	Projected concrete cone area
$A^0_{c,N}$	Reference projected concrete cone area
$\psi_{s,N}$	Effect of the disturbance of the distribution of stresses in the concrete due to edges
$\psi_{re,N}$	Effect of shell spalling
$\psi_{ec,N}$	Effect of the eccentricity of the load

Since the current study presented in section 4.3 is on anchor plates far from concrete edges and loaded centrically, the concrete cone failure resistance reduction factors $\psi_{s,N}$ and $\psi_{ec,N}$ are assigned the value 1.0. However, according to CEN/TS the effect of shell spalling needs to be considered for anchors with embedment depths h_{ef} < 100 mm. The reduction is calculated as:

$$\psi_{re,N} = 0.5 + \frac{h_{ef}}{200} \leq 1 \quad \text{(Eq. 4-4)}$$

Irrespective of the embedment of the anchor, $\psi_{re,N}$ may be taken as 1.0 if:

- Reinforcement is provided at a spacing ≥ 150 mm, or
- Reinforcement with a diameter of 10 mm or less is provided at a spacing ≥ 100 mm

4.3.3. Analysed configurations

The following three geometry constellations are studied:

- Single anchor with embedment depth h_{ef} = 50 mm
- Single anchor with embedment depth h_{ef} = 100 mm
- Group of four anchors with embedment depth h_{ef} = 100 mm

Following amount of surface reinforcement in two orthogonal directions are studied:

- No reinforcement
- ϕ12cc300
- ϕ12cc200
- ϕ12cc150
- ϕ12cc100
- ϕ16cc300
- ϕ16cc200
- ϕ16cc150
- ϕ16cc100

Irrespective of reinforcement dimension, the concrete cover is set to 30 mm. The geometry of the anchor and steel plate is presented in Figure 4-2 and the concrete specimen geometry is presented in Figure 4-3. The plate is not embedded in the concrete.

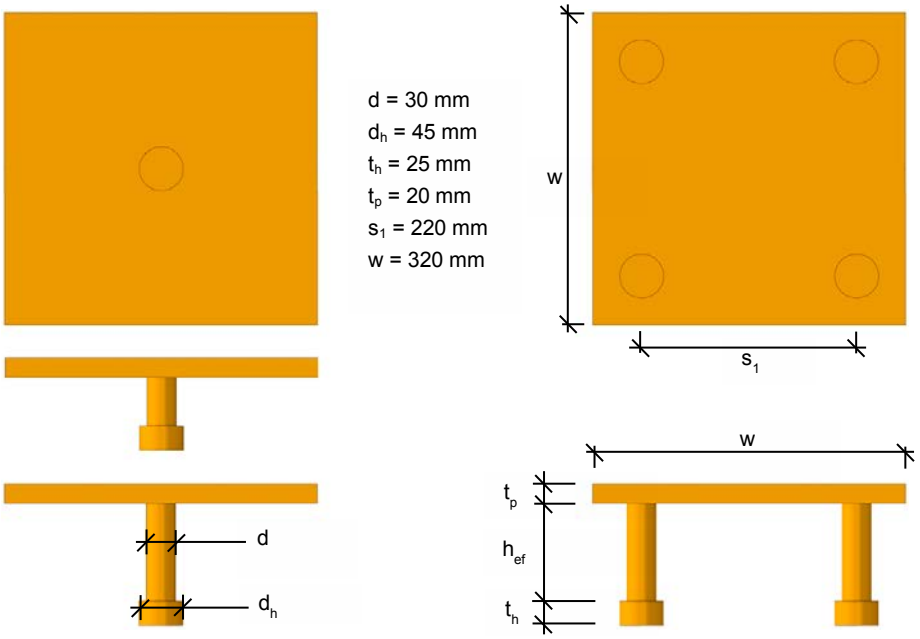

Figure 4-2 Dimensions of anchors and non-embedded steel plate that are studied.

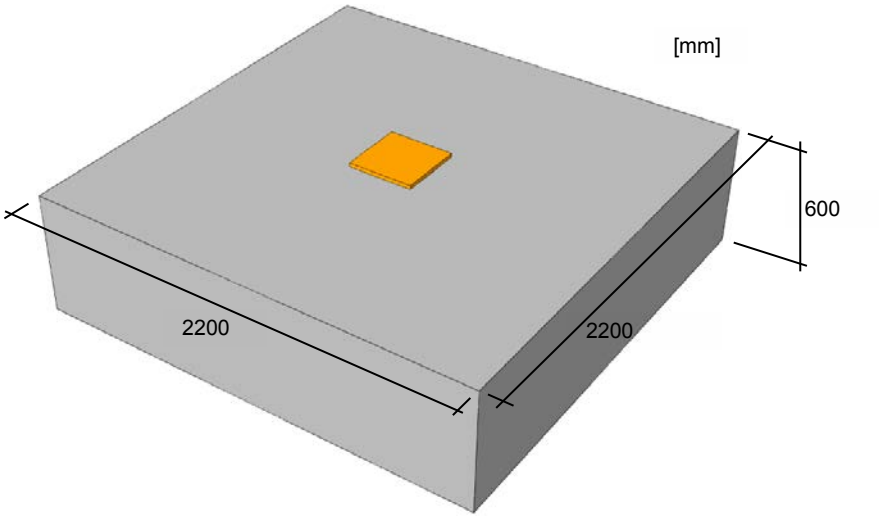

Figure 4-3 Dimensions of the concrete specimen that is studied.

4.3.4. Finite element model

Due to symmetry, only half of the structural geometry is modelled. The finite element mesh of a model with a group of four anchors is presented in Figure 4-4 and a detailed presentation in the vicinity of the anchors is shown in Figure 4-5. Corresponding size of the FE-model is presented in Table 4-2.

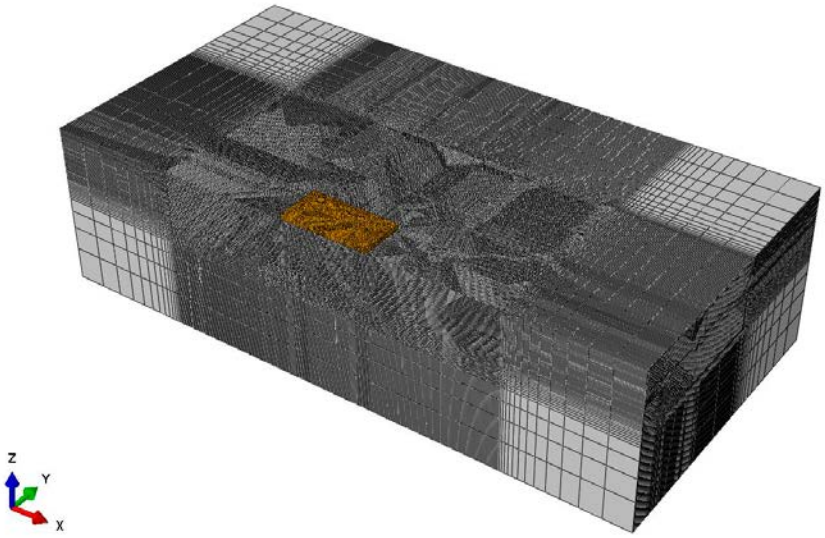

Figure 4-4 Finite element mesh of model constituting a group of four anchors. The element side length in the concrete dense meshed region around the anchors is 5 mm.

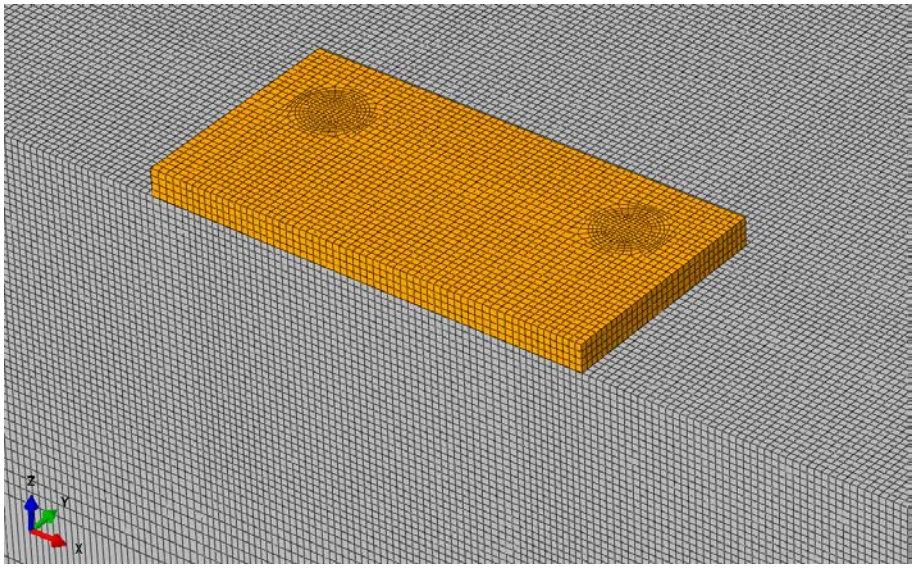

Figure 4-5 Zoomed view of finite element mesh around the anchors. The element side length in the concrete dense meshed region is 5 mm.

Table 4-2 Size of FEA-model constituting a group of four anchors and ϕ12cc100 reinforcement.

Number of nodes	Number of elements	Number of degrees of freedom
~2 224 300	~2 129 000	~6 631 200

Boundary conditions

The nodes on the bottom surface of the concrete member are constrained in all directions, see Figure 4-6. The nodes on the symmetry plane are prevented to translate in the Y-direction, see Figure 4-7.

Apart from the above stated boundary conditions, the models constitute non-linear boundary conditions, i.e. contact definitions. A contact formulation is defined between the anchors and the concrete as well as between the steel plate and the concrete. The contact prevents the different regions to pass each other's exterior surfaces by instead transmitting pressure forces. Further on, the contact formulation allows separation without any tensional stresses and includes friction.

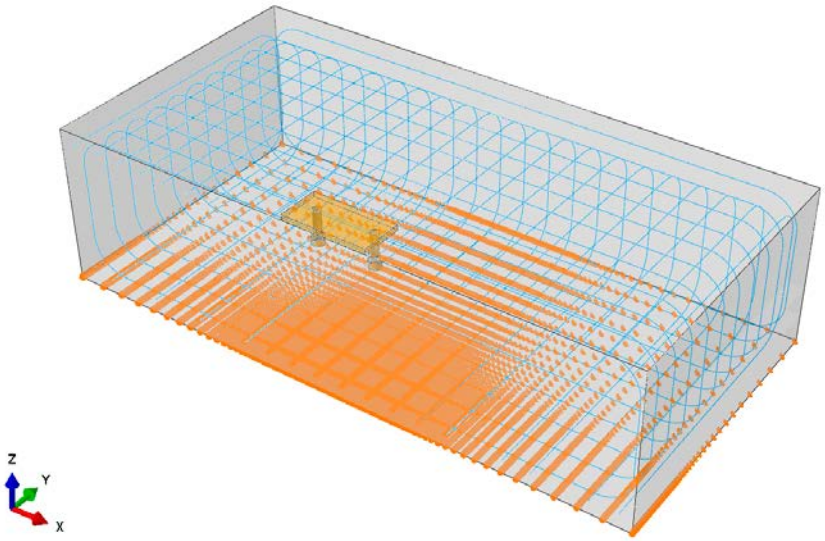

Figure 4-6 Transparent view of model with a group of four anchors in ϕ12cc100 reinforced concrete member. The highlighted nodes on the concrete bottom surface are constrained in all directions.

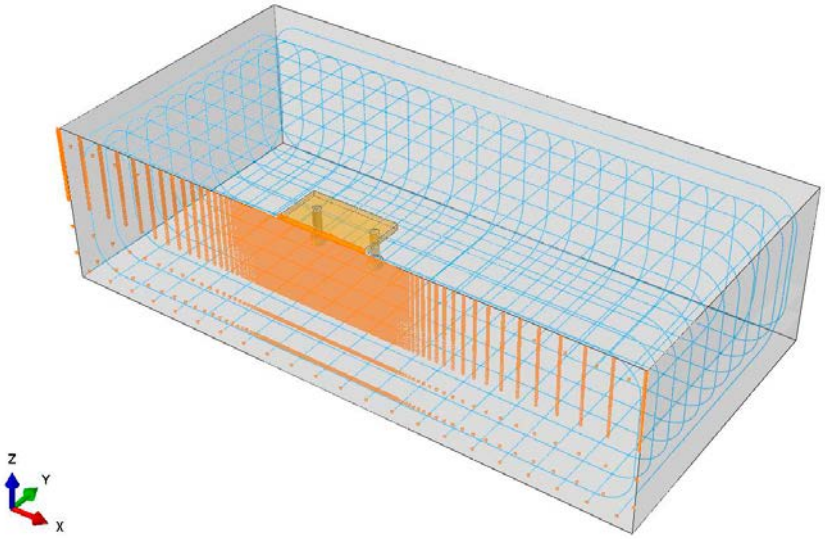

Figure 4-7 Transparent view of model with a group of four anchors in ϕ12cc100 reinforced concrete member. The highlighted nodes on the symmetry plane are restrained to translate in the Y-direction.

Convergence study

Convergence is studied with respect to element mesh size and coefficient of friction. This is mainly done for the model with a single anchor that is embedded 100 mm into a non-reinforced concrete member.

The differently meshed models have element side lengths in the vicinity of the anchor that are 10 mm, 5 mm and 2.5 mm, respectively. The element meshes of these three models are shown in Figure 4-8. Simulated force-displacement curves of the finite element mesh size convergence analyses are presented in Figure 4-9. Displacement in x-direction and shear force are given on x- and y-axis, respectively.

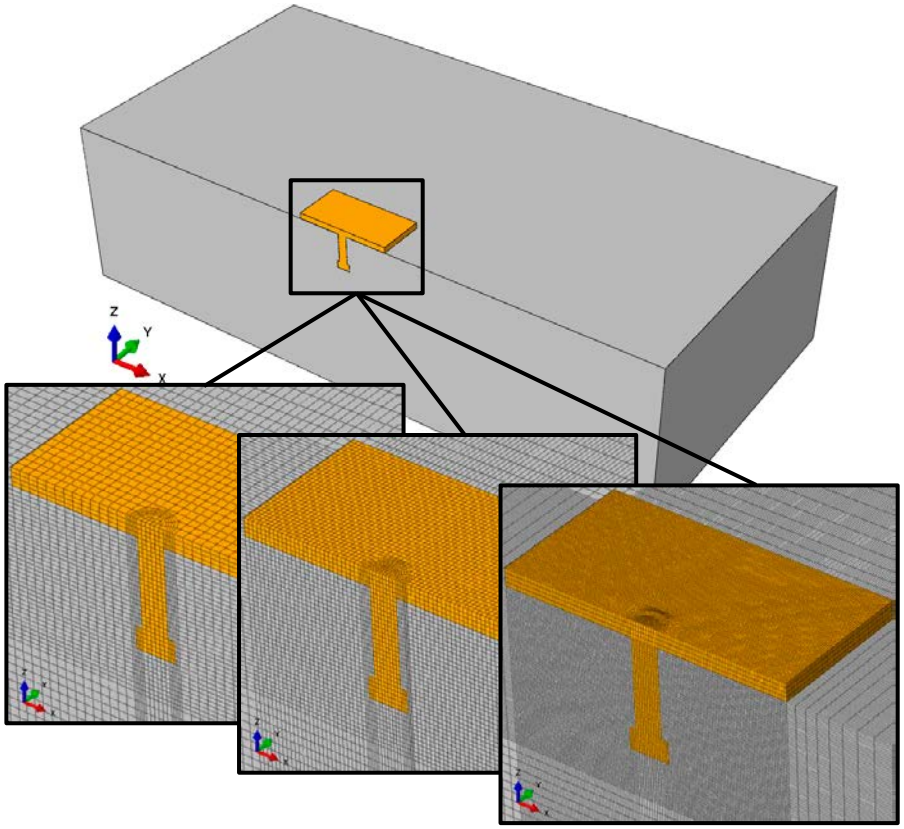

Figure 4-8 Element side lengths from left to right: 10 mm, 5 mm, 2.5 mm

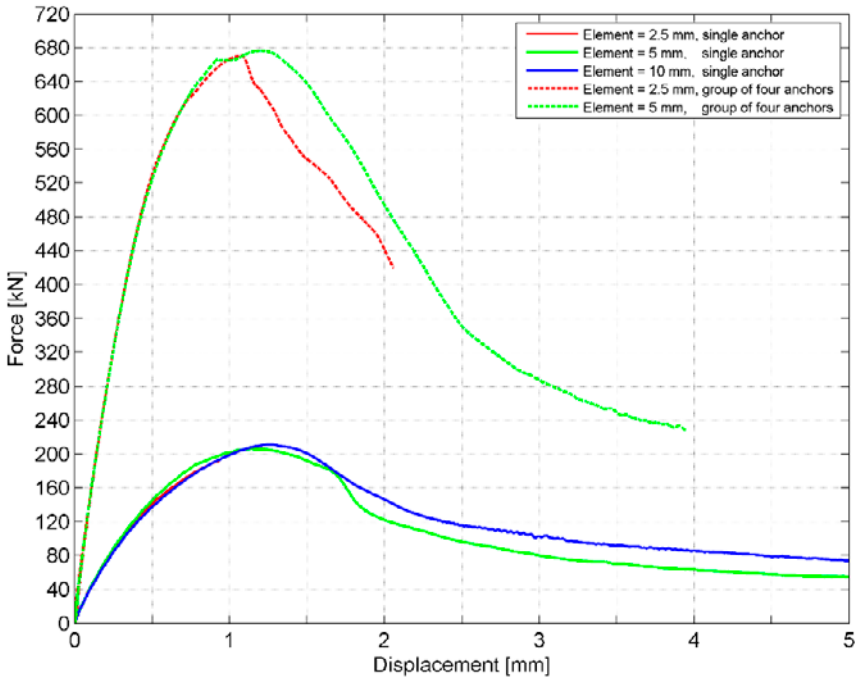

Figure 4-9 Relation between force and displacement for anchor(s) with embedment depth h_{ef} = 100 mm in non-reinforced concrete for three different element meshes. Results from analyses with coefficient of friction μ = 0.4.

Analyses of the non-reinforced models having an element side length of 5 mm can be driven further than the other model meshes, see Figure 4-9. Model with element size 2.5 mm shows negligible difference in failure load and fracture surface development compared to the model with element size 5 mm. Using models with concrete element side length 5 mm around the anchors is therefore regarded to be sufficient for the current study.

Since the analyses include friction contact, its impact on the simulation results is investigated for several values on the coefficient of friction. Relations between force and displacement are presented in Figure 4-10. The structural response is shown stiffer with increasing coefficient of friction. According to [Boverket 2004], the coefficient of friction between concrete and steel may vary in the range $0.2 \leq \mu \leq 0.6$. A value of $\mu = 0.4$ is considered appropriate for the task at hand and is used in the simulations if not otherwise stated.

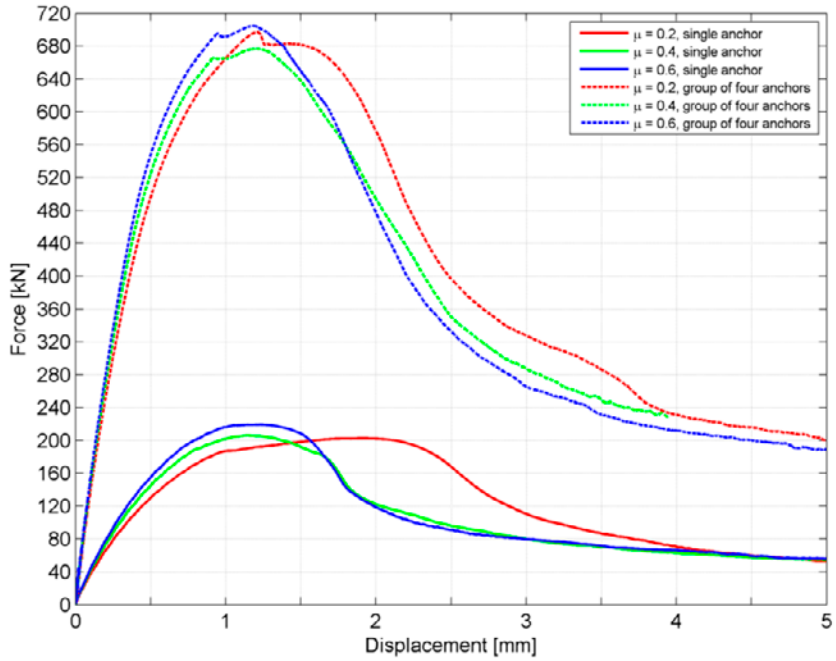

Figure 4-10 Relation between force and displacement for anchors with embedment depth h_{ef} = 100 mm in non-reinforced concrete for different coefficients of friction.

4.3.5. Finite element analysis

The analyses are conducted by displacing the steel plate in the x-direction. This is done at the level of the steel plate upper surface where the steel beam attaches the steel plate. The displacement output information is registered throughout the analyses in the centre of the attachment region.

4.3.6. Results for non-reinforced concrete

For comparison with a design code, the concrete pry-out failure load is predicted for non-cracked concrete based on [CEN/TS 1992-4-2 2009]. The concrete pry-out failure resistance is highly dependent on corresponding concrete cone failure resistance, see section 4.3.2. The characteristic concrete cone failure resistance

according to CEN/TS for a single anchor $N^0_{Rk,c}$ corresponds to the 5 % fractile of the physical failure load. Hence, the value is multiplied with 1.33 to get the mean value before it is compared with simulated failure loads. Furthermore, the characteristic compressive cube strength $f_{ck,cube}$ is replaced by the mean compressive cube strength $f_{cm,cube}$ for the comparison. The concrete cylindrical compressive strength utilized in the analyses is $\sigma_{cu} = f_{cm,cyl} = 25.0$ MPa, see Table 2-2. This is converted according to [Betonghandbok – Material 2008]:

$$f_{cm,cube} = \frac{f_{cm,cyl}}{0.76} = \frac{25.0}{0.76} = 32.89\ MPa$$

The predicted concrete cone failure load based on CEN/TS is designated $N_{u,CEN/TS}$ and corresponding predicted concrete pry-out failure load is designated $V_{u,CEN/TS}$.

With reference to section 4.3.2 and the above stated modifications of the failure mode resistances according to CEN/TS, $N_{u,CEN/TS}$ and $V_{u,CEN/TS}$ for the studied configurations according to section 4.3.3 are determined.

Single anchor with embedment depth h_{ef} = 50 mm

$N_{u,CEN/TS} = 11.9 \cdot \sqrt{32.89} \cdot 50^{1.5} \cdot 1.33 = 32.1\ kN$
$V_{u,CEN/TS} = k_3 \cdot N_{u,CEN/TS} = 1 \cdot 32.1 = 32.1\ kN$

When effect of shell spalling needs to be considered, i.e. when relatively dense reinforcement is provided around the anchor (see section 4.3.2), the predicted concrete cone failure load and consequently the predicted pry-out failure load is multiplied with a factor:

$\psi_{re,N} = 0.5 + \frac{h_{ef}}{200} = 0.5 + \frac{50}{200} = 0.75$
$V_{u,CEN/TS} = 32.1 \cdot 0.75 = 24.1\ kN$

Single anchor with embedment depth h_{ef} = 100 mm

$N_{u,CEN/TS} = 11.9 \cdot \sqrt{32.89} \cdot 100^{1.5} \cdot 1.33 = 90.8\ kN$
$V_{u,CEN/TS} = k_3 \cdot N_{u,CEN/TS} = 2 \cdot 90.8 = 181.5\ kN$

Group of four anchors with embedment depth h_{ef} = 100 mm

The difference between $N_{u,CEN/TS}$ for the group of anchors compared to the single anchor is taken into account by the factor $A_{c,N}/A^0_{c,N}$. The factor represents the relation between a theoretical projected fracture surface area for the anchor group and corresponding area for a single anchor without disturbance of nearby anchors or concrete edges.

$A^0_{c,N} = s_{cr,N} \cdot s_{cr,N} = \left(3 \cdot h_{ef}\right)^2 = (3 \cdot 100)^2 = 90\ 000\ mm^2$
$A_{c,N} = \left(0.5 \cdot s_{cr,N} + s_1 + 0.5 \cdot s_{cr,N}\right)^2$ since $s_1 \leq s_{cr,N}$ (see Figure 4-2)
$\rightarrow A_{c,N} = \left(3 \cdot h_{ef} + s_1\right)^2 = (3 \cdot 100 + 220)^2 = 270\ 400\ mm^2$
$V_{u,CEN/TS} = 181.5 \cdot \frac{270\ 400}{90\ 000} = 545.5\ kN$

In Table 4-3 and Figure 4-11, results from numerical simulations and predicted concrete pry-out failure loads based on CEN/TS are compared. For all studied configurations, the numerical simulations predict higher failure loads than CEN/TS does. For single anchors with embedment depth h_{ef} = 50 mm, the deviation in failure load is remarkably high. An explanation for this is that the factor k_3 for anchors with

short embedment depths equals one (k_3 = 1.0), but suddenly becomes twice as big for a certain length of embedment. This certain length is not specified in CEN/TS but is h_{ef} = 63.5 mm (2.5 inches) according to [ACI 349-13].

Table 4-3 Comparison of failure loads from numerical simulations and predictions based on [CEN/TS 1992-4-2 2009].

Anchor configuration	$V_{u,simulation}$ [kN]	$V_{u,CEN/TS}$ [kN]	$\frac{V_{u,simulation}}{V_{u,CEN/TS}}$
Single anchor, h_{ef} = 50 mm	106.7	32.1	3.32
Single anchor, h_{ef} = 100 mm	206.3	181.5	1.14
Group of four anchors, h_{ef} = 100 mm	676.8	545.5	1.24

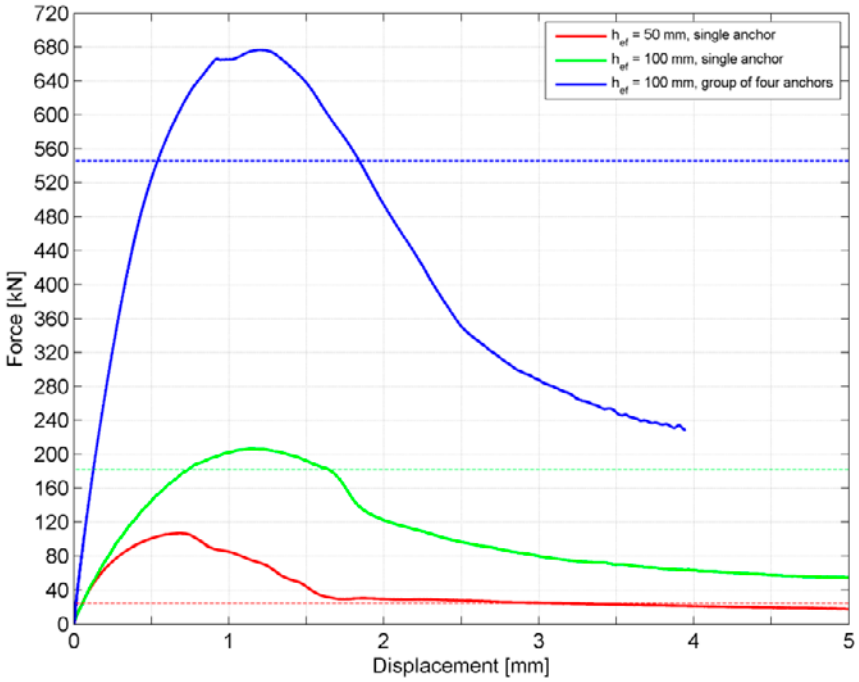

Figure 4-11 Relation between force and displacement for different anchor constellations in non-reinforced concrete. The dashed lines show corresponding predicted concrete pry-out failure load based on CEN/TS, i.e. $V_{u,CEN/TS}$.

An increase of the embedment depth increases the concrete pry-out failure load. As does the number of anchors. The different fracture surfaces are presented as contour plots of the damage tension parameter at failure load in Figure 4-12 to Figure 4-14. The figures clearly show a developed concrete pry-out failure cone.

Additional figures of concrete fracture surfaces are presented in appendix 2.

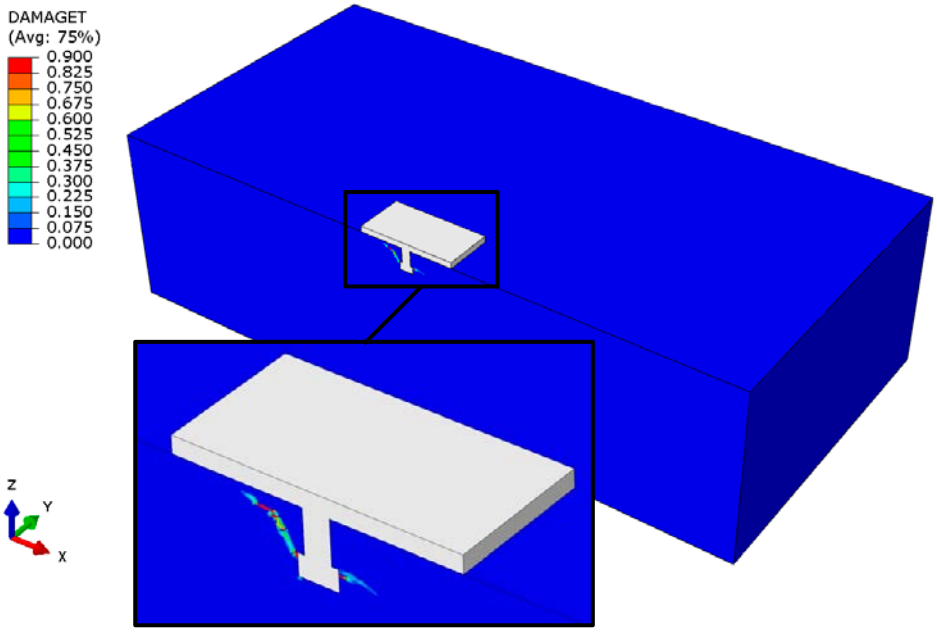

Figure 4-12 Damage tension parameter (DAMAGET) at failure load (106.7 kN) for model with a single anchor with embedment depth h_{ef} = 50 mm. The X-Z plane is a symmetry plane.

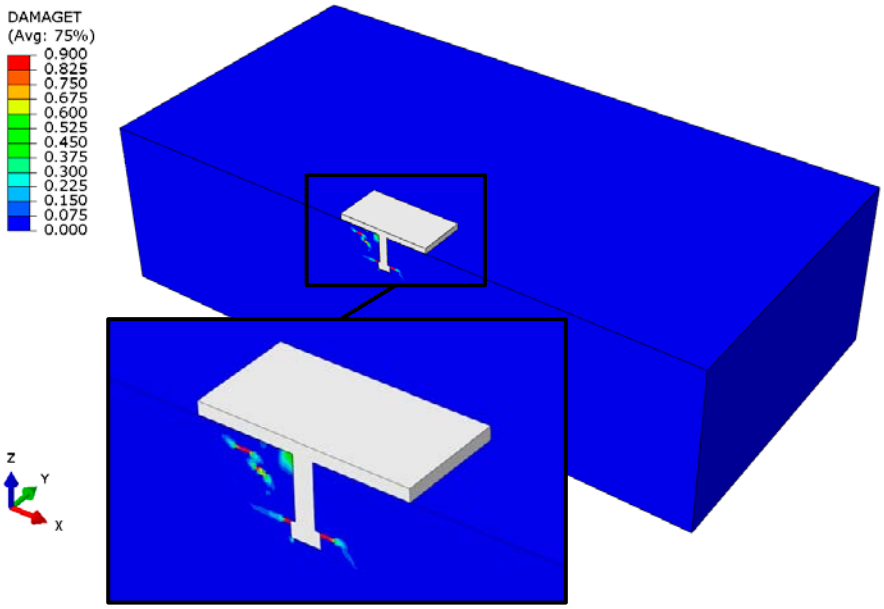

Figure 4-13 Damage tension parameter (DAMAGET) at failure load (206.3 kN) for model with a single anchor with embedment depth h_{ef} = 100 mm. The X-Z plane is a symmetry plane.

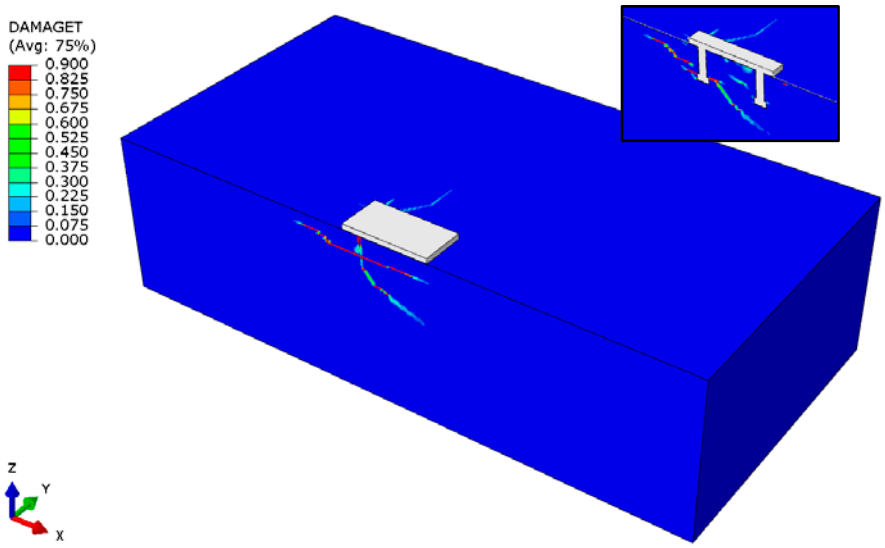

Figure 4-14 Damage tension parameter (DAMAGET) at failure load (676.8 kN) for model with a group of four anchors. The X-Z plane is a symmetry plane. The recessed figure to the right show corresponding result in the section across the anchors, i.e. at a distance $s_1/2$ = 110 mm from the symmetry plane.

4.3.7. Results for reinforced concrete

In general, the numerical simulations show that the amount of surface reinforcement has little or no impact on the concrete pry-out failure load. For the analysis model of a single anchor with embedment depth h_{ef} = 50 mm, the difference in results is negligible as seen in Figure 4-15. The reason is that the rebars barely cross the concrete fracture surface as seen in Figure 4-16. Consequently, there is no reinforcement tying the concrete breakout body to the concrete member.

Corresponding force-displacement curves for the single anchor with embedment depth h_{ef} = 100 mm are shown in Figure 4-17, and for a group of four anchors in Figure 4-18 and Figure 4-19. These numerical simulations show that the surface reinforcement have greatest impact on the single anchor stud, for which the failure load increases with 5 % to 15 % depending on rebar diameter. As the surface reinforcement spacing increases from 100 mm to 200 mm, the reinforcement does not have any significant effect on either failure load or post failure behaviour. For the group of four anchors, Figure 4-18 and Figure 4-19 show that reinforcement in general makes the failure more ductile.

For anchors loaded in tension, the plane of the surface reinforcement is oriented perpendicular to the tension load. The tension load is therefore not easily transferred to the reinforcement bars, see section 3.4.7. Even though the shear load is acting parallel to the reinforcement, the surface reinforcement is in the numerical simulations shown only to have little impact also on the concrete pry-out failure load. The main reason for this is that the shear load give rise to a pressure force between the steel plate and the concrete which is balanced by a tensile force in the anchor. The concrete pry-out failure mode is hence much alike the concrete cone failure mode. This is also reflected by the concrete cone- and concrete pry-out failure mode resistance expressions in CEN/TS.

Additional figures of concrete fracture surfaces are presented in appendix 2.

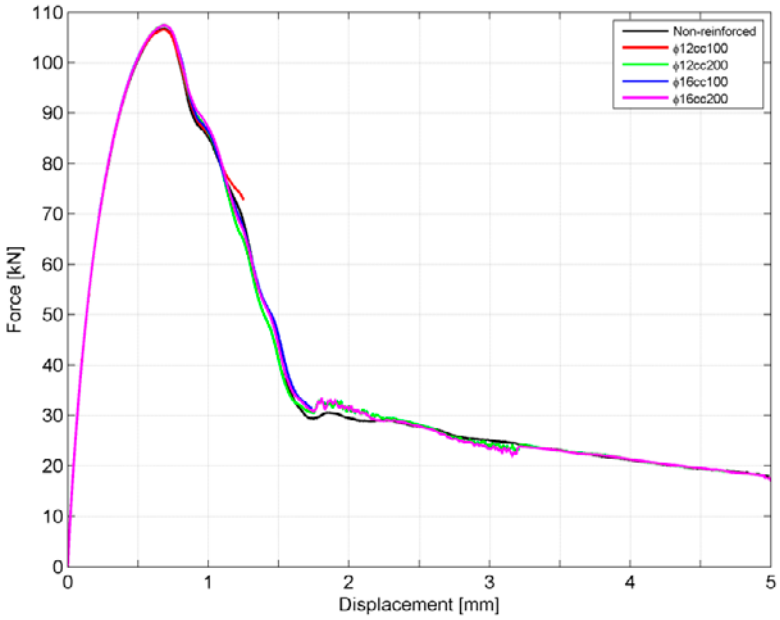

Figure 4-15 Relation between force and displacement for a single anchor with embedment depth h_{ef} = 50 mm for different reinforcement setups. Results for model with element side length = 2.5 mm.

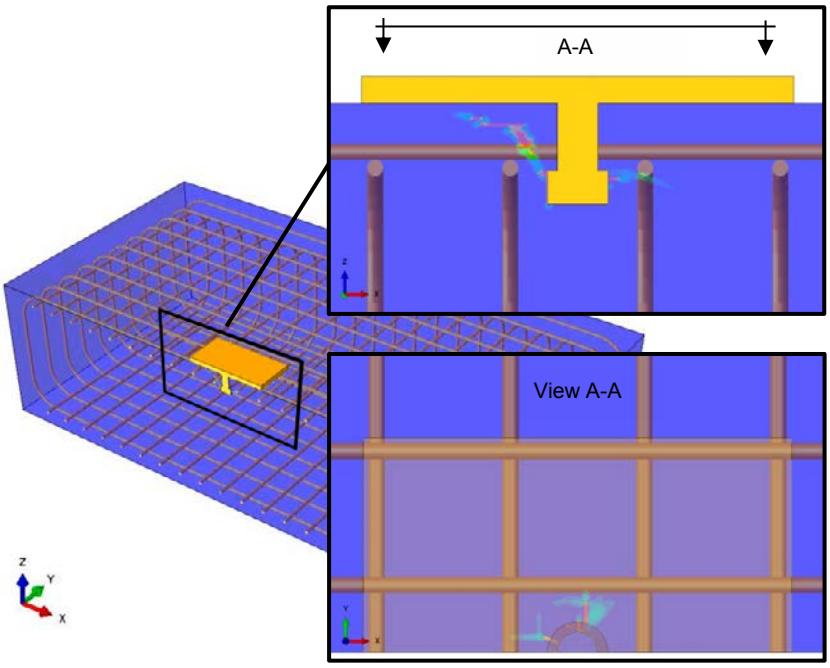

Figure 4-16 Transparent view of concrete fracture surface contour plot showing the reinforcement position in relation to the breakout cone. The X-Z plane is a symmetry plane. Model with h_{ef} = 50 mm and ϕ12cc100.

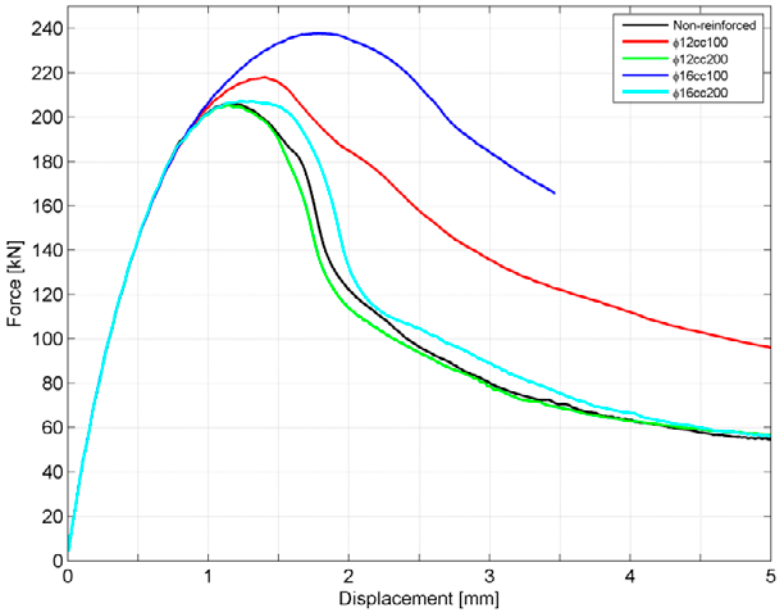

Figure 4-17 Relation between force and displacement for a single anchor with embedment depth h_{ef} = 100 mm for different reinforcement setups.

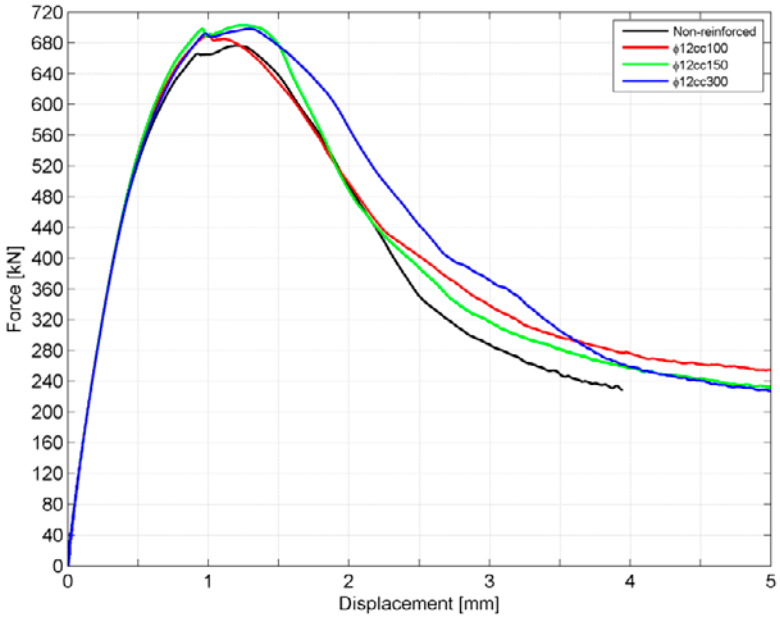

Figure 4-18 Relation between force and displacement for a group of four anchors with embedment depth h_{ef} = 100 mm for different reinforcement setups with ϕ12 mm.

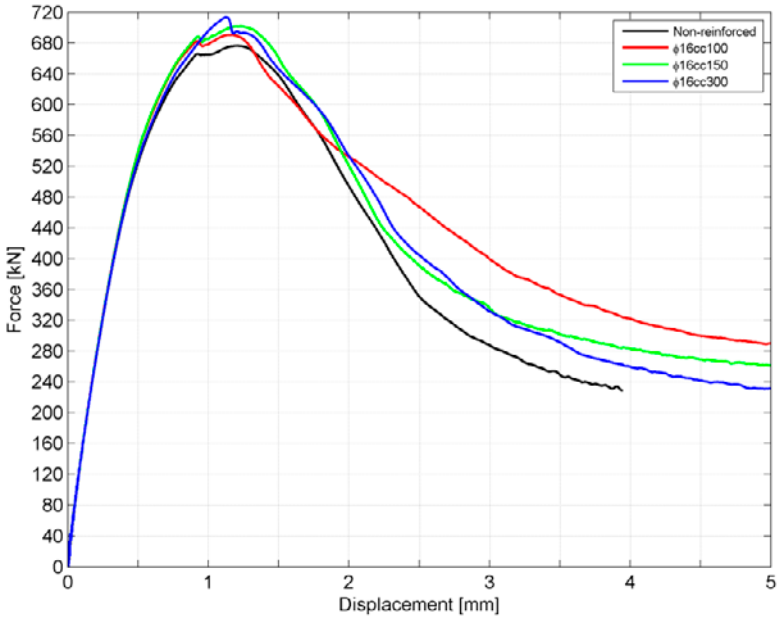

Figure 4-19 Relation between force and displacement for a group of four anchors with embedment depth h_{ef} = 100 mm for different reinforcement setups with ϕ16 mm.

5. Anchor plates loaded in tension and shear

5.1. General

The methodology in CEN/TS, when designing anchorage in concrete, is to show that the design effect of actions does not exceed the design value of resistance. Design values are determined by means of partial factors. The design methodology applies for all failure modes, but tension and shear failure modes are treated separately. The governing failure mode will limit the final capacity in tension (N_{Rd}) and shear (V_{Rd}), respectively. For anchors loaded in both tension and shear simultaneously, corresponding interaction verification needs to be conducted.

Within chapter 5, one anchor plate configuration is studied by means of numerical simulations, comprising four headed anchor studs with embedment depth h_{ef} = 100 mm. The anchor plate is positioned far from concrete edges. The geometry setup thus eliminates the concrete blow-out failure mode and the concrete edge failure mode. The study includes anchor plates centrically and eccentrically loaded in tension and simultaneously loaded in shear in non-reinforced and reinforced concrete. The simulated concrete failures are compared with corresponding interaction of combined tension and shear loads according to [CEN/TS 1992-4-2 2009]. The main objective is to study the effect of surface reinforcement and the relation between tension and shear load on the concrete failure capacity.

5.2. Centrically loaded far from concrete edges

5.2.1. General

The studies conducted and reported within section 5.2 comprises numerical simulations where the combination of tension and shear load is applied centrically on the steel plate, i.e. without eccentricities giving rise to bending moments.

5.2.2. Combined tension and shear load according to CEN/TS

According to section 6.4.1 in [CEN/TS 1992-4-2:2009], the combined tension and shear action shall be verified differently depending on whether the governing tension failure mode and shear failure mode is ductile.

Required verification when steel failure is decisive for both tension and shear load:

$$\beta_N^2 + \beta_V^2 \leq 1 \qquad \text{(Eq. 5-1)}$$

where
$\beta_N = N_{Ed}/N_{Rd} \leq 1$
$\beta_V = V_{Ed}/V_{Rd} \leq 1$

When other modes of failure are decisive, either of following equations shall be satisfied:

$$\beta_N + \beta_V \leq 1.2 \qquad \text{(Eq. 5-2)}$$

$$\beta_N^{1.5} + \beta_V^{1.5} \leq 1 \qquad \text{(Eq. 5-3)}$$

where
$\beta_N = N_{Ed}/N_{Rd} \leq 1$
$\beta_V = V_{Ed}/V_{Rd} \leq 1$

An interaction diagram for combined tension and shear loads, i.e. a diagram of equations 5-1, 5-2 and 5-3 is presented in Figure 5-1.

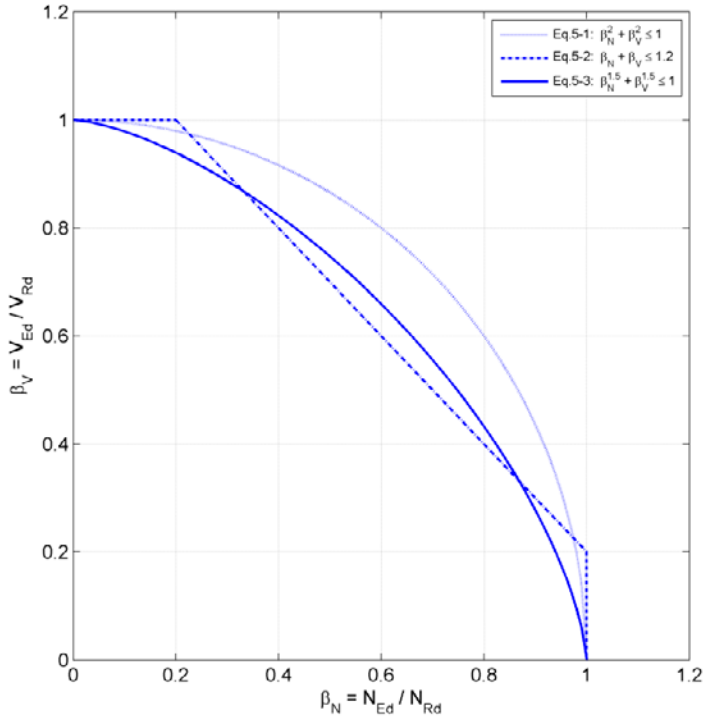

Figure 5-1 Interaction diagram for combined tension and shear loads according to [CEN/TS 1992-4-2:2009].

5.2.3. Analysed configurations

A group of four anchors with embedment depth h_{ef} = 100 mm is studied. The geometry of the anchors and steel plate is presented to the right in Figure 4-2 and the concrete specimen is presented in Figure 4-3. Investigated amount of surface reinforcement (in both orthogonal directions) is

- No reinforcement
- ϕ16cc300
- ϕ16cc150
- ϕ16cc100

5.2.4. Finite element model and analysis

The studied model is loaded in tension, shear and simultaneous tension and shear in separate numerical simulations by means of displacement controlled analyses. This is done in order to see the effect of different loading scenarios on the same finite element model. The load ratio relation between tension and shear is also investigated, i.e. alteration of the applied displacement rates in the vertical and transverse directions. The finite element model is described in section 4.3.4. All presented displacement results are registered at the steel plate centre point throughout the analyses.

5.2.5. Results for non-reinforced concrete

For the non-reinforced concrete specimen, different relations between tension and shear are investigated. Since the simulations are driven as displacement controlled analyses, the presented tension and shear forces are reactions to the applied vertical and transverse displacements. Figure 5-2 shows the convention of displacement directions.

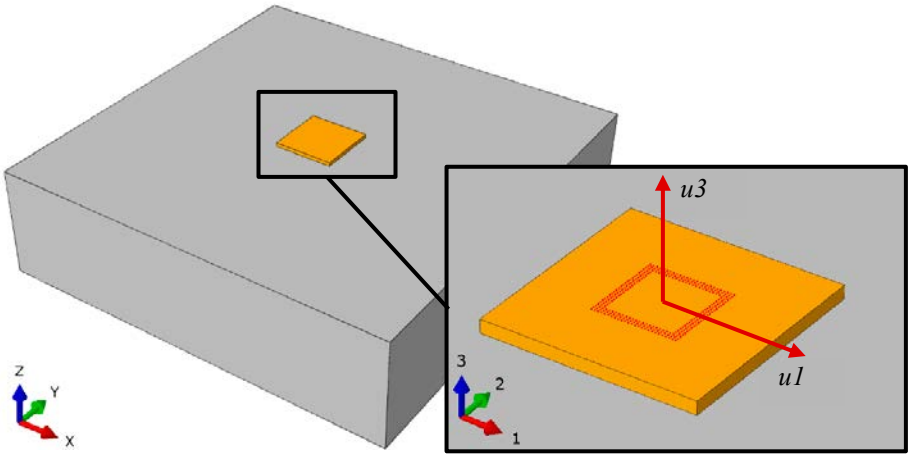

Figure 5-2 Transverse displacement (*u1)* giving rise to shear reaction and vertical displacement (*u3)* giving rise to tensile reaction.

As the structural response depends on both the vertical and the transverse displacement rate, different mutual displacement rates are investigated. Relations between force and corresponding displacement in the centre of the steel plate are shown in Figure 5-3. Due to the different rates, the results are also presented in the time domain, i.e. corresponding relation between force and time is presented in Figure 5-4. The simulated failure loads are compiled in Table 5-1.

Table 5-1 Numerically simulated failure loads.

Simulated loading scenario	$N_{u,simulation}$ [kN]	$V_{u,simulation}$ [kN]
Only loaded in tension, $\dot{u}3$=50 mm/s	294.9	-
Only loaded in shear, $\dot{u}1$=25 mm/s	-	666.9
$\dot{u}1$=25 mm/s and $\dot{u}3$=75 mm/s	193.2	312.9
$\dot{u}1$=25 mm/s and $\dot{u}3$=50 mm/s	156.5	400.5
$\dot{u}1$=25 mm/s and $\dot{u}3$=25 mm/s	100.5	563.3
$\dot{u}1$=25 mm/s and $\dot{u}3$=12.5 mm/s	37.7	680.1

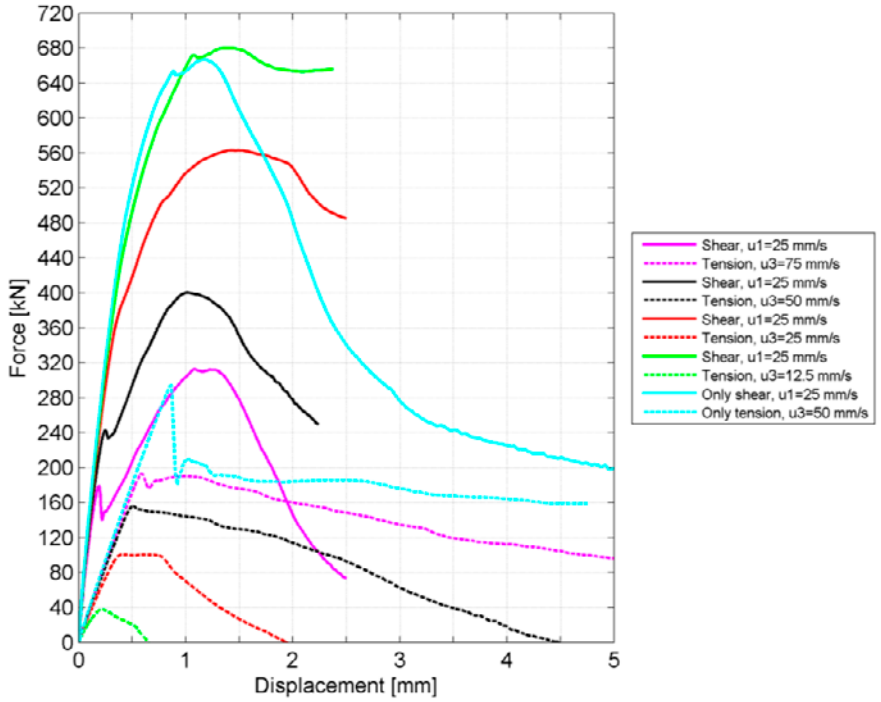

Figure 5-3 Relation between force and displacement for different loading rates. Solid lines show shear force and dashed lines show corresponding tension force. The two cyan coloured curves are results from analyses where the steel plate only gets loaded in shear or tension.

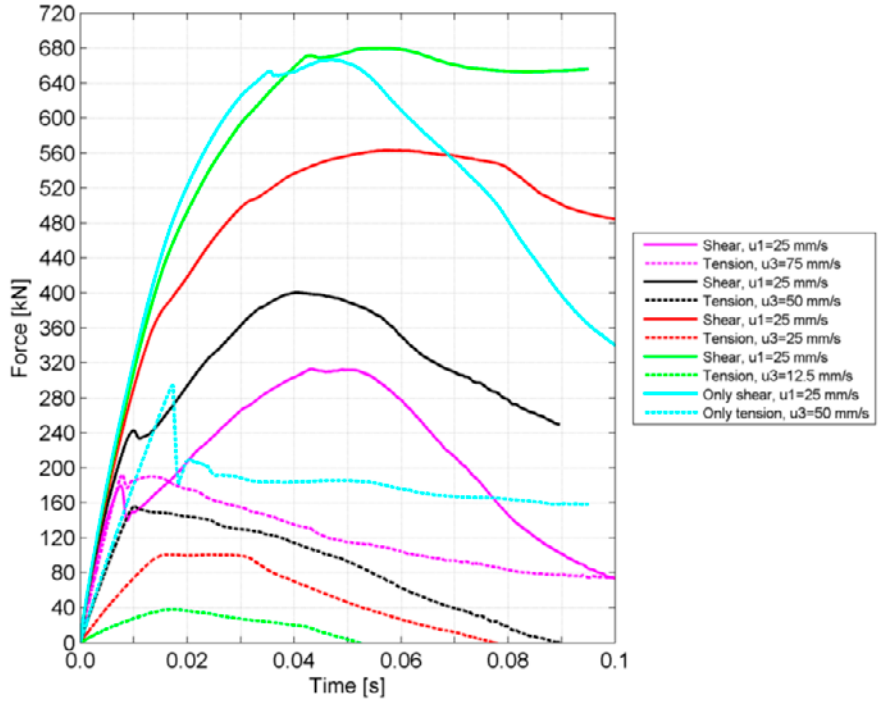

Figure 5-4 Relation between force and time for different loading rates. Solid lines show shear force and dashed lines show corresponding tension force. The two cyan coloured curves are results from analyses where the steel plate only gets loaded in shear or tension.

By keeping the transverse displacement rate constant for all analyses and alter the vertical displacement rate, results show that the relation between tension and shear load is important for corresponding ultimate failures. A low vertical displacement rate in relation to the transverse displacement rate leads to a failure behaviour governed by shear. Consequently, the shear failure load is approximately the same as for a model only loaded in shear. If the vertical displacement rate instead is three times as high as the transverse displacement rate, the tension concrete failure occur sooner and characterizes the failure to a greater extent. This conclusion is also reflected in the fracture surfaces seen in Figure 5-5 and Figure 5-6. With a constant transverse displacement rate, the tension concrete failure naturally gets more prominent with increasing vertical displacement rate. Meaning higher vertical displacement rate leads to higher tension failure load. Corresponding shear failure load decreases due to the already evolved concrete failure due to tension.

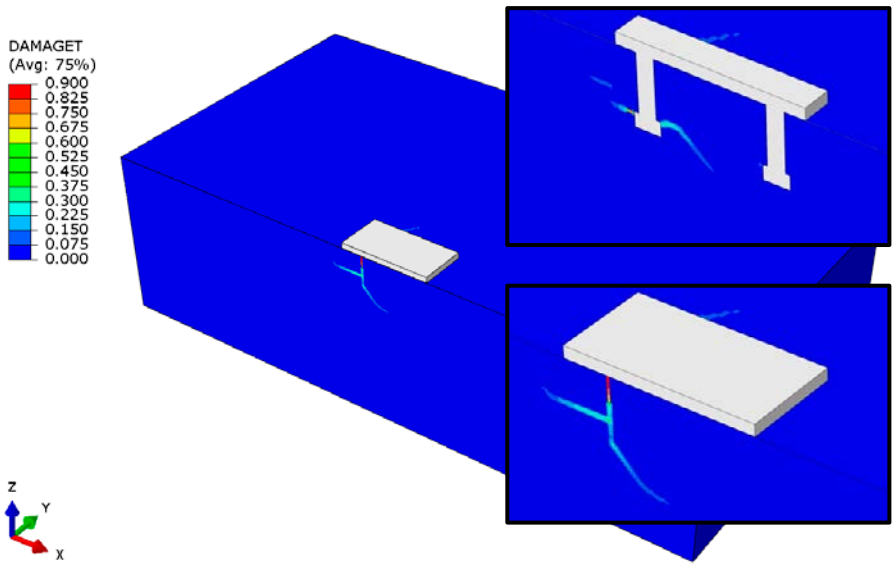

Figure 5-5 Fracture surface at time of maximum tension load (t = 0.019 s) for model with $\dot{u}3$ = 12.5 mm/s (and $\dot{u}1$ = 25 mm/s). The X-Z plane is a symmetry plane.

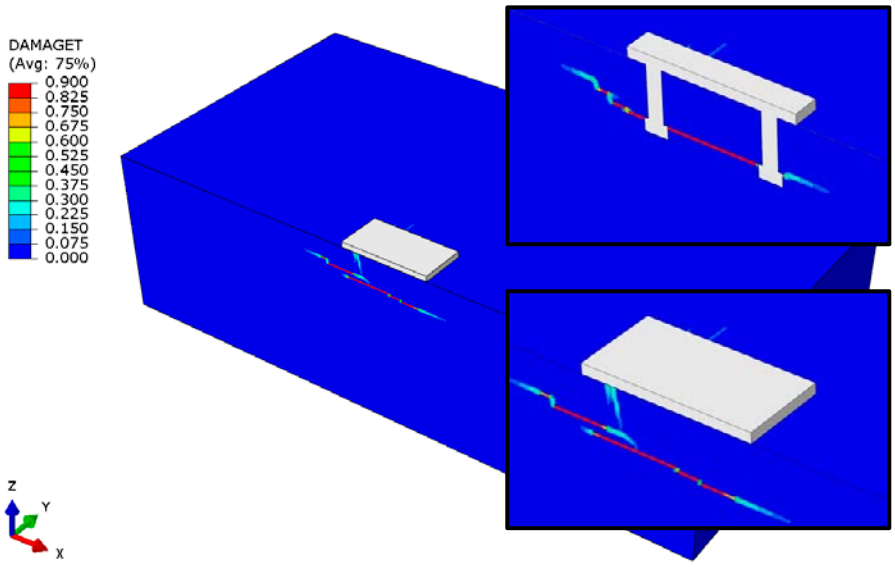

Figure 5-6 Fracture surface at time of maximum tension load (t = 0.009 s) for model with $\dot{u}3$ = 75 mm/s (and $\dot{u}1$ = 25 mm/s). The X-Z plane is a symmetry plane.

A comparison with the interaction equations in CEN/TS 1992-4-2 section 6.4.1.2 is presented in Table 5-2 and Figure 5-7. In the comparison, the simulated tension failure load of the model that is only loaded in tension is regarded as N_{Rd}. Correspondingly, the simulated shear failure load of the model that is only loaded in shear is regarded as V_{Rd}.

Table 5-2 Numerically simulated failure loads and corresponding interaction verifications according to CEN/TS 1992-4-2 section 6.4.1.2.

Simulated loading scenario	$N_{u,simulation}$ [kN]	$V_{u,simulation}$ [kN]	Eq.5-2 (≤ 1.2)	Eq.5-3 (≤ 1.0)
Only loaded in tension, $\dot{u}3$=50 mm/s	294.9	-		
Only loaded in shear, $\dot{u}1$=25 mm/s	-	666.9		
$\dot{u}1$=25 mm/s and $\dot{u}3$=75 mm/s	193.2	312.9	1.12	0.85
$\dot{u}1$=25 mm/s and $\dot{u}3$=50 mm/s	156.5	400.5	1.13	0.85
$\dot{u}1$=25 mm/s and $\dot{u}3$=25 mm/s	100.5	563.3	1.19	0.98
$\dot{u}1$=25 mm/s and $\dot{u}3$=12.5 mm/s	37.7	680.1	1.15	1.08

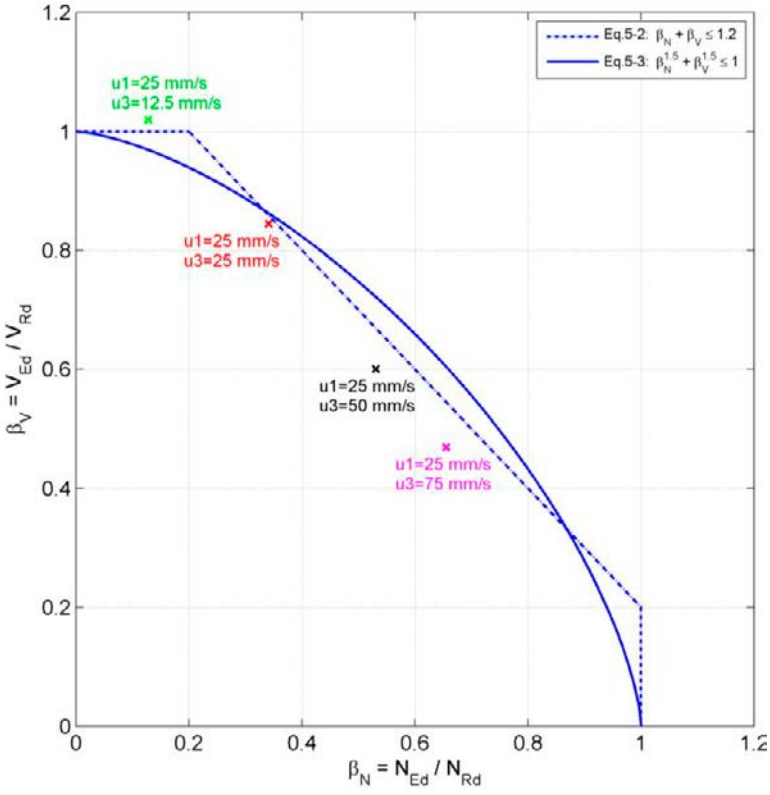

Figure 5-7 Interaction diagram for combined tension and shear loads for simulated cases.

As seen in Figure 5-7, the simulated results show good agreement with the interaction verification equations according to [CEN/TS 1992-4-2:2009].

5.2.6. Results for reinforced concrete

As shown in section 5.2.5, it is difficult to have the tension and shear failures occur at the same time. At least this is the case for the studied model. Figure 5-8 and Figure 5-9 present results where the applied displacement rates are kept constant in shear ($\dot{u}1$ = 25 mm/s) and tension ($\dot{u}3$ = 50 mm/s) for different reinforcement contents. Results show that surface reinforcement only has a minor impact on the failure load magnitudes. The post tension failure behaviour is nevertheless shown more ductile than for a model without reinforcement.

Figures of concrete fracture surfaces are presented in appendix 3.

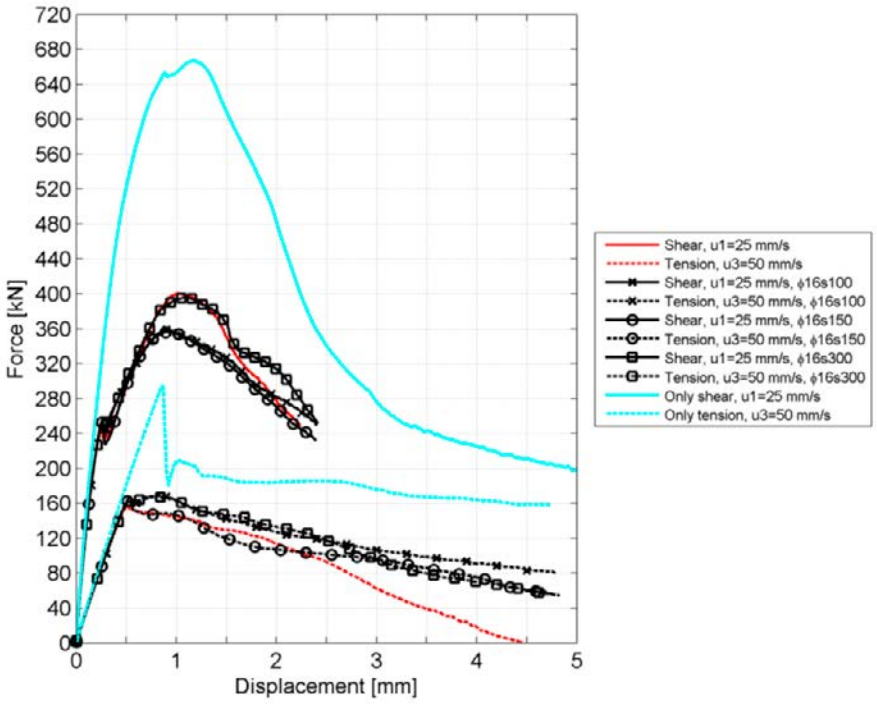

Figure 5-8 Relation between force and displacement for different reinforcement setups. Solid lines show shear force and dashed lines show corresponding tension force. The two cyan coloured curves are results from analyses where the steel plate only gets loaded in shear or tension.

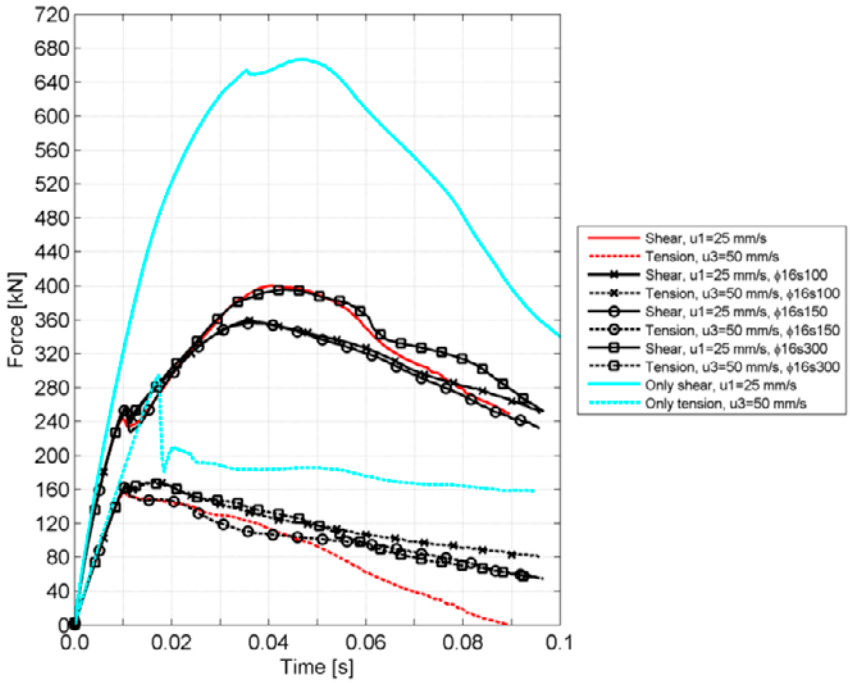

Figure 5-9 Relation between force and time for different reinforcement setups. Solid lines show shear force and dashed lines show corresponding tension force. The two cyan coloured curves are results from analyses where the steel plate only gets loaded in shear or tension.

5.3. Eccentrically loaded far from concrete edges

5.3.1. General

The studies conducted and reported within section 5.3 comprises numerical simulations where the vertical displacement is applied eccentrically with respect to the steel plate centre point. The transverse displacement is however always applied centrically on the steel plate. Hence, studied anchor plates are loaded in both tension (N), shear (V) and with a bending moment (M). All presented displacement results are registered at the steel plate centre point throughout the analyses.

5.3.2. Definition of eccentricity

Figure 5-10 shows the convention of displacement directions. The eccentricity of the vertical displacement is defined as stated in section 3.4.2, i.e. accordingly:

$$e = \frac{M/s_1}{N/2}$$

Investigated eccentricities are

e = 0, 1, 2 and 5

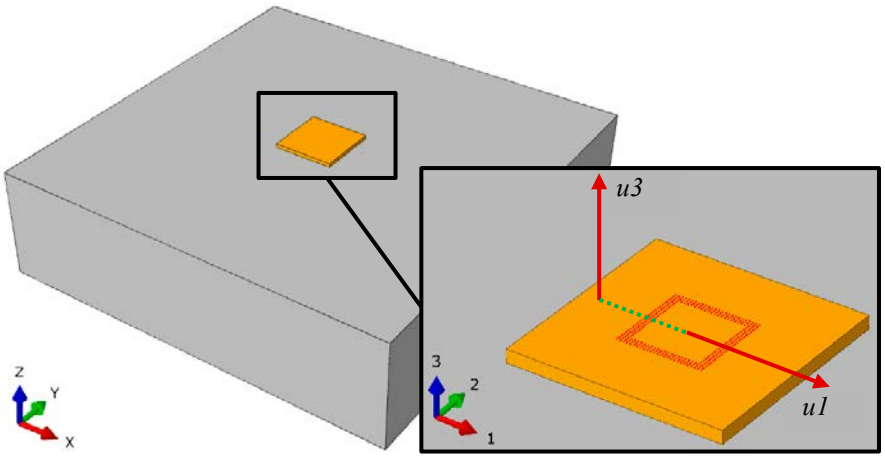

Figure 5-10 Transverse displacement (*u1)* giving rise to shear reaction (*V*) and eccentric vertical displacement (*u3)* giving rise to tensile reaction (*N*) and bending moment (*M*). The green dashed line, i.e. the eccentricity distance, is modelled as a rigid beam.

5.3.3. Results for non-reinforced concrete

Two analysis approaches are conducted. One where the vertical displacement rate $\dot{u}3$ is kept constant irrespective of eccentricity and another approach where the angular velocity of the steel plate is kept constant, i.e. an increasing vertical displacement rate with increasing eccentricity. The transverse displacement rate is kept constant for all analyses ($\dot{u}1$ = 25 mm/s).

Constant vertical displacement rate

Relations between force and corresponding displacement in the centre of the steel plate as well as force and time for analyses where the applied vertical displacement rate is 50 mm/s and transverse displacement rate is 25 mm/s, are presented in Figure 5-11 and Figure 5-12, respectively. The failure loads and corresponding failure moment are summarised in Table 5-3.

Table 5-3 Failure loads and failure moment for non-reinforced concrete analysis model and different eccentricities.

Setup	Ecc. [mm]	Simulated loading scenario	$N_{u,simulation}$ [kN]	$V_{u,simulation}$ [kN]	$M_{u,simulation}$ [kNm]
e = 0	0	$\dot{u}1$=25 mm/s & $\dot{u}3$=50 mm/s	156.5	400.5	-
e = 1	110	$\dot{u}1$=25 mm/s & $\dot{u}3$=50 mm/s	77.8	502.0	8.6
e = 2	220	$\dot{u}1$=25 mm/s & $\dot{u}3$=50 mm/s	39.0	570.1	8.6
e = 5	550	$\dot{u}1$=25 mm/s & $\dot{u}3$=50 mm/s	8.2	666.0	4.5

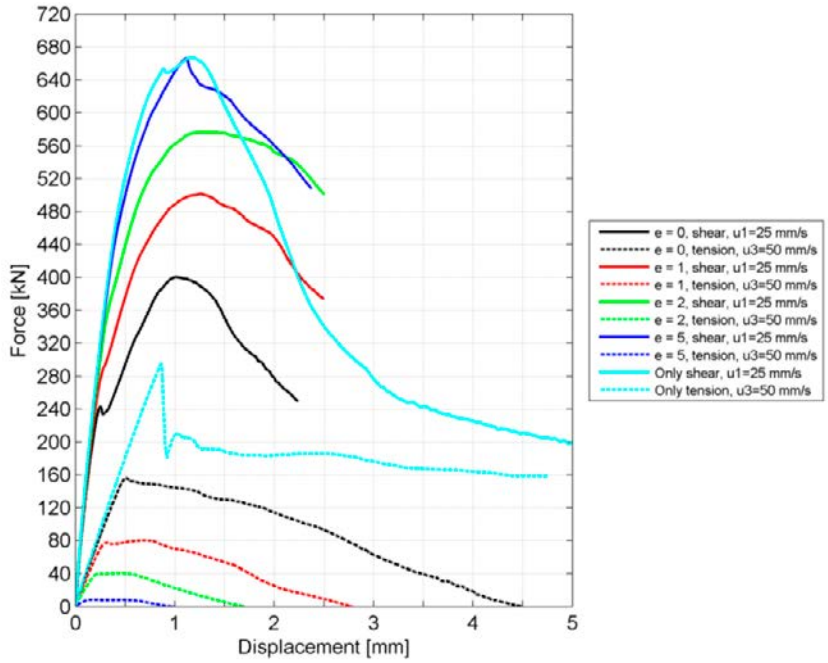

Figure 5-11 Relation between force and corresponding displacement in the centre of the steel plate for different eccentricities of the applied vertical displacement. Solid lines show shear force and dashed lines show corresponding tension force. The two cyan coloured curves are results from analyses where the steel plate only gets loaded in shear or tension. Applied vertical displacement rate $\dot{u}3$ = 50 mm/s and transverse displacement rate $\dot{u}1$ = 25 mm/s.

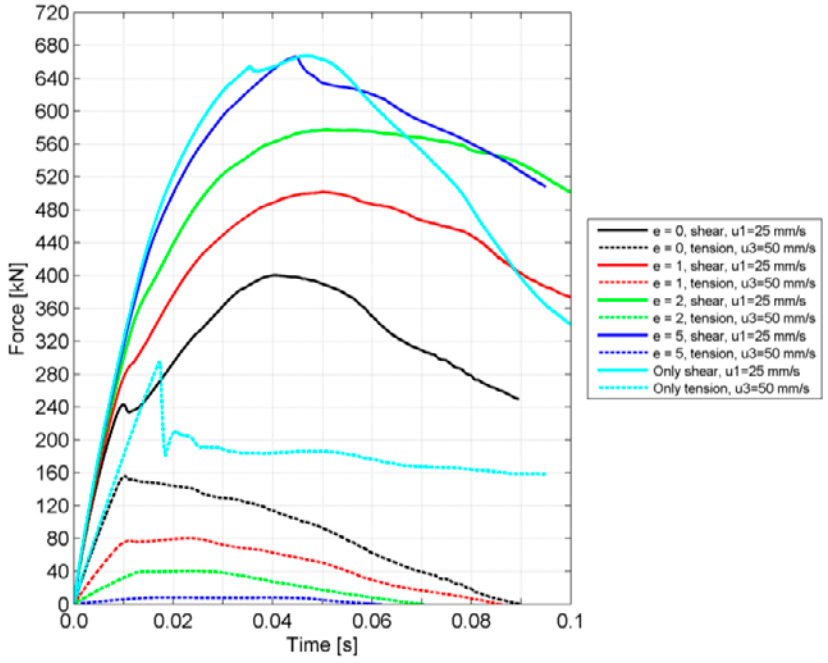

Figure 5-12 Relation between force and time for different eccentricities of the applied vertical displacement. Solid lines show shear force and dashed lines show corresponding tension force. The two cyan coloured curves are results from analyses where the steel plate only gets loaded in shear or tension. Applied vertical displacement rate $\dot{u}3$ = 50 mm/s and transverse displacement rate $\dot{u}1$ = 25 mm/s.

The results show that the tension failure load decreases with increasing eccentricity, while the shear failure load increases. As the applied vertical displacement rate is the same for all analysed eccentricities, the angular velocity of the steel plate rotation decreases with increasing eccentricity. This results in decreasing tension and moment response with increasing eccentricity. As the applied transverse displacement rate is the same for all analysed eccentricities and always is applied at the centre of the steel plate, consequently the concrete shear failure will govern the failure to a greater extent with increasing eccentricity.

Constant angular velocity of steel plate

Relations between force and displacement as well as between force and time for analyses where the applied vertical displacement rate increases with increasing eccentricity are presented in Figure 5-13 and Figure 5-14, respectively. Failure loads and corresponding failure moments are summarised in Table 5-4.

Table 5-4 Failure loads and failure moments for non-reinforced concrete analysis model and different eccentricities. The angular velocity of the steel plate is kept constant irrespective of eccentricity.

Setup	Ecc. [mm]	Simulated loading scenario	$N_{u,simulation}$ [kN]	$V_{u,simulation}$ [kN]	$M_{u,simulation}$ [kNm]
e = 0	0	$\dot{u}1$=25 mm/s & $\dot{u}3$=50 mm/s	156.5	400.5	-
e = 1	110	$\dot{u}1$=25 mm/s & $\dot{u}3$=50 mm/s	80.4	501.6	8.8
e = 2	220	$\dot{u}1$=25 mm/s & $\dot{u}3$=100 mm/s	82.1	374.2	18.1
e = 5	550	$\dot{u}1$=25 mm/s & $\dot{u}3$=250 mm/s	47.2	354.8	26.0

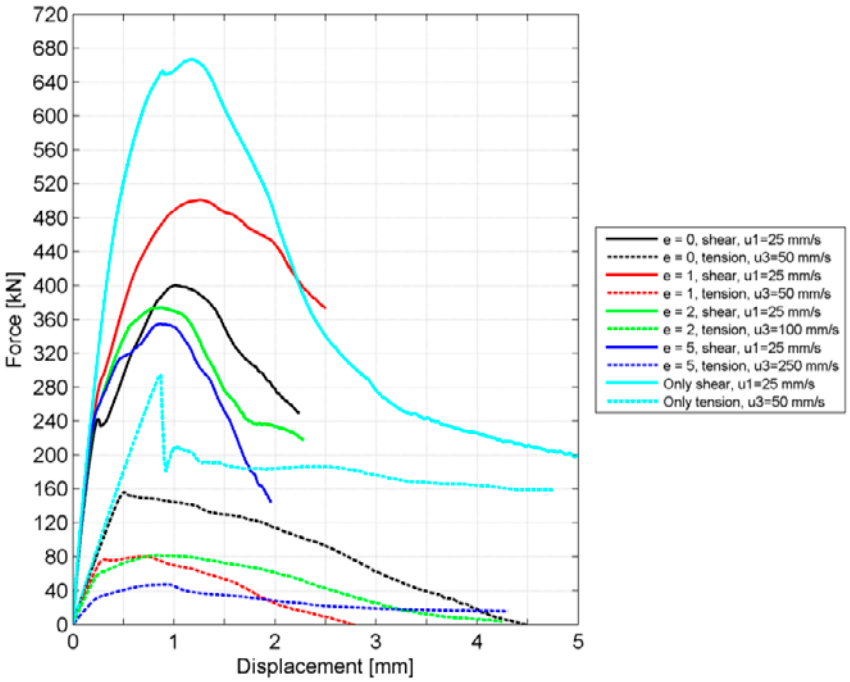

Figure 5-13 Relation between force and corresponding displacement in the centre of the steel plate for different eccentricities of the applied vertical displacement rate ($\dot{u}3$). Solid lines show shear force and dashed lines show corresponding tension force.

The two cyan coloured curves are results from analyses where the steel plate only gets loaded in shear or tension.

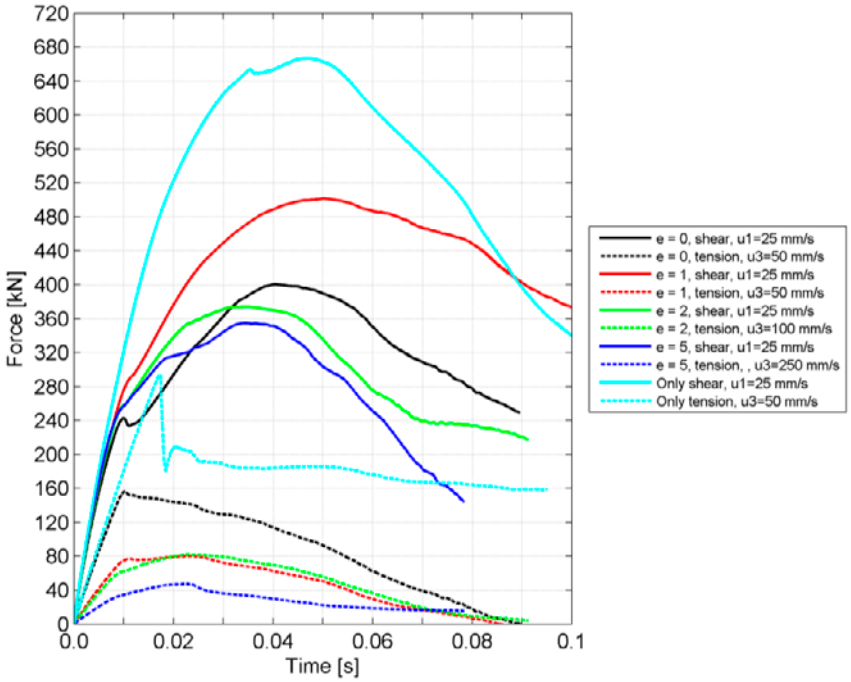

Figure 5-14 Relation between force and time for different eccentricities of the applied vertical displacement rate ($\dot{u}3$). Solid lines show shear force and dashed lines show corresponding tension force. The two cyan coloured curves are results from analyses where the steel plate only gets loaded in shear or tension.

In general, the results show that the tension failure load decreases with increasing eccentricity of the applied vertical displacement. This is also the case for the simulated shear failure loads, except for the non-eccentric setup (e = 0). A distinct peak tension failure is achieved for the model with no eccentricity e = 0, which is also shown to affect the behaviour in shear (see black curves in Figure 5-14).

The inclination of the tension response curves in Figure 5-13 shows that the structural stiffness is similar for cases e = 0 and e = 1. Thus it can be concluded that all four anchors are in tension for the considered constellations. However, the same relation for cases e = 0 and e = 1 is not shown in the time domain (see Figure 5-14), meaning the applied transverse displacement affects the fracturing process to a greater extent for case e = 1. The reason for the higher shear failure load for e = 1 compared to e = 0 is also explained by studying the fracture surfaces in Figure 5-15 and Figure 5-16. The figures show that one joint concrete cone is developed for the group of anchors in both cases, but for e = 1 the front of the concrete fracture surface is pointing further down into the concrete specimen. The small eccentricity, giving rise to a bending moment, thus alters the direction of the concrete crack plane and increases the shear capacity.

The decrease in tension and shear failure load for models with eccentricities e = 2 and e = 5 is due to the increased bending moment which reduces or eliminates the tension forces in two of the anchors. Figure 5-18 clearly shows that a concrete cone is developed for the two back row anchors, i.e. the two anchors in negative x-direction aligned in the y-direction. The same tendency is shown for setup e = 2 in Figure 5-17.

Additional figures of concrete fracture surfaces are presented in appendix 3.

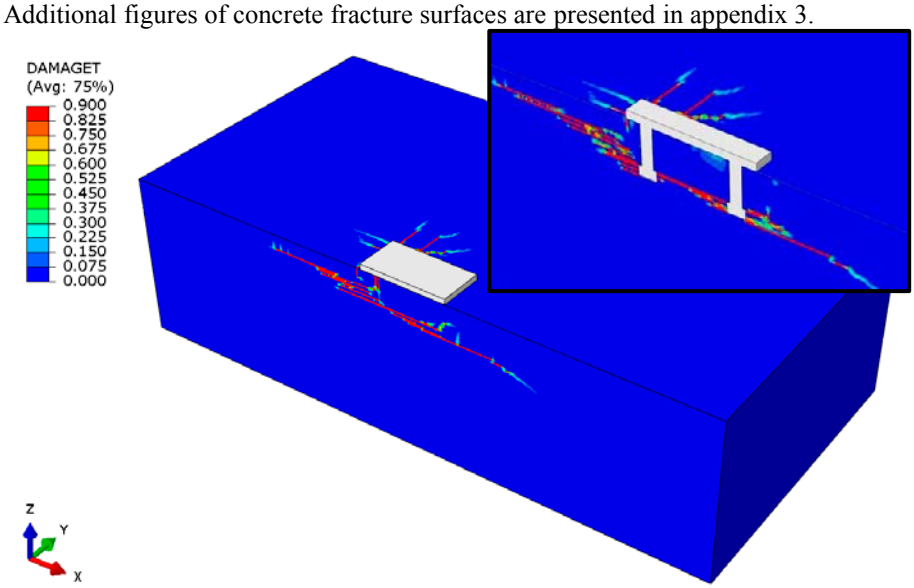

Figure 5-15 Fracture surface at time t = 0.05 s (see **Figure 5-14**) for model with eccentricity e = 0, $\dot{u}3$ = 50 mm/s (and $\dot{u}1$ = 25 mm/s). The X-Z plane is a symmetry plane.

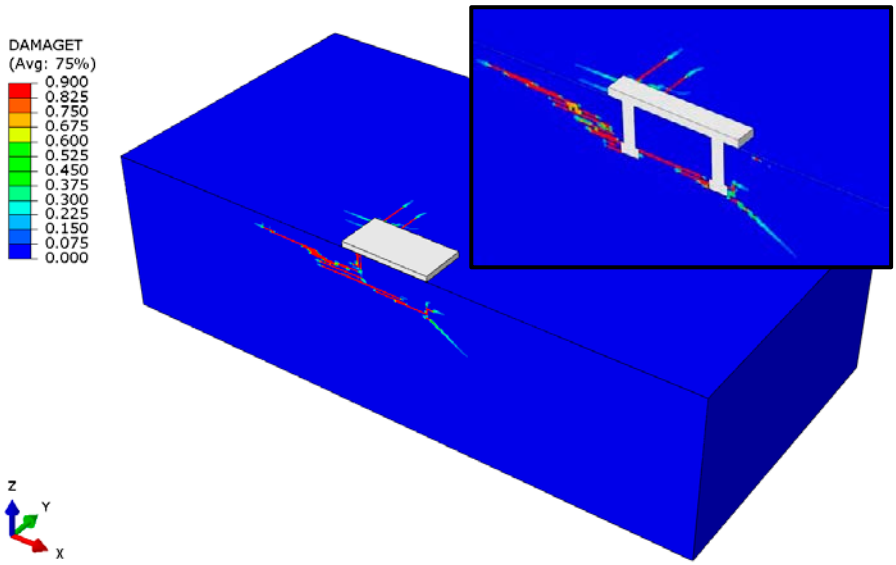

Figure 5-16 Fracture surface at time t = 0.05 s (see **Figure 5-14**) for model with eccentricity e = 1, $\dot{u}3$ = 50 mm/s (and $\dot{u}1$ = 25 mm/s). The X-Z plane is a symmetry plane.

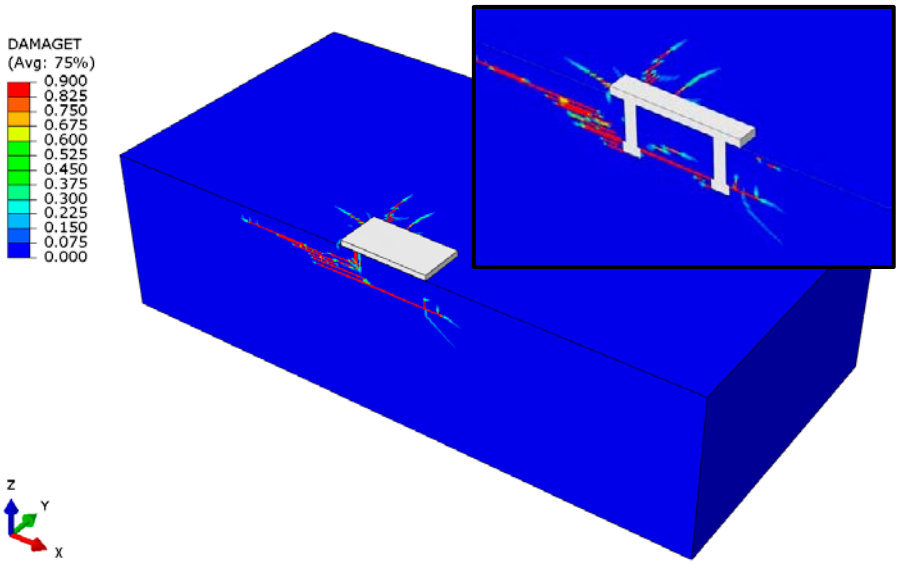

Figure 5-17 Fracture surface at time t = 0.05 s (see **Figure 5-14**) for model with eccentricity e = 2, $\dot{u}3$ = 100 mm/s (and $\dot{u}1$ = 25 mm/s). The X-Z plane is a symmetry plane.

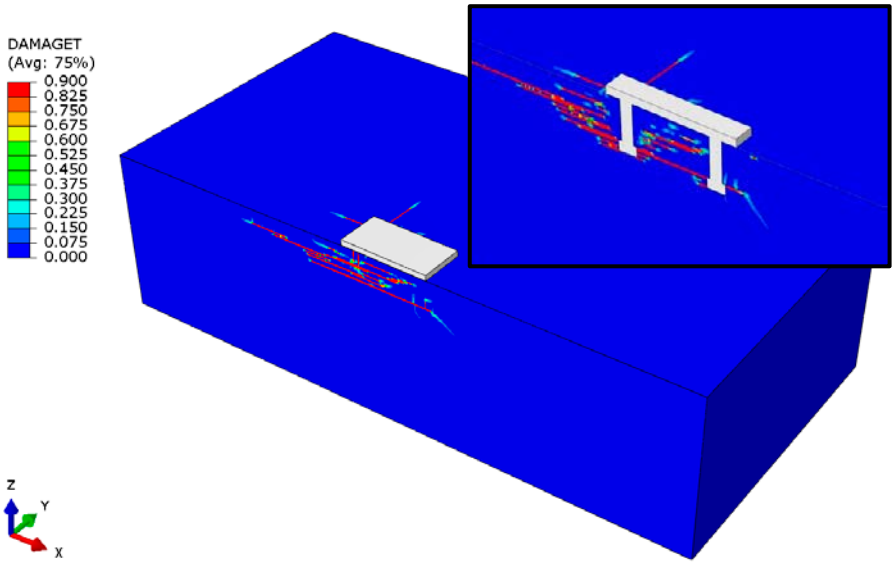

Figure 5-18 Fracture surface at time t = 0.05 s (see **Figure 5-14**) for model with eccentricity e = 5, $\dot{u}3$ = 250 mm/s (and $\dot{u}1$ = 25 mm/s). The X-Z plane is a symmetry plane.

5.3.4. Results for reinforced concrete

The numerical simulations in which reinforcement is included in the model, are conducted by keeping the angular velocity of the steel plate constant irrespective of eccentricity, see Table 5-4. Relations between force and displacement as well as between force and time are presented in Figure 5-19 and Figure 5-20, respectively.

Results show that the dense reinforcement setup (ϕ16 with a spacing of 100 mm) only has a minor effect on the simulated failure loads. Less reinforcement will most likely not contribute to higher failure loads. In general, the reinforcement makes the post failure behaviour more ductile. Figures of concrete fracture surfaces are presented in appendix 3.

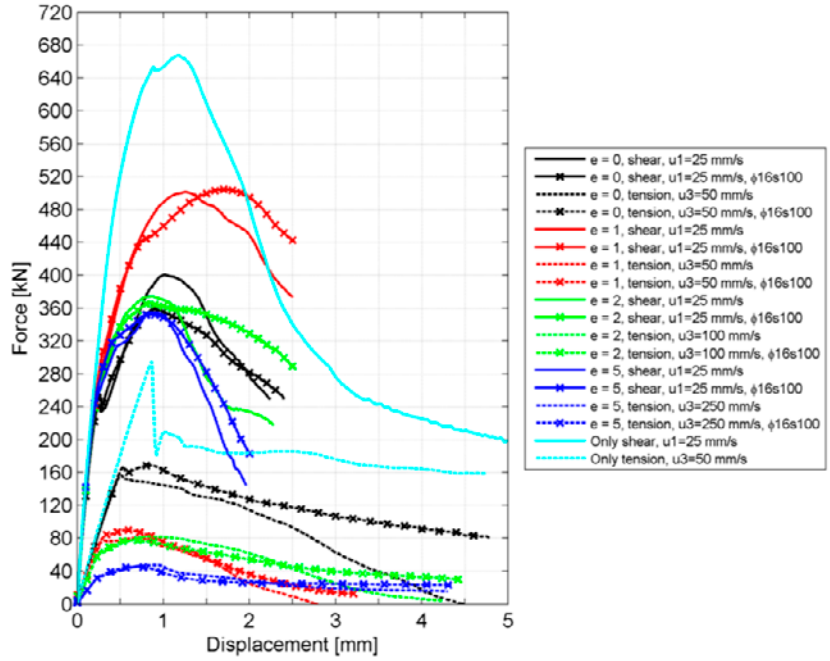

Figure 5-19 Relation between force and corresponding displacement in the centre of the steel plate for different eccentricities of the applied vertical displacement. The figure includes both non-reinforced and relatively dense reinforced concrete. Solid lines show shear force and dashed lines show corresponding tension force. The two cyan coloured curves are results from analyses where the steel plate only gets loaded in shear or tension.

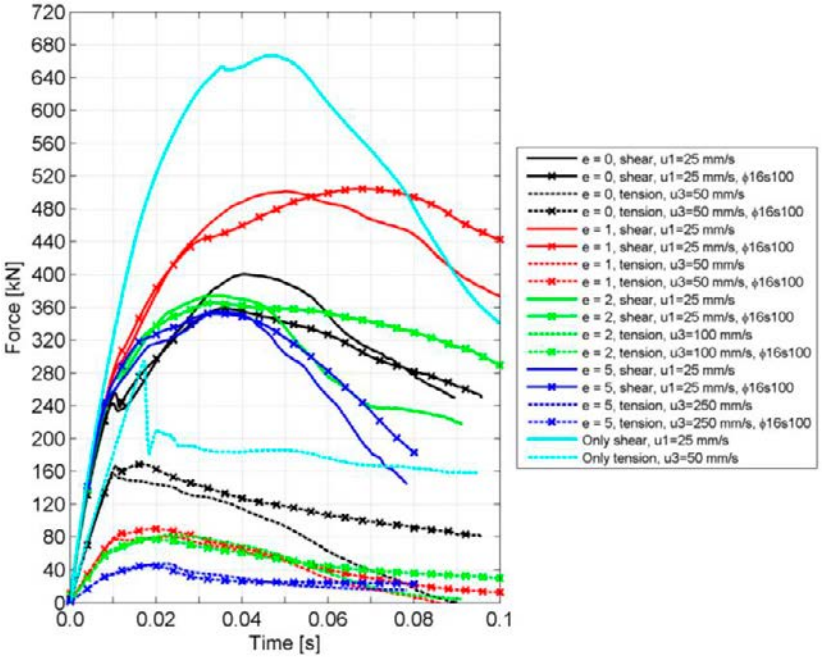

Figure 5-20 Relation between force and time for different eccentricities of the applied vertical displacement. The figure includes both non-reinforced and relatively dense reinforced concrete. Solid lines show shear force and dashed lines show corresponding tension force. The two cyan coloured curves are results from analyses where the steel plate only gets loaded in shear or tension.

6. Discussion

The response of mechanically loaded anchors in reinforced concrete structures can only be understood by a combination of testing and numerical simulations. As concrete is a complex material, interaction between anchors, reinforcement and concrete is consequently also complex. Reported work within this area in the open literature is limited why efforts are needed to fill this gap.

One important result from the previous project [SSM Research Project 2013:27] was that splitting of the concrete structure could limit the tension capacity of the anchor plate if the bending stiffness of the structure was too low. The thickness of the structure had a big impact of the bending stiffness and thereby also the tension failure mode. An increase from 300 to 600 mm resulted in a change in failure mode from a combination of concrete cone and splitting failure to a pure concrete cone failure. Not only thickness of the structure but also the amount of surface reinforcement and the boundary conditions at the edges of the structure influenced the bending stiffness. These parameters were also looked at in the previous project. In order to investigate the local interaction between tension loaded anchor plates and the concrete structure, i.e. the concrete cone failure mode, splitting is supressed in the present simulations.

In the present research project, the response of headed anchors in non-reinforced and reinforced concrete structures is investigated by means of finite element simulations. Based on work done in a previous project [SSM Research Project 2013:27], the following configurations are investigated:

- eccentrically tension loaded anchors far from concrete edges,
- centrically tension loaded anchor plates close to a free concrete edge,
- centrically tension loaded anchor plates with shear reinforcement far from concrete edges,
- centrically shear loaded anchor plates far from concrete edges,
- centrically shear loaded and eccentrically tension loaded anchor plates far from concrete edges.

With respect to the concrete cone failure mode, surface reinforcement has a negligible influence on the failure load level. The main reason is that the tension load is acting perpendicular to the reinforcement which means that it is difficult to transfer load into the rebars. One exception is anchor plates in shear reinforced concrete. As the shear reinforcement links enclose the surface reinforcement, load transfer from the links into the concrete structure is further facilitated by the surface reinforcement.

The location of shear reinforcement links is of importance for the tension capacity of anchor plates in shear reinforced structures. Simulation results clearly show that all links located in the cone breakout prism cannot be fully utilized. For a case with 16 links (four in each direction), only those four links closest to the anchors reach full yielding. The remaining twelve links only contribute with about 35% to the failure load capacity. The deflection of the cone breakout prism controls the distribution of the tension load to the links.

For the case with only four shear reinforcement links, the distance between the links and the anchors should not exceed $0.3h_{ef}$ if full utilization of the links is expected. If the same distance exceeds $0.75h_{ef}$, the links do not contribute to the tension capacity.

For anchor plates far from concrete edges and loaded in shear, the surface reinforcement has only a small effect on the pry-out failure load level. The reason for this is that the shear load gives rice to a pressure force between the steel plate and the concrete and a corresponding tensile force in the anchors located outside the contact zone. This tension load is not easily transferred to the surface reinforcement since the reinforcement is oriented perpendicular to the tension load.

The results from the simulations of anchor plates loaded in shear correspond well with capacities according to CEN/TS 1992-4-2, except from the case when embedment depth gets below the value when the factor k_3 used in CEN/TS is reduced from 2 to 1. A reasonable explanation for this is that CEN/TS underestimates the capacity of embedment depths just below the limit where k_3 is reduced, since it is not likely that the capacity suddenly drops 50% when the embedment depth decreases only a few millimetres.

The simulations of anchor plates simultaneously loaded in tension and shear, clearly show that the ratio between the tension load and the shear load is of great importance. In the case of a dominant tension force the combined failure mode will be characterized by tension concrete failure. When the shear load is dominant the combined failure mode will to a greater extent be governed by a shear failure mode. In general, the simulations show agreement with the interaction verification equations in CEN/TS, but for some ratios between tension load and shear load the simulations show slightly lower capacity than CEN/TS.

For anchor groups simultaneously loaded in shear and eccentric tension, the simulations show a complex relationship between the shear capacity and the eccentricity of the tension load. For small eccentricities, the shear capacity increases when eccentricity of the tension load is increased. When the eccentricity is large, the shear capacity will instead decrease when the eccentricity is increased. The results from the simulations show that the reason for this behaviour is that the concrete cone failure prism is large and enclose all anchors when the eccentricity is small, but when the eccentricity gets larger only two of the four anchors in the group is in tension resulting in a smaller concrete cone failure prism and thereby a lower pry-out failure capacity.

For all configurations investigated, surface reinforcement benefits to the ductility of the failure process.

Material properties used for the reinforcement vary with type of configuration. If the rebar is expected to yield, elastic perfectly plastic properties are chosen. This is the case for the anchor plates with shear reinforcement. For the remaining cases, elastic properties are chosen for the reinforcement.

Comparisons between numerical simulations and CEN/TS 1992-4-2 show good agreement for investigated non-reinforced structures. This gives confidence in the numerical approach used in this investigation.

7. Conclusions

The present research project together with the ANKARM project [SSM Research Report 2013:27] have resulted in the following conclusions:

1. Concrete failure of headed anchors and anchor groups in non-reinforced as well as reinforced concrete can be simulated with confidence using finite element analyses.

2. The simulations show good agreement with results from available physical tests. The failure load is better predicted than force-displacement curves.

3. The concrete damaged plasticity constitutive model in Abaqus is found to work very well for the simulation of the failure modes investigated.

4. The use of mean concrete cylinder compressive strength together with corresponding tensile strength in the concrete damaged plasticity constitutive model seems to be most appropriate for simulation of the physical response of concrete structures.

5. In general, reinforcement makes the failure of anchors loaded in tension or shear more ductile.

6. Global stiffness of the concrete structure is not considered by design codes such as CEN/TS in the design of anchors. For anchor groups loaded in tension, this lack might result in reduced safety margin against concrete cone failure if the concrete structure is too flexible. This is particularly true when non-cracked concrete is assumed.

7. The simulations show that reinforcement in the direction of the applied load leads to a distinct increase of the concrete edge failure capacity. However, the simulations show that the normal stress in the reinforcement bars close to the anchors is considerably higher than in the rest of the bars tying the breakout body to the concrete member.

8. Simulated failure loads of eccentrically tension loaded anchor plates in non-reinforced concrete far from concrete edges rather well correspond to predictions made by use of CEN/TS 1992-4-2. For larger eccentricities, the two results start to deviate.

9. Surface reinforcement has a negligible impact on simulated failure loads of eccentrically tension loaded anchor plates far from concrete edges.

10. Simulated failure loads of centrically tension loaded anchor plates in non-reinforced concrete close to a free concrete edge rather well correspond to predictions made by use of CEN/TS 1992-4-2.

11. Edge reinforcement increases failure load of centrically tension loaded anchor plates close to a free concrete edge. Failure load increases with reinforcement density.

12. Edge reinforcement increases failure ductility of centrically tension loaded anchor plates close to a free concrete edge. Failure ductility increases slightly with reinforcement density.

13. Shear reinforcement links should be located close enough to the anchor plate in order to fully contribute to concrete cone tension capacity. For investigated configurations, full contribution is obtained if the distance between anchors and shear reinforcement links does not exceed $0.3h_{ef}$.

14. Shear reinforcement links have a beneficial impact on failure ductility of tension loaded anchor plates. For investigated configurations, this effect is largest if the distance between anchors and shear reinforcement links does not exceed $0.4h_{ef}$.

15. For anchor plates in non-reinforced concrete far from concrete edges and loaded in shear, the simulated capacities correspond well with the capacities according to CEN/TS 1992-4-2. For embedment depth 100 mm the simulations show good agreement with CEN/TS both for single anchors and anchor groups. For shorter anchors (50 mm) simulation shows significant higher load capacity than CEN/TS. The reason is mainly that the factor k_3 used in CEN/TS drops from 2 to 1 for small embedment depths.

16. In general, the numerical simulations show that the amount of surface reinforcement only has little impact on the concrete pry-out failure load. The main reason for this is that the shear load gives rise to a pressure force between the steel plate and the concrete which is balanced by a tensile force in the anchor. The tension load is not easily transferred to the perpendicular oriented surface reinforcement bars.

17. For anchors simultaneously loaded in tension and shear, the relation between applied tension displacement rate and shear displacement rate in the simulation is important for the resulting failure capacity. A low tension displacement rate in relation to the shear displacement rate leads to a failure behaviour governed by shear. On the contrary, if the tension displacement rate is high in relation to the shear displacement rate, the tension concrete failure occurs sooner and characterizes the combined failure to a greater extent. If the concrete tension failure is more prominent, corresponding shear failure load decreases due to the already evolved tension failure.

18. For investigated configurations of anchor plates in non-reinforced concrete far from concrete edges and centrically loaded both in tension and shear, the simulations in general show good agreement with predictions made by use of CEN/TS 1992-4-2. Simulation has been carried out for different ratios between tension load and shear load (i.e. different rations between tension displacement rate and shear displacement rate). In all cases, the results show good agreement with the interaction verification equations in CEN/TS 1992-4-2. For some ratios between tension load and shear load, the simulations show slightly lower capacity than the prediction using the interaction verification equations.

19. For the studied anchor groups simultaneously loaded in shear and eccentric tension, the simulations show that the shear failure capacity increases when the eccentricity of the tension load increases but only as long as concrete-cone failure and pry-out failure can share the same fracture surface. As the eccentricity gets large enough, the concrete-cone failure prism encloses only two of the four anchors, i.e. the volume of the concrete breakout body gets reduced. Consequently, the shear failure load decreases.

8. Recommendations

Recommendations for numerical simulation of mechanically loaded anchor plates in non-reinforced and reinforced concrete are given as follows:

1. The constitutive model for the concrete material must be able to capture phenomena such as cracking in tension and plastic deformation in compression. In Abaqus, the concrete damaged plasticity model is most suitable.

2. An elastic material model is, in most cases, sufficient in modelling surface reinforcement. Shear reinforcement links and hairpins need to be modelled with an elastic-plastic material model.

3. In order to capture the evolution of damage in the concrete, the concrete element size should be sufficiently small. In the present study an element size of 5 mm worked satisfactorily.

4. The material behaviour of concrete is highly non-linear. In order to avoid numerical problems, it is recommended to conduct the numerical simulations with an explicit solver and as displacement controlled analyses.

5. Second order effects (NLGEOM=YES in Abaqus) might be necessary to considered in numerical simulation of failure load of anchor plates in reinforced concrete structures if the failure process is ductile. Simulation of failure load of tension loaded anchor plates in shear reinforced concrete is such an example.

6. It is recommended that the length of the elements representing the reinforcement rebars is similar to the side length of the concrete elements. When using EMBEDDED ELEMENT in Abaqus to connect the reinforcement to the concrete, two crossing rebars are connected to each other where their respective nodes are located in the same concrete element.

7. Friction between the anchor plate and the concrete surface might have an important impact on the results when the anchor plate is loaded in shear. It is therefore important to include friction in the contact properties.

Acknowledgements

The Swedish Radiation Safety Authority (SSM) has sponsored this research project. This support is acknowledged.

References

ACI 349-13, 2013. Code Requirements for Nuclear Safety-Related Concrete Structures (ACI 349-13) and Commentary. American Concrete Institute.

Betonghandbok - Material, 2008. Betonghandbok - Material, utgåva 2. Svensk Byggtjänst.

Boverket, 2004. Boverkets handbok om betongkonstruktioner, BBK04. Karlskrona, 2004.

CEN/TS 1992-4-2, 2009. European committee for standardization. Design of fastenings for use in concrete – Part 4-2: Headed fasteners. Brussels, May 2009.

Cornelissen H, Hordijk D, Reinhardt H, 1986. Experimental determination of crack softening characteristics of normalweight and lightweight concrete. Delft University of Technolog, pp. 50-51, 1986.

Dassault Systémes, 2014. Abaqus *Analysis User's Manual Volume I-V*, *Version 6.14*, Abaqus INC.

Eligehausen R, Bouska P, Cervenka V, Pukl R, 1992. Size effect of the concrete cone failure load of anchor bolts. In: Bazant, Z.P. (Editor), Fracture Mechanics of Concrete Structures, pp. 517-525, Elsevier Applied Science, London, New York.

Lee J, Fenves G, 1998. Plastic-Damage Model for Cyclic Loading of Concrete Structures, Journal of Engineering Mechanics, vol. 124, no. 8, pp. 892-900, 1998.

Lubliner J, Oliver J, Oller S, Oñate E, 1989. A Plastic-Damage Model for Concrete, International Journal of Solids and Structures, vol. 25, pp. 299-329, 1989.

SSM Research Report 2013:27, 2013. Numerical simulations of headed anchors break in reinforced and non-reinforced concrete structures.

APPENDIX 1

Extended result figures regarding numerical simulation of anchors loaded in tension

In this Appendix, figures with the damage tension parameter (DAMAGET) are presented at failure load and at end of simulation for a number of anchor groups loaded in tension. The anchor configurations are summarised in Table A1-1, Table A1-2, Table A1-3 and Table A1-4, respectively.

Table A1-1 Summary of results from numerical simulations of eccentrically loaded anchor plates far from concrete edges.

No.	Surface reinforcement	Eccentricity *e* [-]	$N_{u,simulation}$ [kN]
1	-	0	364
2	-	1	321
3	-	2	220
4	-	5	112
5	-	10	63
6	ϕ12cc300	0	360
7	ϕ12cc300	1	321
8	ϕ12cc300	2	221
9	ϕ12cc200	0	360
10	ϕ12cc200	1	324
11	ϕ12cc200	2	221
12	ϕ12cc100	0	362
13	ϕ12cc100	1	323
14	ϕ12cc100	2	219
15	ϕ12cc100	5	116
16	ϕ12cc100	10	62

Table A1-2 Summary of results from numerical simulations of centrically loaded anchor plates close to free concrete edge. c_1 is the distance from the anchors to the edge.

No.	Surface reinforcement	c_1 [mm]	$N_{u,simulation}$ [kN]
1	-	75	152
2	-	150	218
3	-	200	262
4	ϕ12cc300	75	154
5	ϕ12cc300	150	229
6	ϕ12cc300	200	265
7	ϕ12cc200	75	172
8	ϕ12cc200	150	268
9	ϕ12cc200	200	272
10	ϕ12cc100	75	181
11	ϕ12cc100	150	312
12	ϕ12cc100	200	283

Table A1-3 Summary of results from numerical simulations of centrically loaded anchor plates far from concrete edges with four shear reinforcement links at a distance *a* from the anchors. Surface reinforcement is ϕ12cc100.

No.	*a* [mm]	$N_{u,simulation}$ [kN]
1	$0.15h_{ef} = 29.3$	897
2	$0.3h_{ef} = 58.5$	892
3	$0.4h_{ef} = 78.0$	800
4	$0.5h_{ef} = 97.5$	650
5	$0.625h_{ef} = 121.9$	485
6	$0.75h_{ef} = 146.3$	397
7	$1.0h_{ef} = 195.0$	363
8	$1.25h_{ef} = 243.8$	350

Table A1-4 Summary of results from numerical simulation a centrically loaded anchor plate far from concrete edges with 16 shear reinforcement links. Surface reinforcement is ϕ12cc100.

No.	Location of links from anchors [mm]	$N_{u,simulation}$ [kN]
1	$0.15h_{ef}, 0.5h_{ef}, 0.85h_{ef}, 1.2h_{ef}$	1300

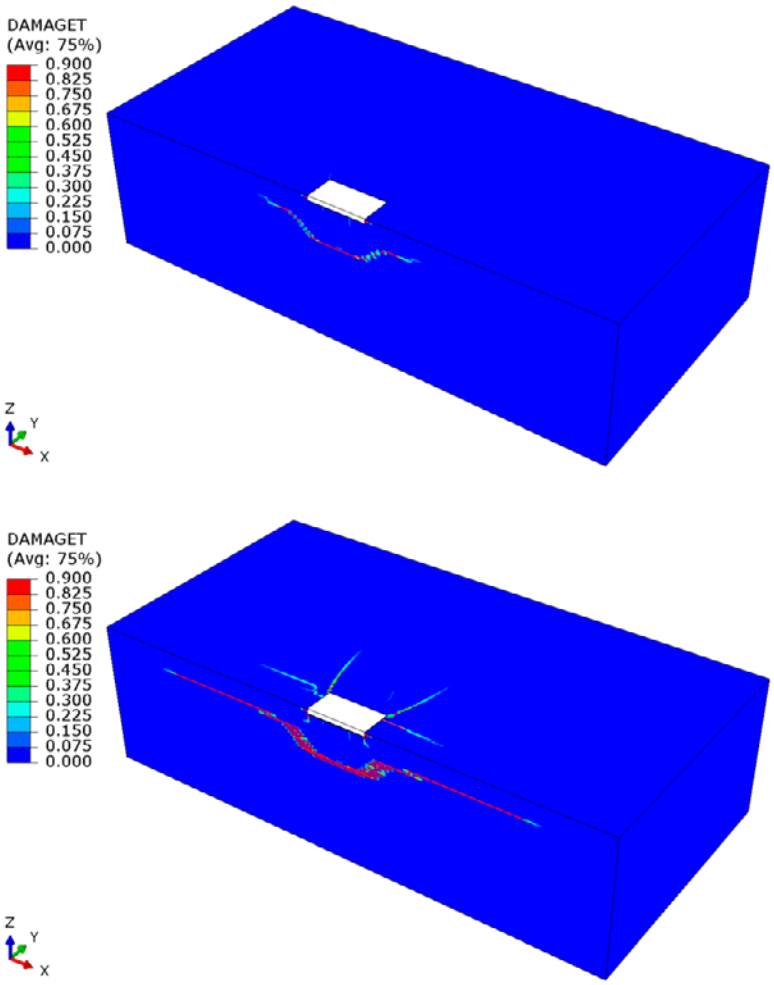

Figure A1-1 Damage tension parameter (DAMAGET) at failure load and at end of simulation for configuration 1 in Table A1-1. No surface reinforcement. Eccentricity $\boldsymbol{e} = \mathbf{0}$.

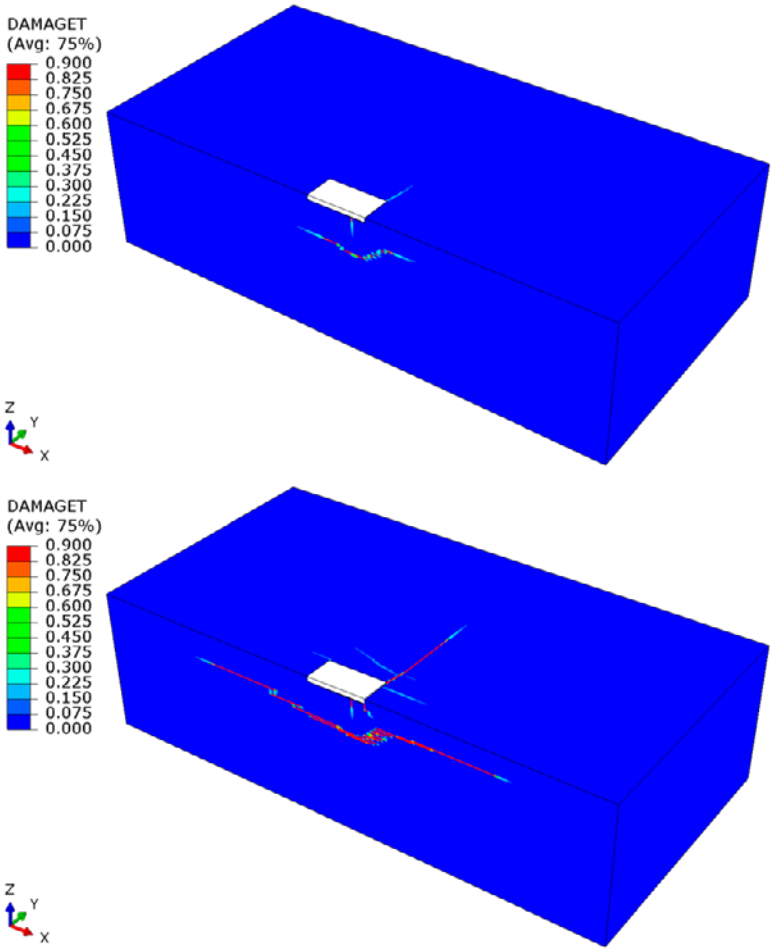

Figure A1-2 Damage tension parameter (DAMAGET) at failure load and at end of simulation for configuration 2 in Table A1-1. No surface reinforcement. Eccentricity $\boldsymbol{e = 1}$.

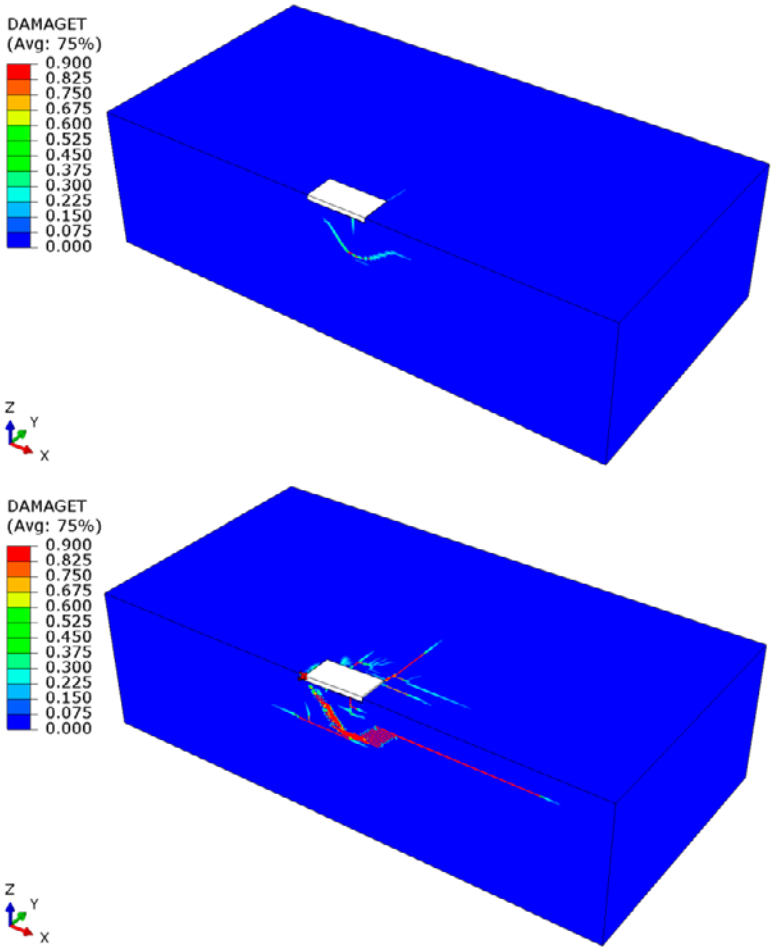

Figure A1-3 Damage tension parameter (DAMAGET) at failure load and at end of simulation for configuration 3 in Table A1-1. No surface reinforcement. Eccentricity $e = 2$.

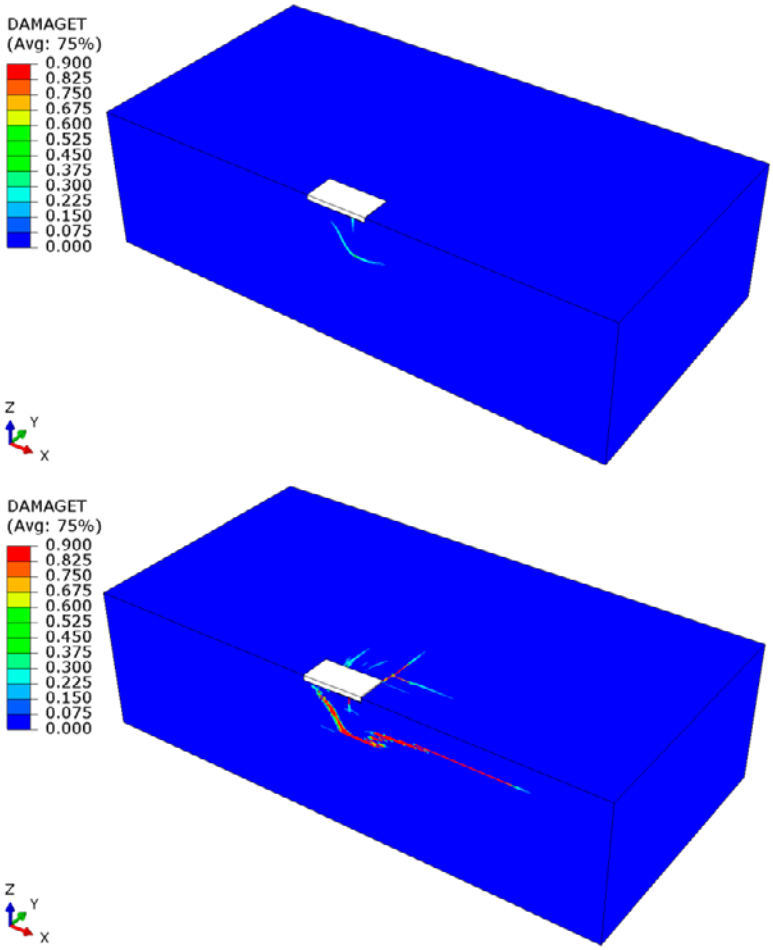

Figure A1-4 Damage tension parameter (DAMAGET) at failure load and at end of simulation for configuration 4 in Table A1-1. No surface reinforcement. Eccentricity $e = 5$.

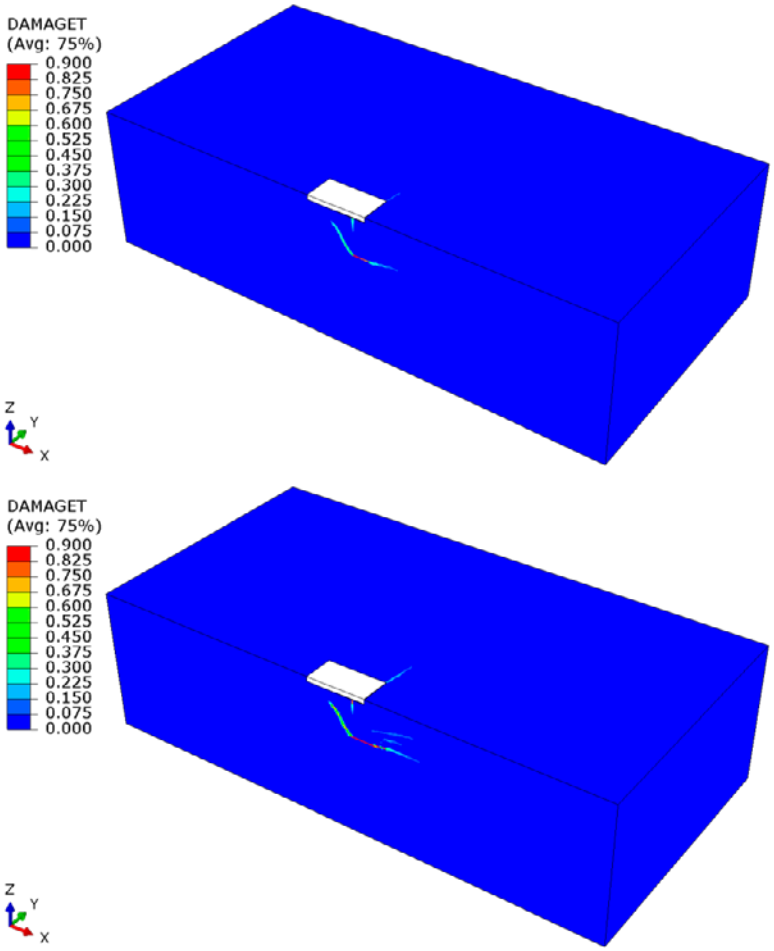

Figure A1-5 Damage tension parameter (DAMAGET) at failure load and at end of simulation for configuration 5 in Table A1-1. No surface reinforcement. Eccentricity $\boldsymbol{e = 10}$.

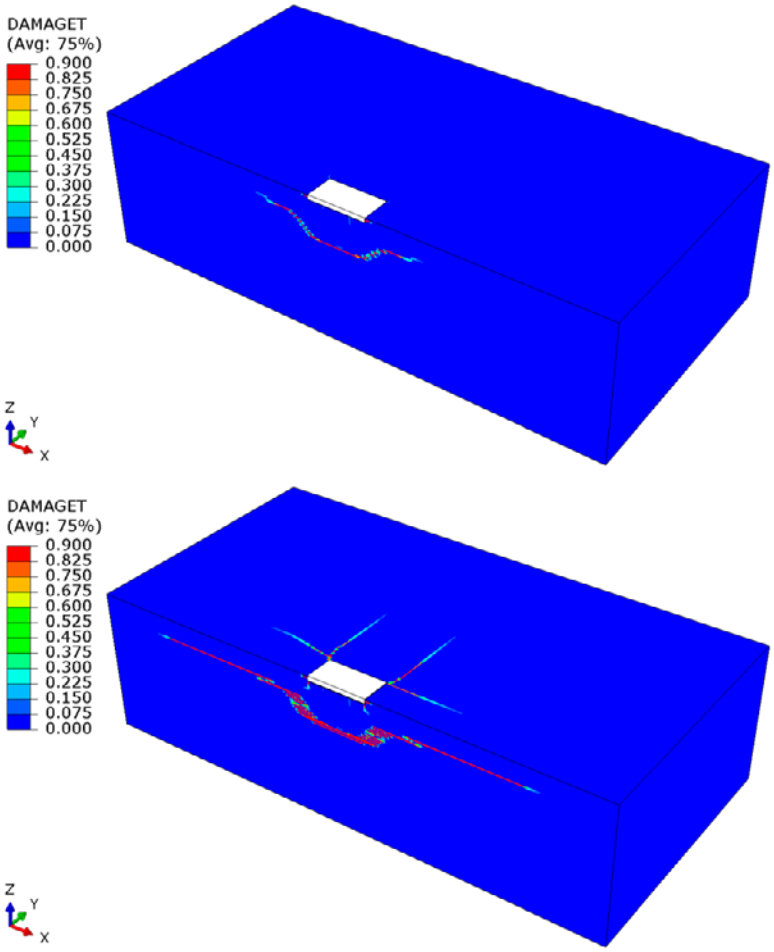

Figure A1-6 Damage tension parameter (DAMAGET) at failure load and at end of simulation for configuration 6 in Table A1-1. Surface reinforcement ϕ12cc300. Eccentricity $\boldsymbol{e} = \mathbf{0}$.

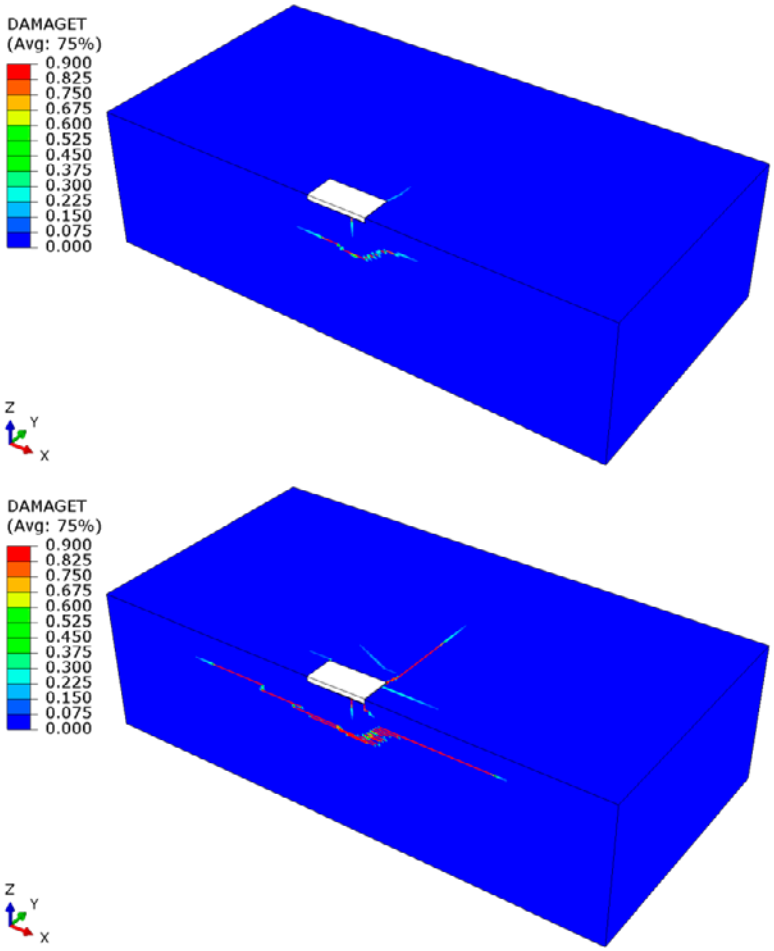

Figure A1-7 Damage tension parameter (DAMAGET) at failure load and at end of simulation for configuration 7 in Table A1-1. Surface reinforcement ϕ12cc300. Eccentricity $\boldsymbol{e = 1}$.

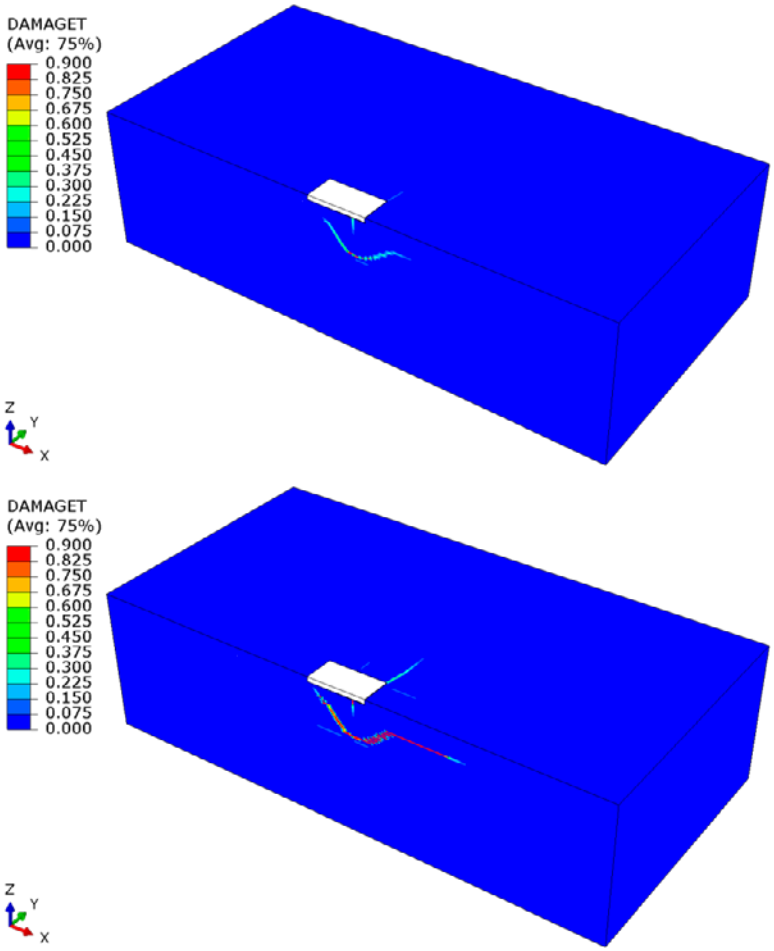

Figure A1-8 Damage tension parameter (DAMAGET) at failure load and at end of simulation for configuration 8 in Table A1-1. Surface reinforcement ϕ12cc300. Eccentricity $\boldsymbol{e = 2}$.

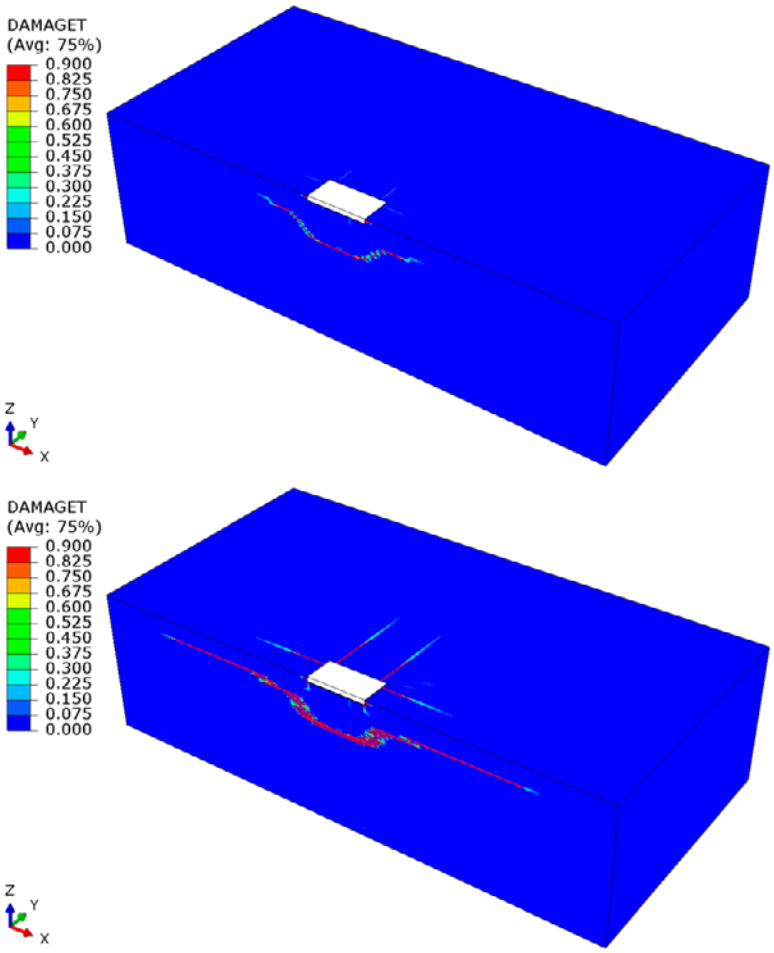

Figure A1-9 Damage tension parameter (DAMAGET) at failure load and at end of simulation for configuration 9 in Table A1-1. Surface reinforcement ϕ12cc200. Eccentricity $\boldsymbol{e} = \mathbf{0}$.

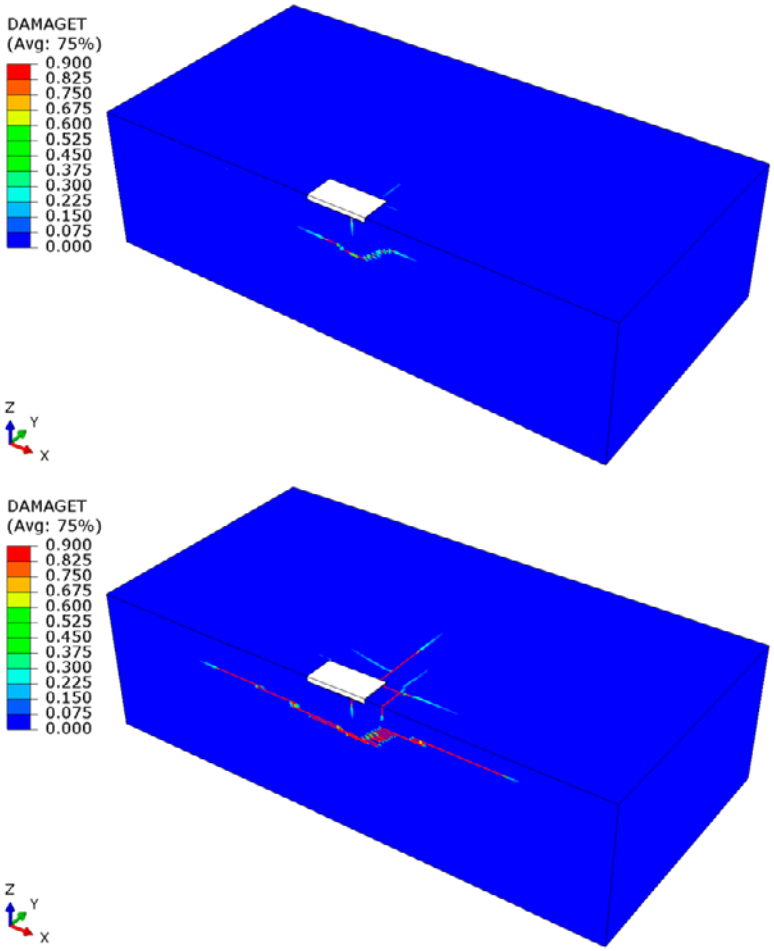

Figure A1-10 Damage tension parameter (DAMAGET) at failure load and at end of simulation for configuration 10 in Table A1-1. Surface reinforcement ϕ12cc200. Eccentricity $\boldsymbol{e} = \mathbf{1}$.

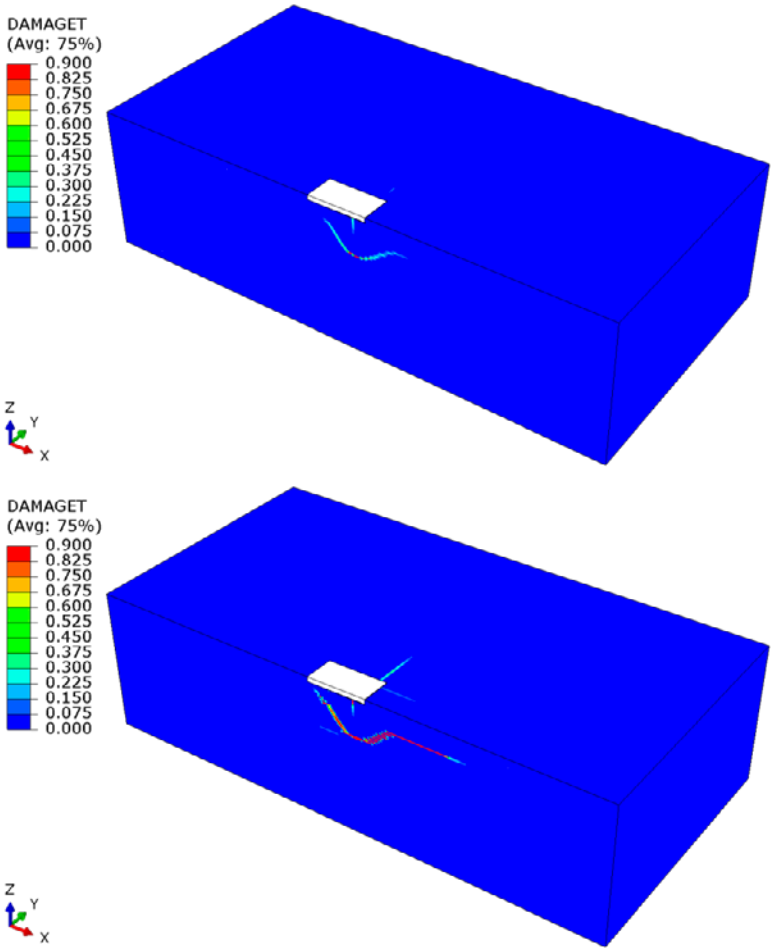

Figure A1-11 Damage tension parameter (DAMAGET) at failure load and at end of simulation for configuration 11 in Table A1-1. Surface reinforcement ϕ12cc200. Eccentricity $\boldsymbol{e} = \mathbf{2}$.

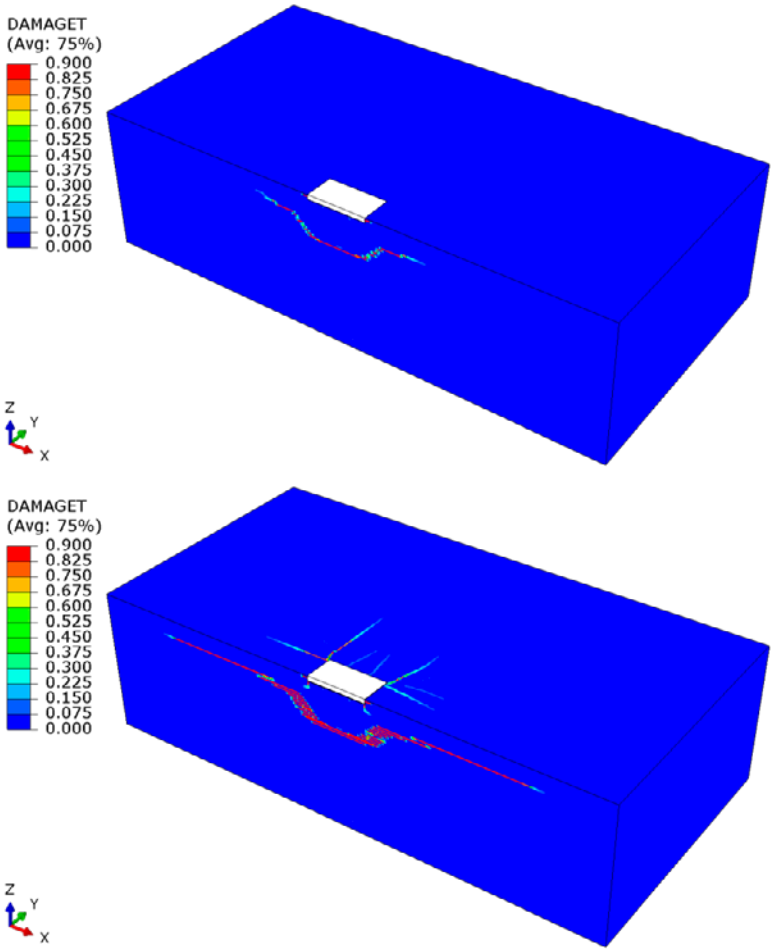

Figure A1-12 Damage tension parameter (DAMAGET) at failure load and at end of simulation for configuration 12 in Table A1-1. Surface reinforcement ϕ12cc100. Eccentricity $\boldsymbol{e} = \mathbf{0}$.

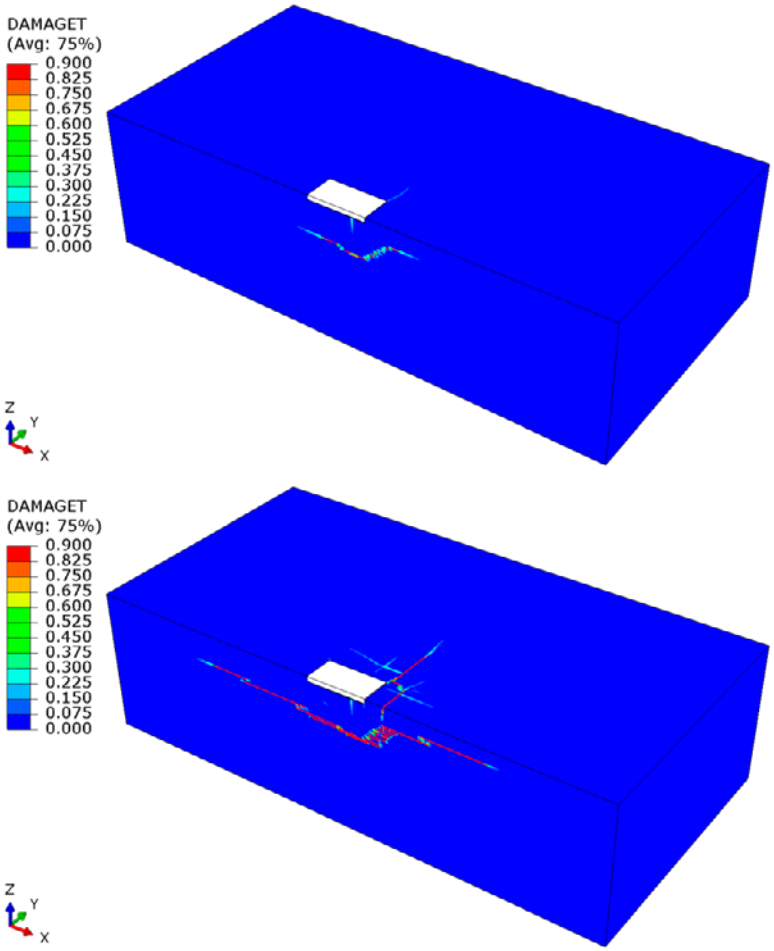

Figure A1-13 Damage tension parameter (DAMAGET) at failure load and at end of simulation for configuration 13 in Table A1-1. Surface reinforcement ϕ12cc100. Eccentricity $\boldsymbol{e} = \mathbf{1}$.

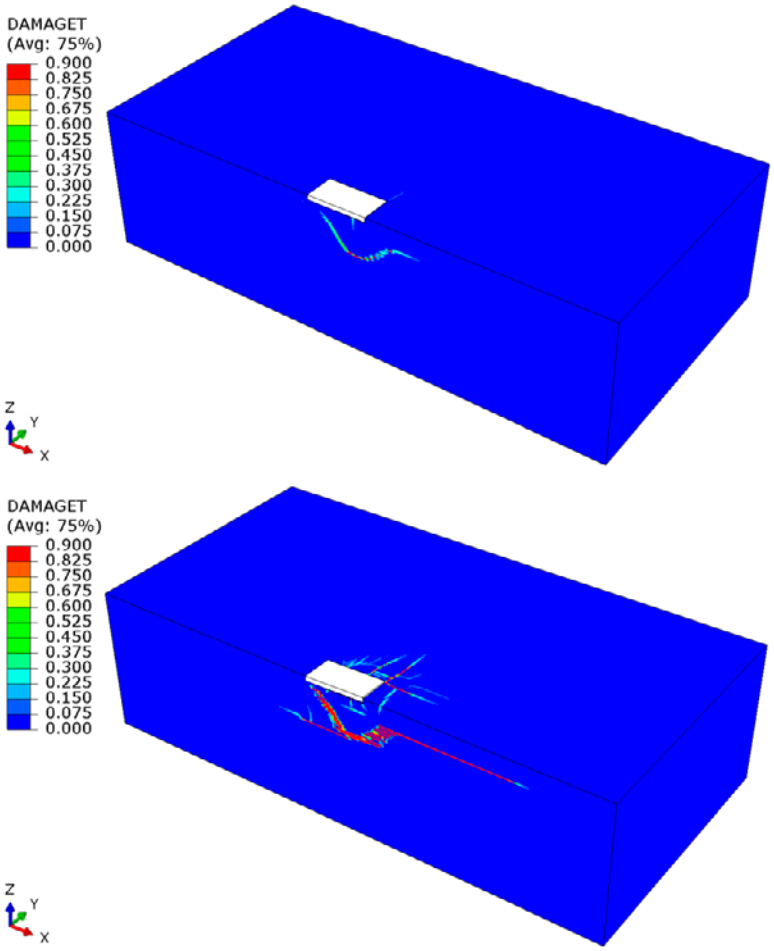

Figure A1-14 Damage tension parameter (DAMAGET) at failure load and at end of simulation for configuration 14 in Table A1-1. Surface reinforcement ϕ12cc100. Eccentricity $\boldsymbol{e} = \mathbf{2}$.

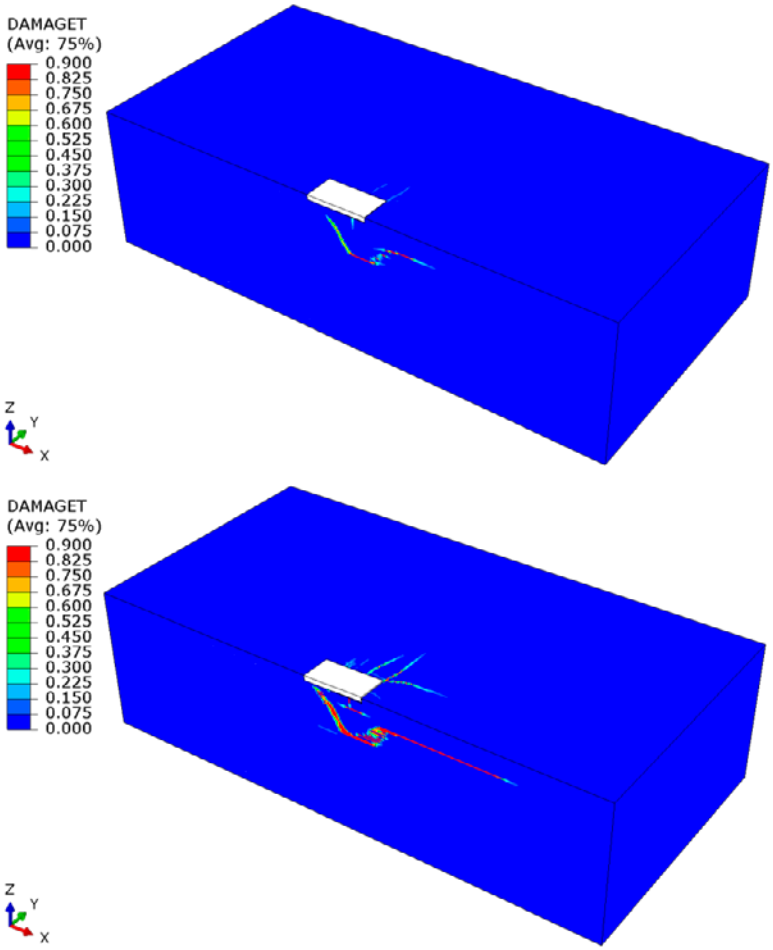

Figure A1-15 Damage tension parameter (DAMAGET) at failure load and at end of simulation for configuration 15 in Table A1-1. Surface reinforcement ϕ12cc100. Eccentricity $\boldsymbol{e} = \mathbf{5}$.

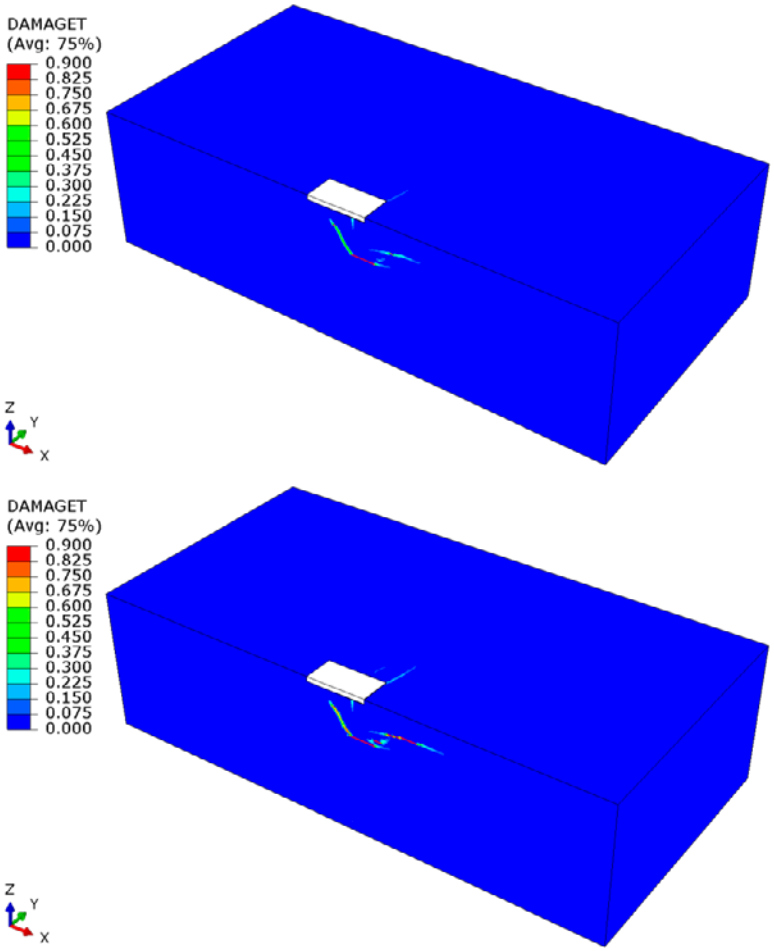

Figure A1-16 Damage tension parameter (DAMAGET) at failure load and at end of simulation for configuration 16 in Table A1-1. Surface reinforcement ϕ12cc100. Eccentricity $\boldsymbol{e = 10}$.

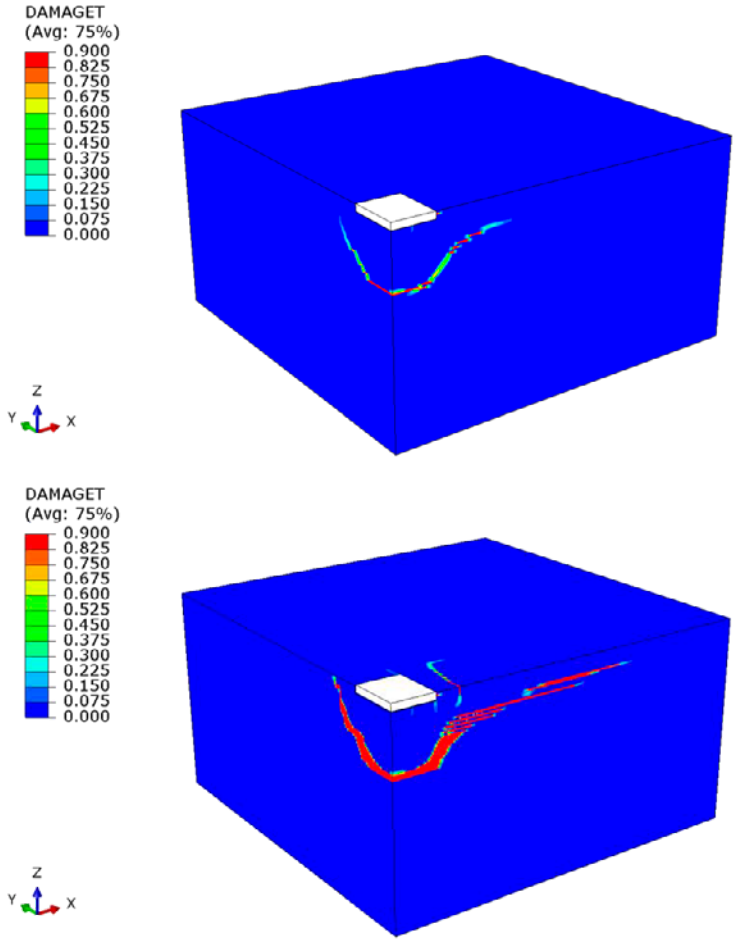

Figure A1-17 Damage tension parameter (DAMAGET) at failure load and at end of simulation for configuration 1 in Table A1-2. No surface reinforcement. Distance from anchors to free concrete edge $c_1 = 75$ mm.

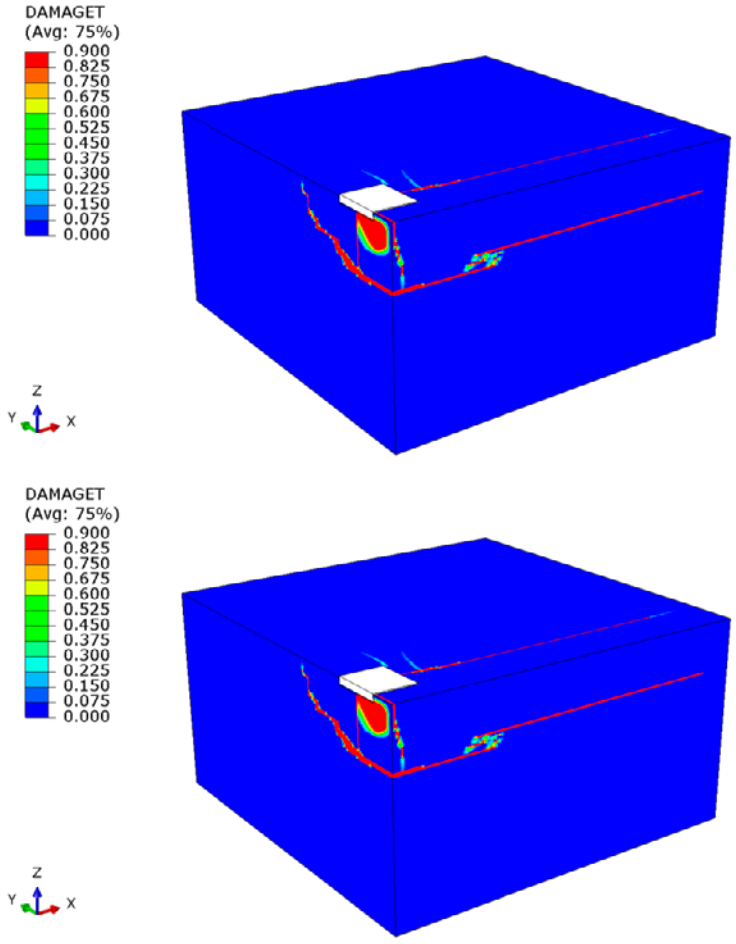

Figure A1-18 Damage tension parameter (DAMAGET) at failure load and at end of simulation for configuration 2 in Table A1-2. No surface reinforcement. Distance from anchors to free concrete edge $c_1 = \mathbf{150}$ mm.

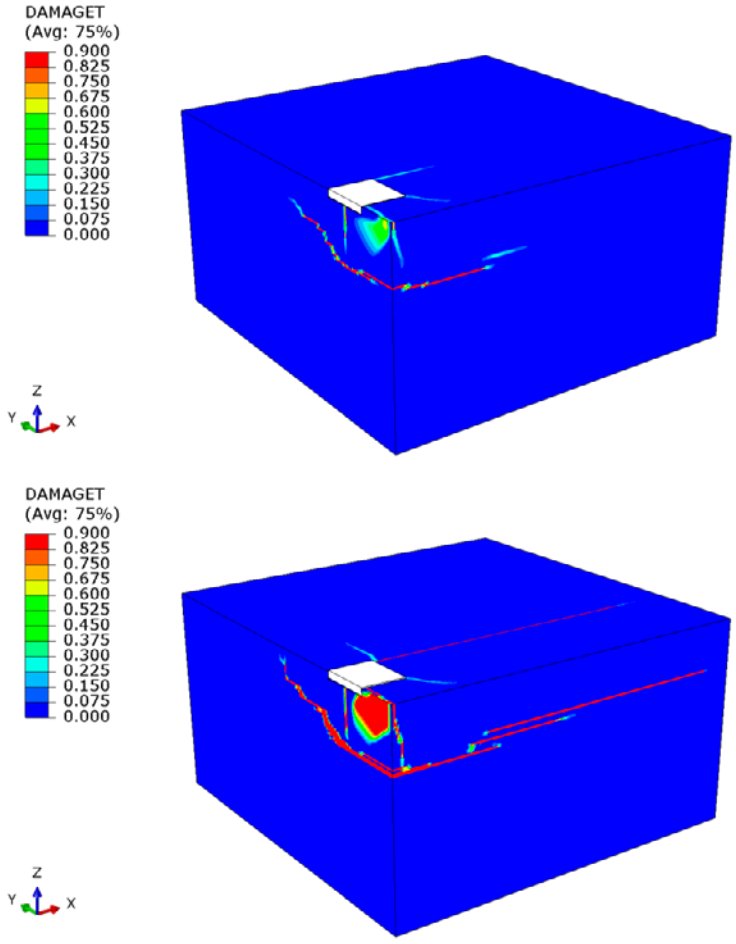

Figure A1-19 Damage tension parameter (DAMAGET) at failure load and at end of simulation for configuration 3 in Table A1-2. No surface reinforcement. Distance from anchors to free concrete edge $c_1 = \mathbf{200}$ mm.

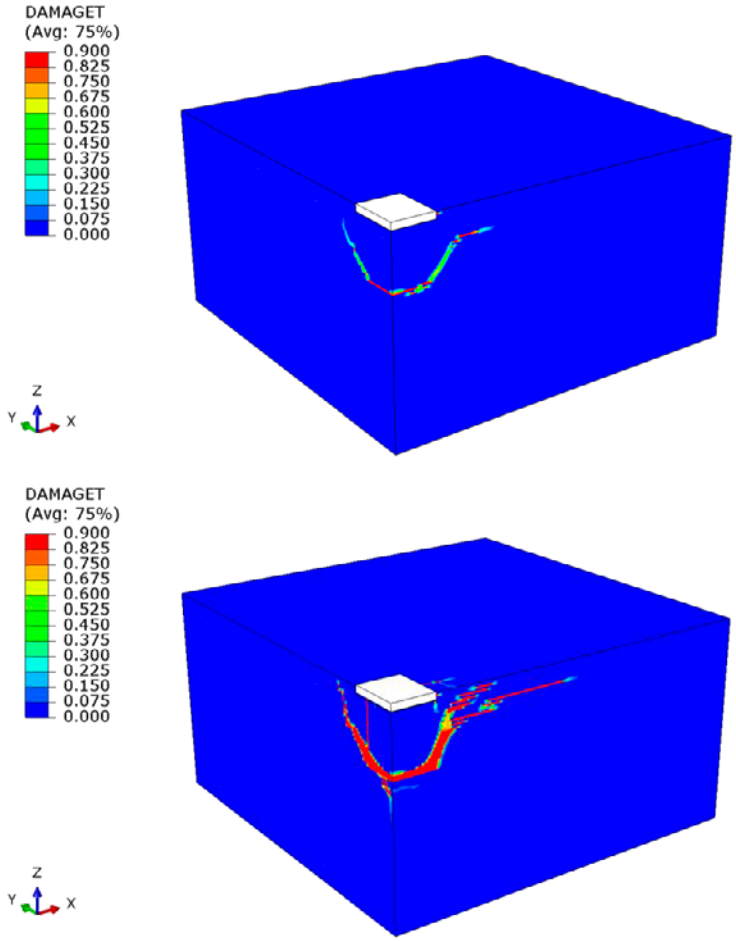

Figure A1-20 Damage tension parameter (DAMAGET) at failure load and at end of simulation for configuration 4 in Table A1-2. Surface reinforcement ϕ12cc300. Distance from anchors to free concrete edge $c_1 = 75$ mm.

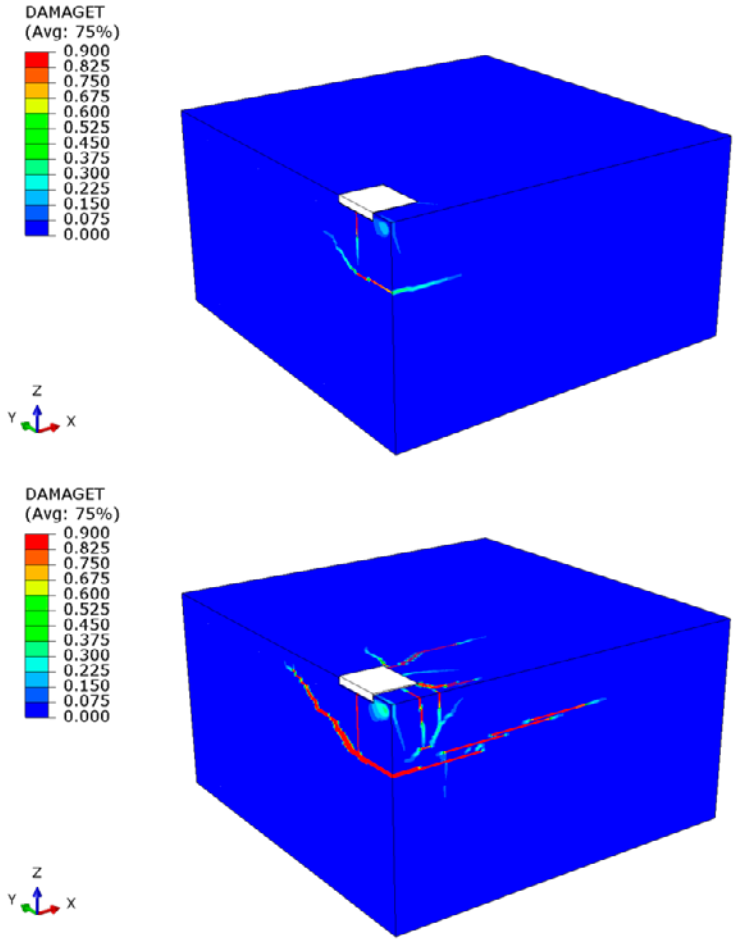

Figure A1-21 Damage tension parameter (DAMAGET) at failure load and at end of simulation for configuration 5 in Table A1-2. Surface reinforcement ϕ12cc300. Distance from anchors to free concrete edge $\boldsymbol{c_1 = 150}$ mm.

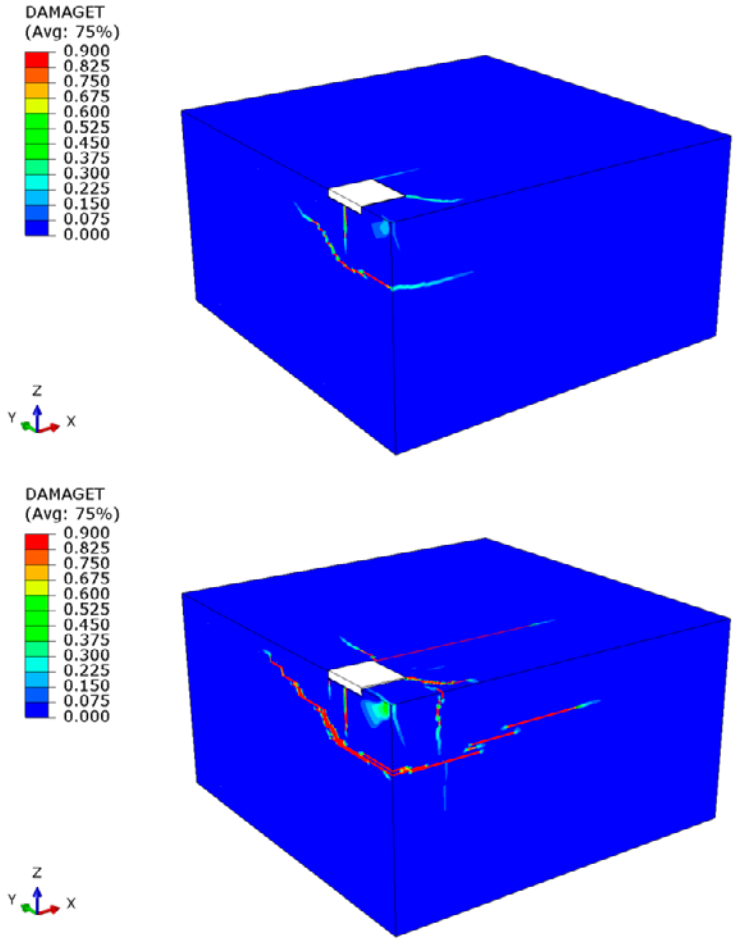

Figure A1-22 Damage tension parameter (DAMAGET) at failure load and at end of simulation for configuration 6 in Table A1-2. Surface reinforcement ϕ12cc300. Distance from anchors to free concrete edge $\boldsymbol{c_1 = 200}$ mm.

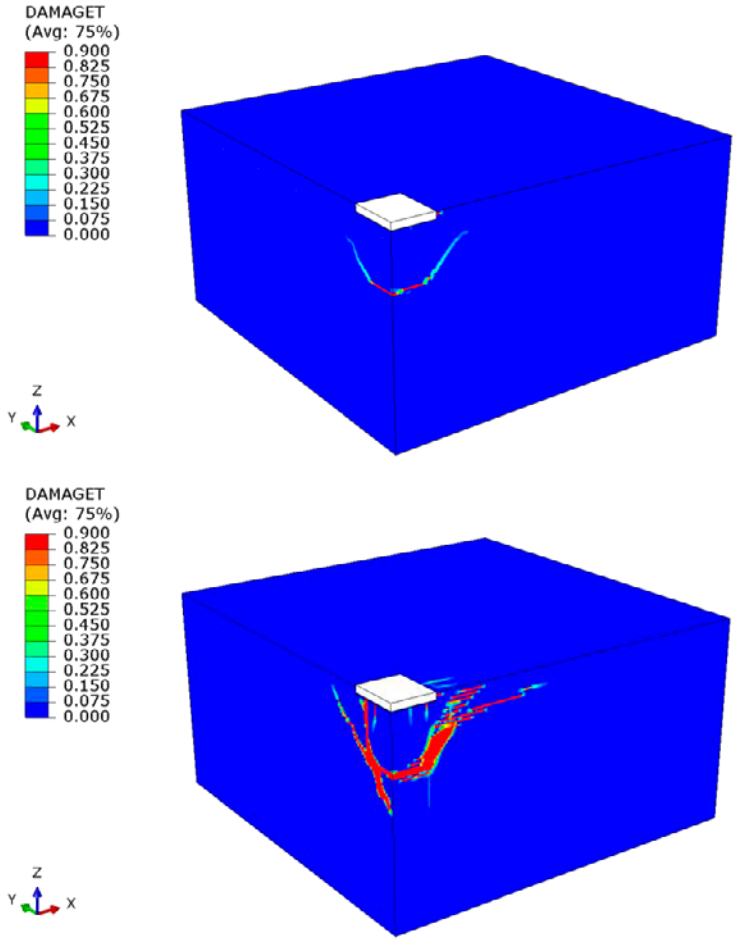

Figure A1-23 Damage tension parameter (DAMAGET) at failure load and at end of simulation for configuration 7 in Table A1-2. Surface reinforcement ϕ12cc200. Distance from anchors to free concrete edge $c_1 = 75$ mm.

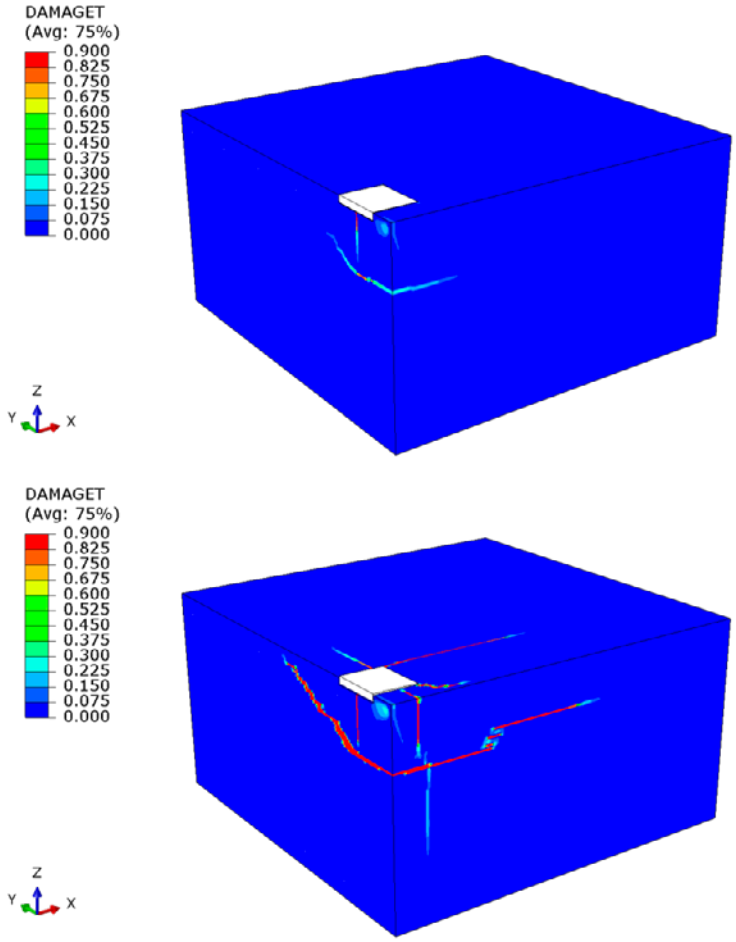

Figure A1-24 Damage tension parameter (DAMAGET) at failure load and at end of simulation for configuration 8 in Table A1-2. Surface reinforcement ϕ12cc200. Distance from anchors to free concrete edge $\boldsymbol{c_1 = 150}$ mm.

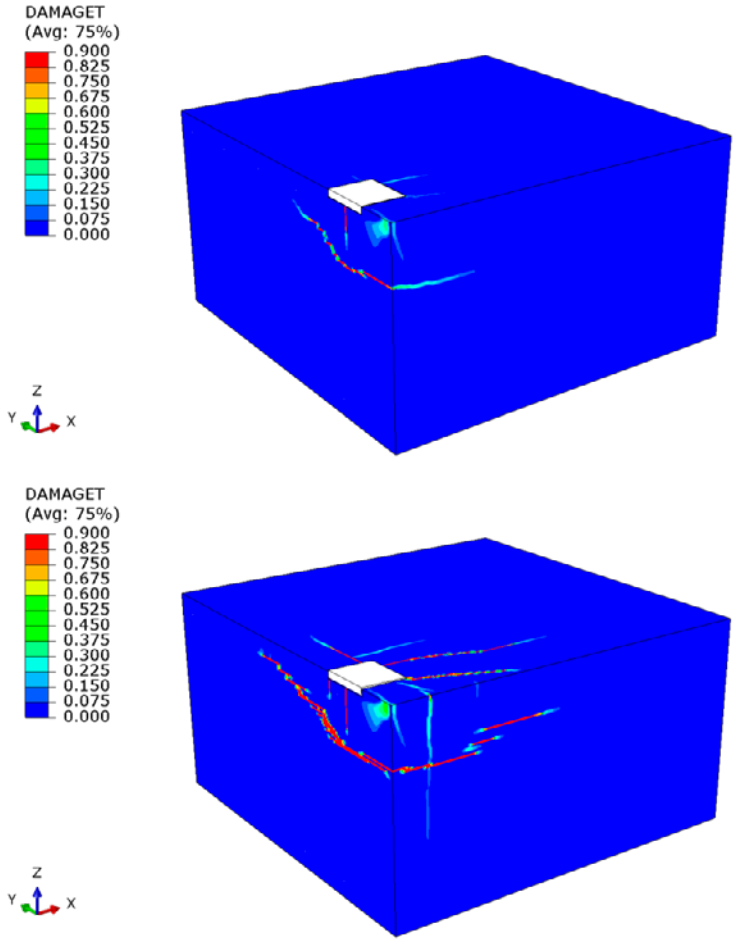

Figure A1-25 Damage tension parameter (DAMAGET) at failure load and at end of simulation for configuration 9 in Table A1-2. Surface reinforcement ϕ12cc200. Distance from anchors to free concrete edge $\boldsymbol{c_1 = 200}$ mm.

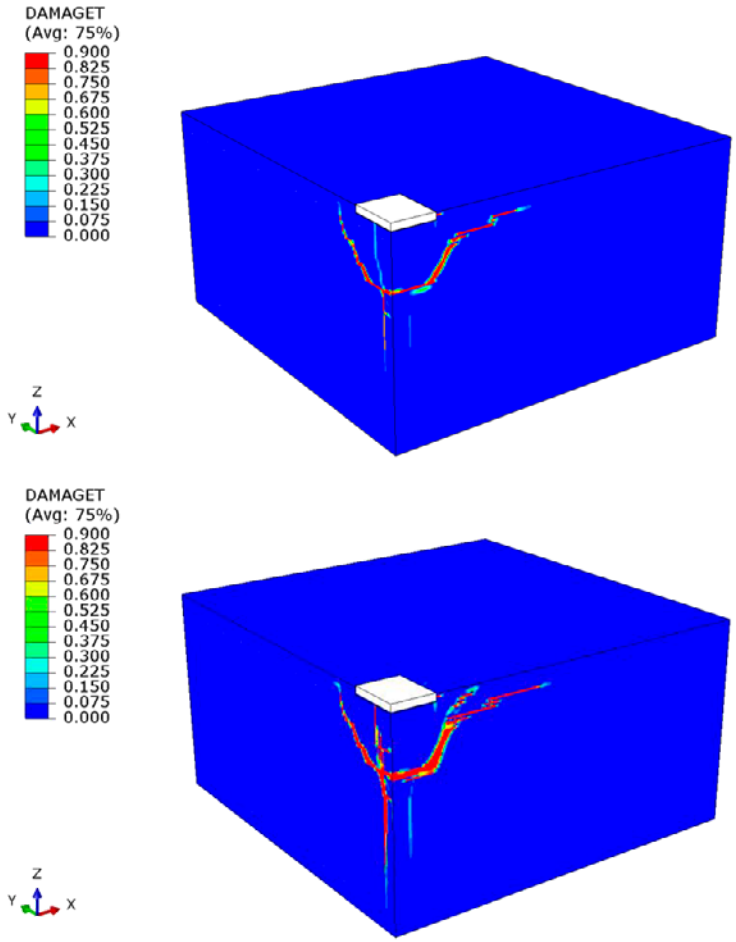

Figure A1-26 Damage tension parameter (DAMAGET) at failure load and at end of simulation for configuration 10 in Table A1-2. Surface reinforcement ϕ12cc100. Distance from anchors to free concrete edge $\boldsymbol{c_1 = 75}$ mm.

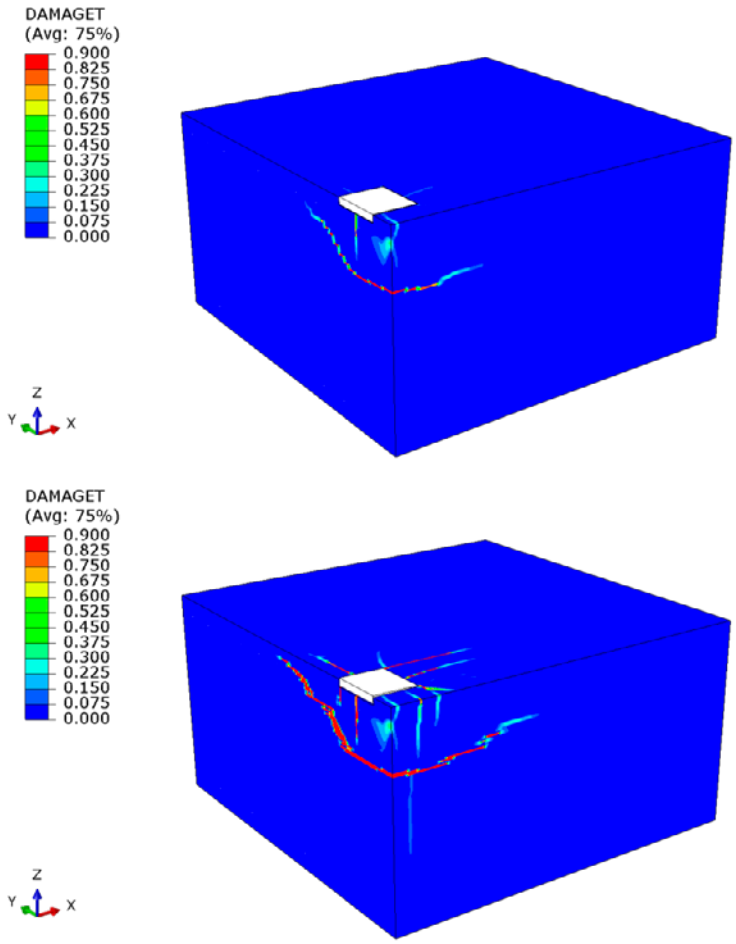

Figure A1-27 Damage tension parameter (DAMAGET) at failure load and at end of simulation for configuration 11 in Table A1-2. Surface reinforcement ϕ12cc100. Distance from anchors to free concrete edge $\boldsymbol{c_1 = 150}$ mm.

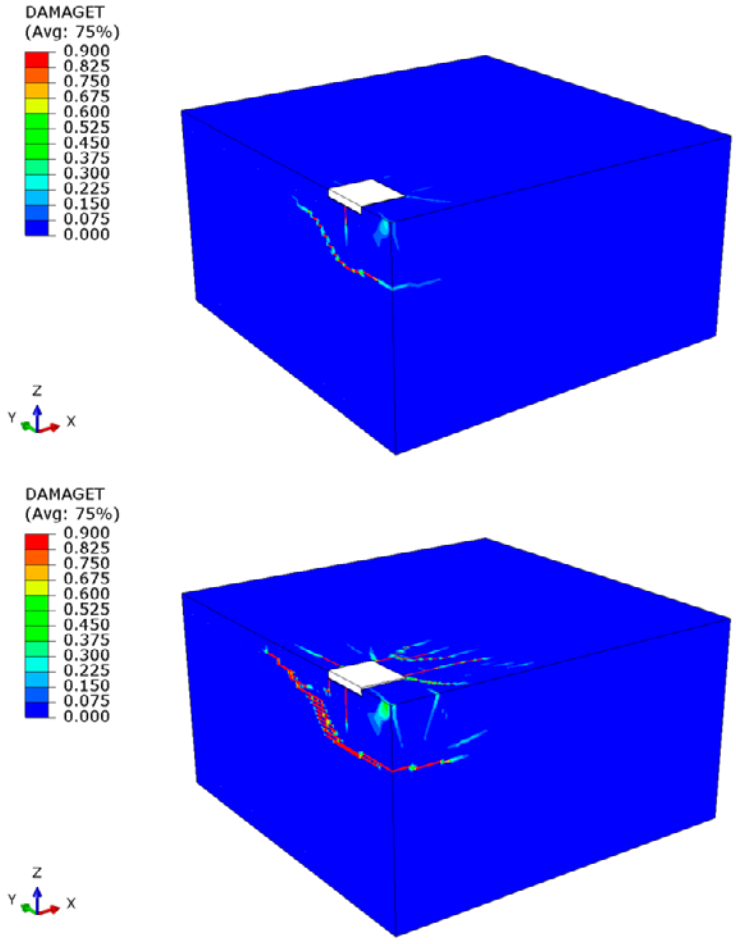

Figure A1-28 Damage tension parameter (DAMAGET) at failure load and at end of simulation for configuration 12 in Table A1-2. Surface reinforcement ϕ12cc100. Distance from anchors to free concrete edge $\boldsymbol{c_1 = 200}$ mm.

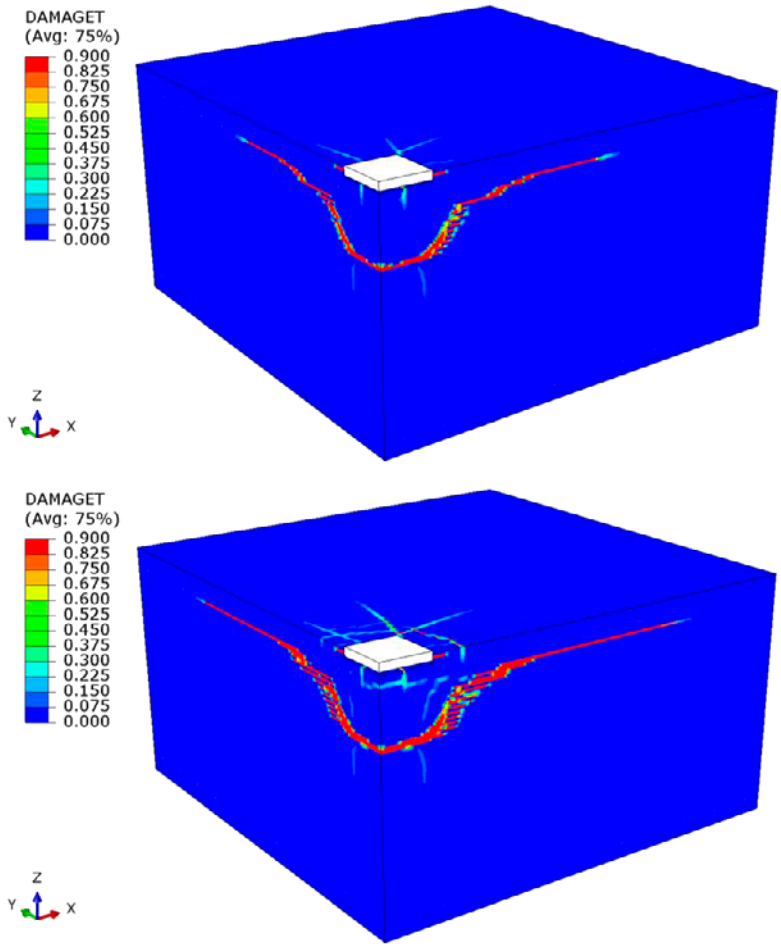

Figure A1-29 Damage tension parameter (DAMAGET) at failure load and at end of simulation for configuration 1 in Table A1-3. Surface reinforcement ϕ12cc100. Four shear reinforcement links with distance from anchors to links $\boldsymbol{a = 0.15h_{ef} = 29.3}$ mm.

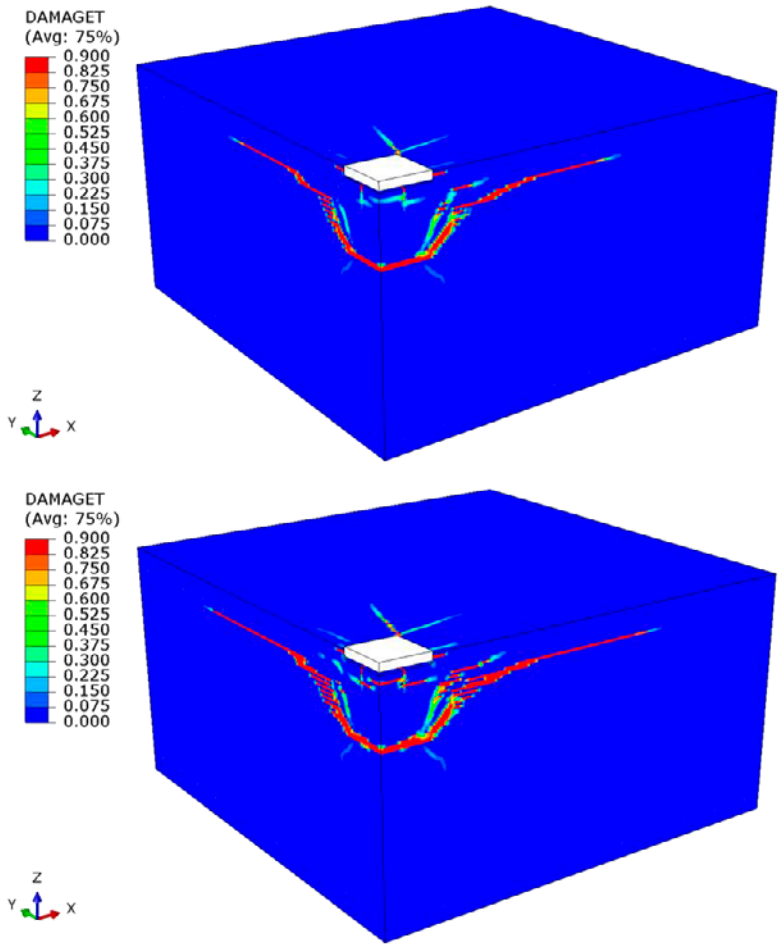

Figure A1-30 Damage tension parameter (DAMAGET) at failure load and at end of simulation for configuration 2 in Table A1-3. Surface reinforcement ϕ12cc100. Four shear reinforcement links with distance from anchors to links $\boldsymbol{a = 0.3h_{ef} = 58.5}$ mm.

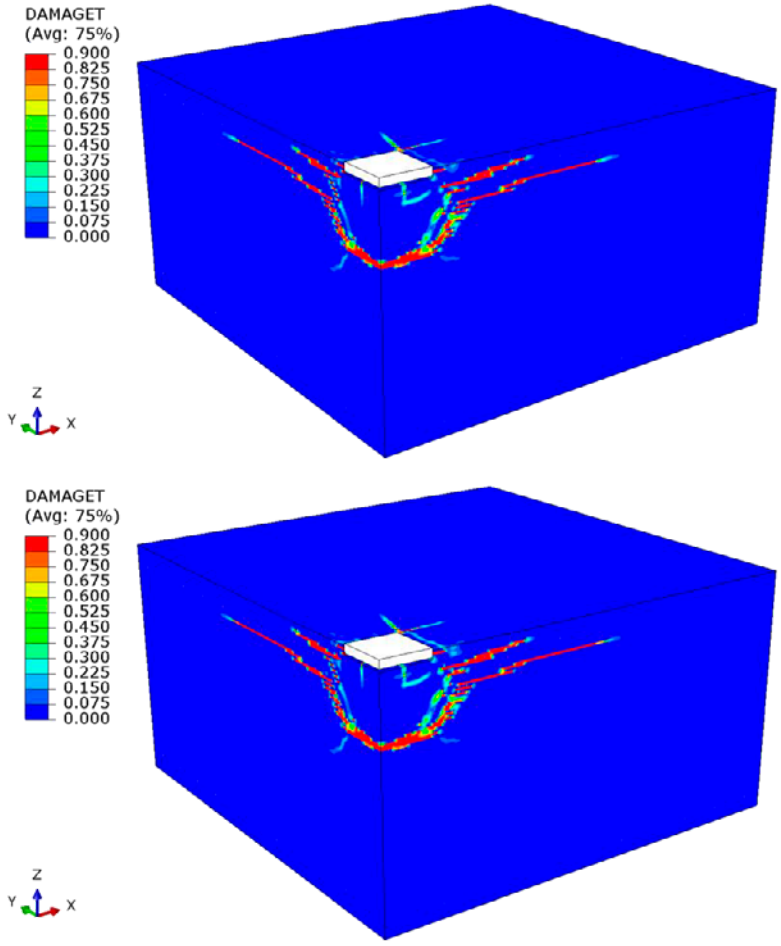

Figure A1-31 Damage tension parameter (DAMAGET) at failure load and at end of simulation for configuration 3 in Table A1-3. Surface reinforcement ϕ12cc100. Four shear reinforcement links with distance from anchors to links $\boldsymbol{a = 0.4h_{ef} = 78.0}$ mm.

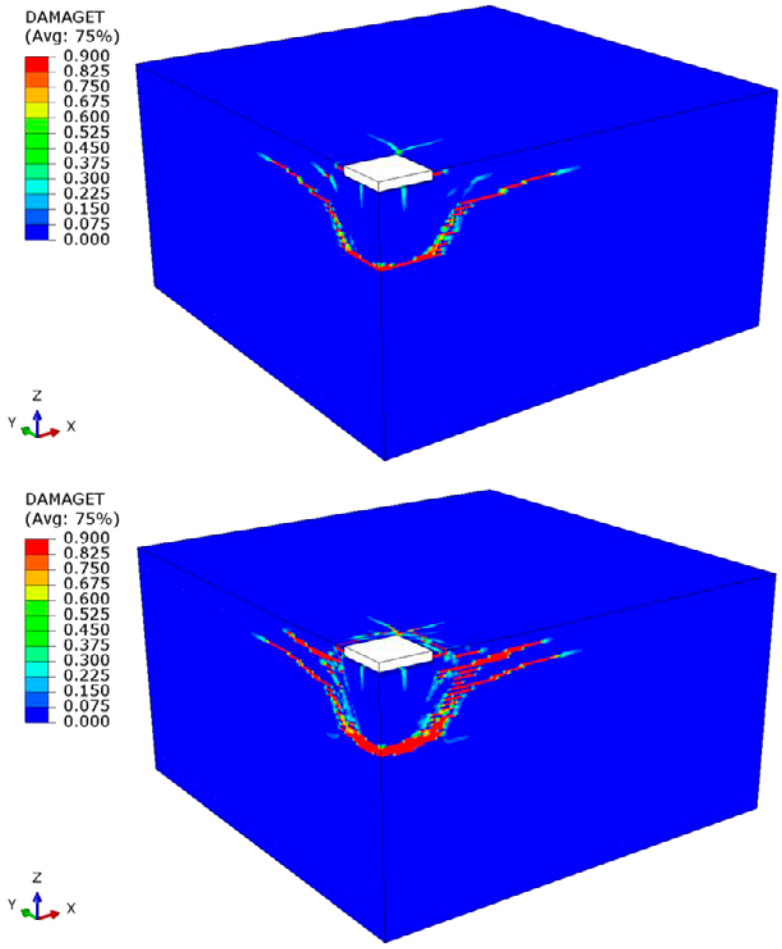

Figure A1-32 Damage tension parameter (DAMAGET) at failure load and at end of simulation for configuration 4 in Table A1-3. Surface reinforcement ϕ12cc100. Four shear reinforcement links with distance from anchors to links $\boldsymbol{a = 0.5h_{ef} = 97.5}$ mm.

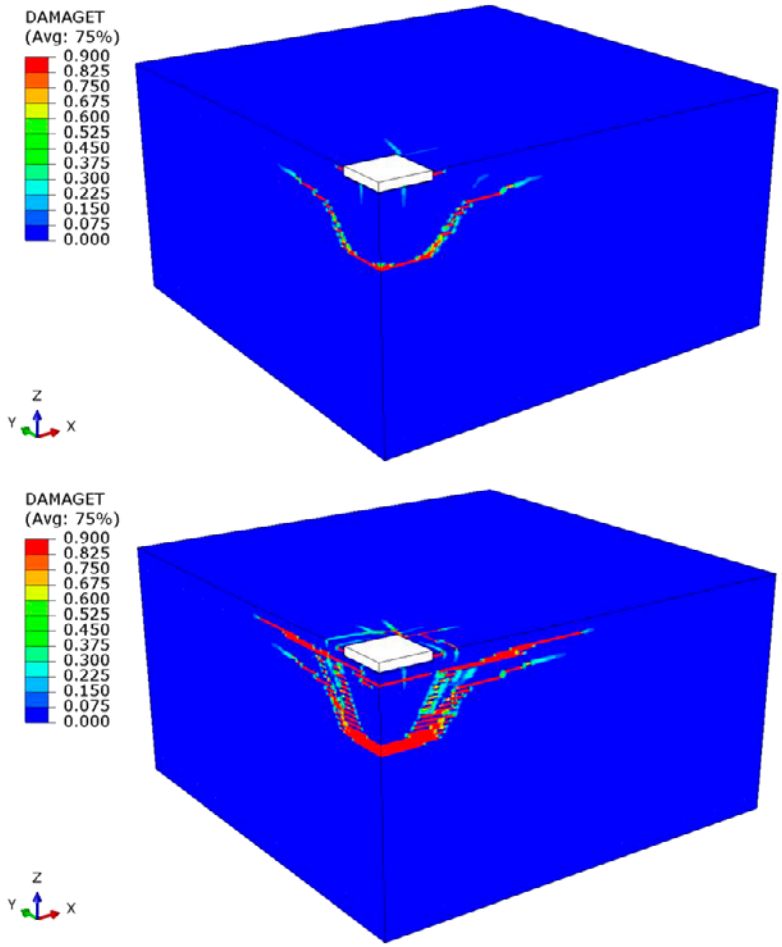

Figure A1-33 Damage tension parameter (DAMAGET) at failure load and at end of simulation for configuration 5 in Table A1-3. Surface reinforcement ϕ12cc100. Four shear reinforcement links with distance from anchors to links $\boldsymbol{a = 0.625 h_{ef} = 121.9}$ mm.

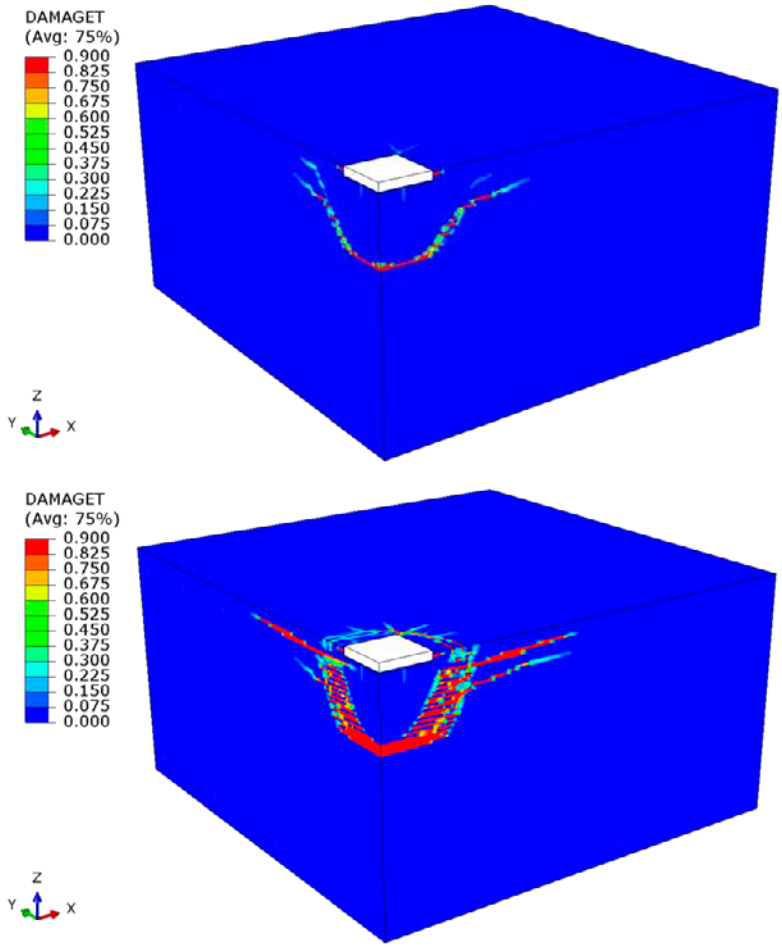

Figure A1-34 Damage tension parameter (DAMAGET) at failure load and at end of simulation for configuration 6 in Table A1-3. Surface reinforcement ϕ12cc100. Four shear reinforcement links with distance from anchors to links $\boldsymbol{a = 0.75h_{ef} = 146.3}$ mm.

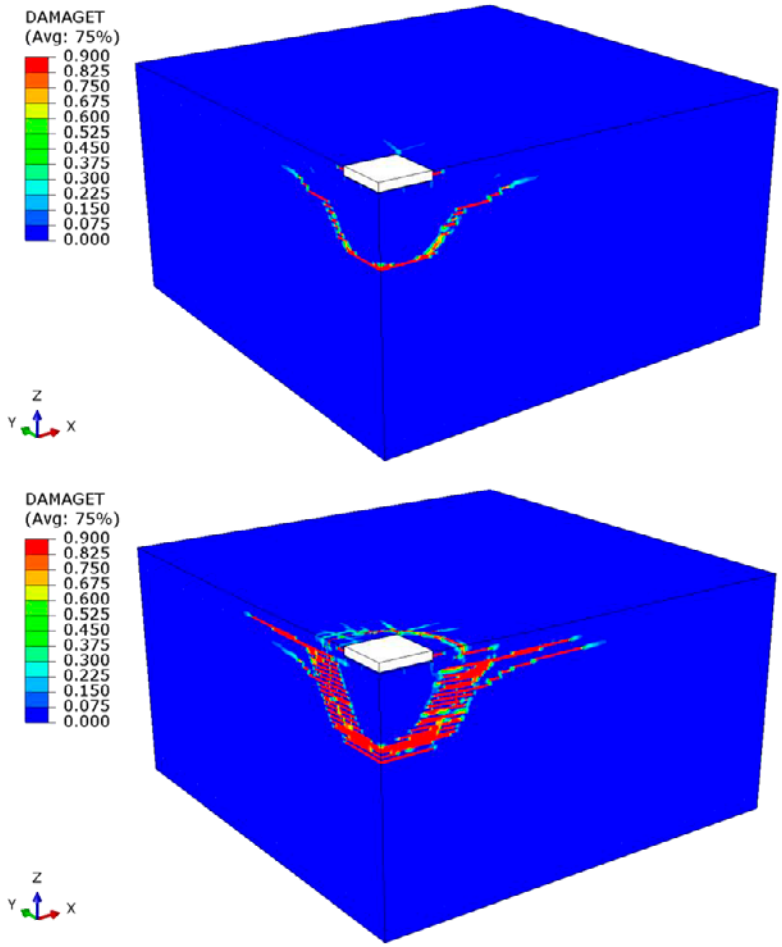

Figure A1-35 Damage tension parameter (DAMAGET) at failure load and at end of simulation for configuration 7 in Table A1-3. Surface reinforcement ϕ12cc100. Four shear reinforcement links with distance from anchors to links $\boldsymbol{a = 1.0 h_{ef} = 195}$ mm.

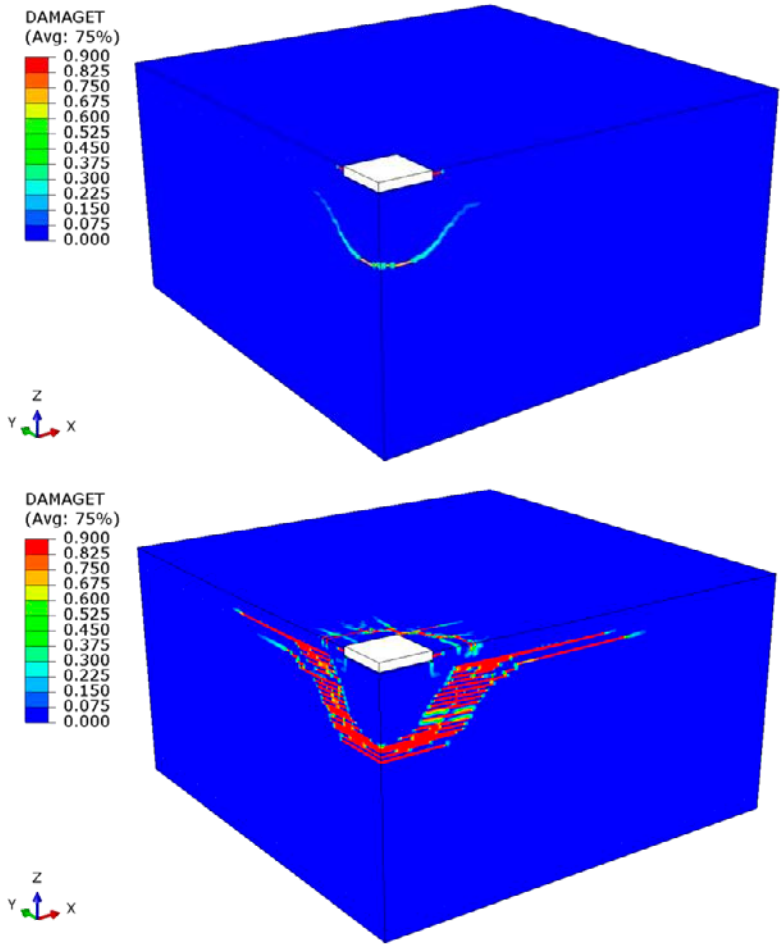

Figure A1-36 Damage tension parameter (DAMAGET) at failure load and at end of simulation for configuration 8 in Table A1-3. Surface reinforcement ϕ12cc100. Four shear reinforcement links with distance from anchors to links $\boldsymbol{a = 1.25h_{ef} = 243.8}$ mm.

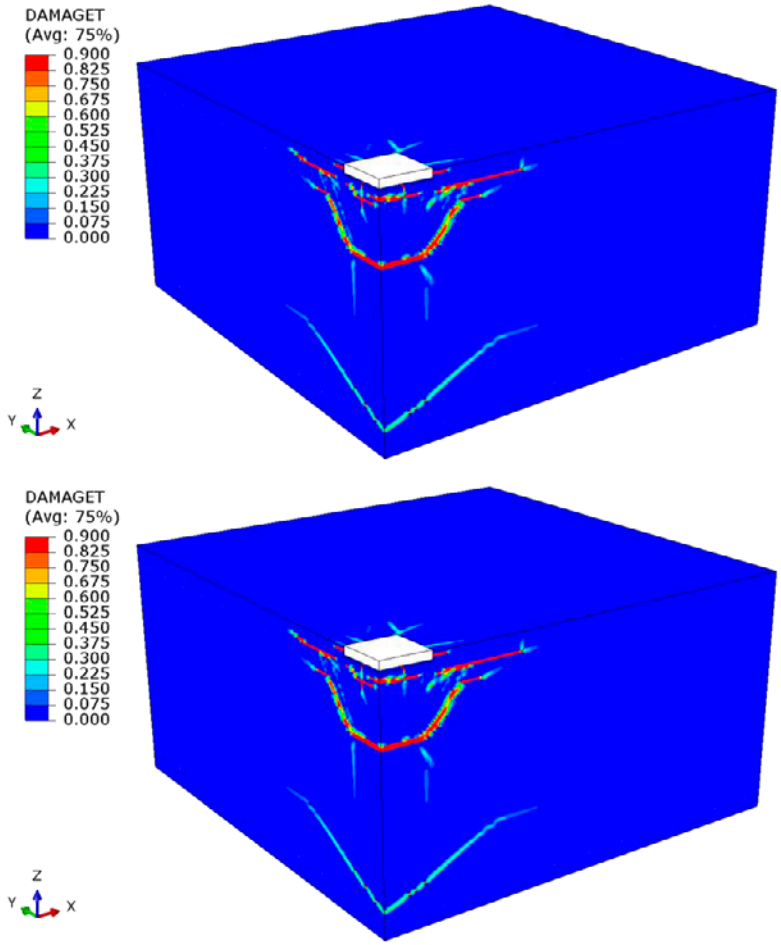

Figure A1-37 Damage tension parameter (DAMAGET) at failure load and at end of simulation for configuration 1 in Table A1-4. Surface reinforcement ϕ12cc100. 16 shear reinforcement links located at $\boldsymbol{a/h_{ef}} = \{\mathbf{0.15}, \mathbf{0.5}, \mathbf{0.85}, \mathbf{1.2}\}$.

APPENDIX 2

Extended result figures regarding numerical simulation of anchors loaded in shear

In this Appendix, figures with the damage tension parameter (DAMAGET) are presented at time of failure load and at end of simulation for single anchors and a group of four anchors, far from concrete edges and loaded in shear. Single anchor configurations and anchor group configurations are summarised in Table A2-1 and Table A2-2, respectively.

Table A2-1 Summary of results from numerical simulations of single anchors.

No.	Surface reinforcement	$V_{u,simulation}$ [kN]
1	-	206.3
2	ϕ12cc200	205.4
3	ϕ12cc100	218.1
4	ϕ16cc200	207.2
5	ϕ16cc100	237.9

Table A2-2 Summary of results from numerical simulations of a group of four anchors.

No.	Surface reinforcement	$V_{u,simulation}$ [kN]
1	-	676.8
2	ϕ12cc300	698.7
3	ϕ12cc150	702.9
4	ϕ12cc100	688.7
5	ϕ16cc300	713.6
6	ϕ16cc150	702.0
7	ϕ16cc100	690.8

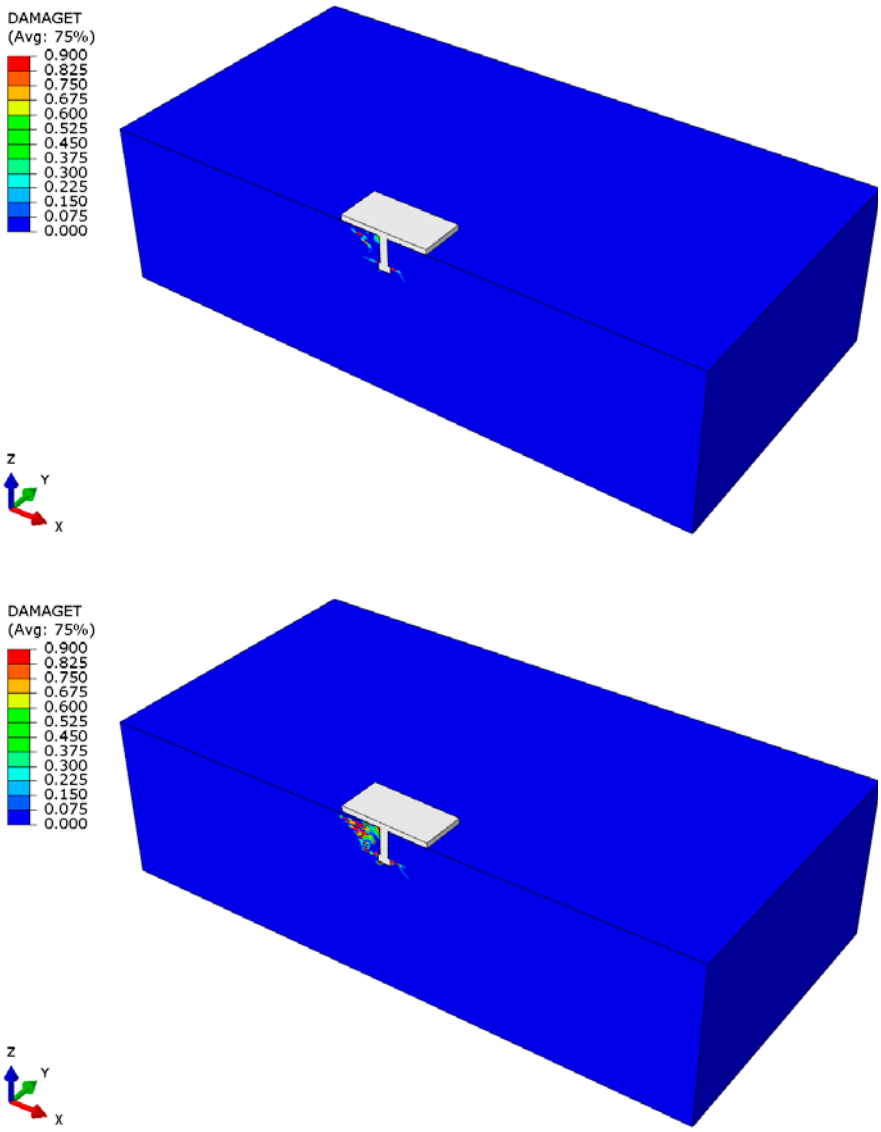

Figure A2-1 Damage tension parameter (DAMAGET) at failure load and at end of simulation for configuration 1 in Table A2-1 (no reinforcement). The X-Z plane is a symmetry plane.

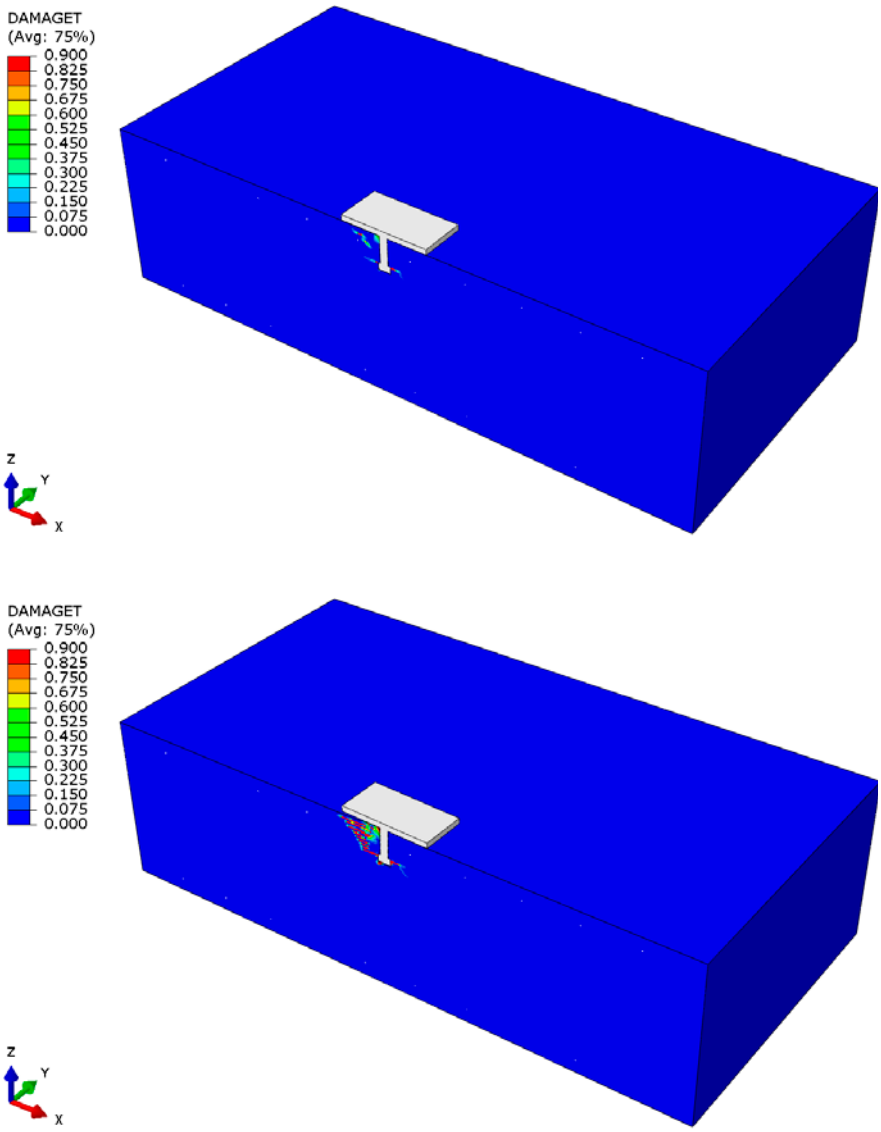

Figure A2-2 Damage tension parameter (DAMAGET) at failure load and at end of simulation for configuration 2 in Table A2-1 (ϕ12cc200). The X-Z plane is a symmetry plane.

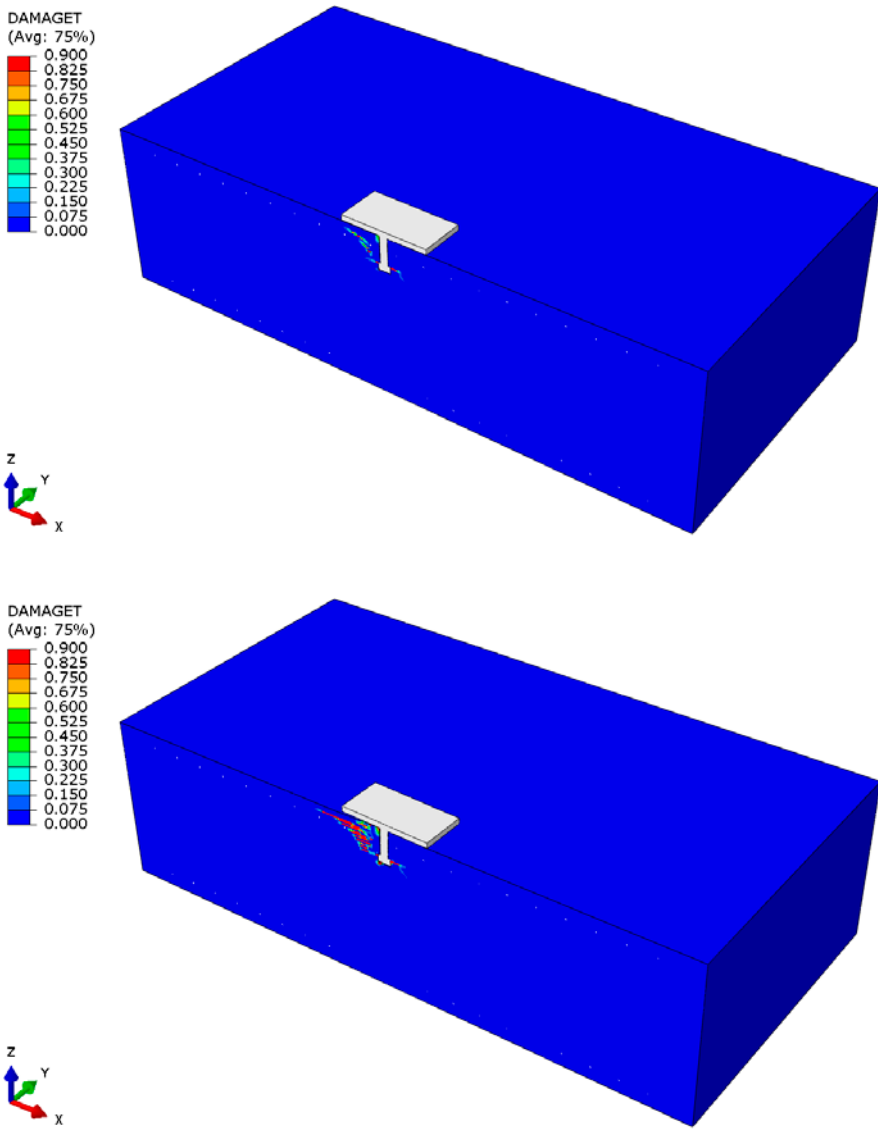

Figure A2-3 Damage tension parameter (DAMAGET) at failure load and at end of simulation for configuration 3 in Table A2-1 (ϕ12cc100). The X-Z plane is a symmetry plane.

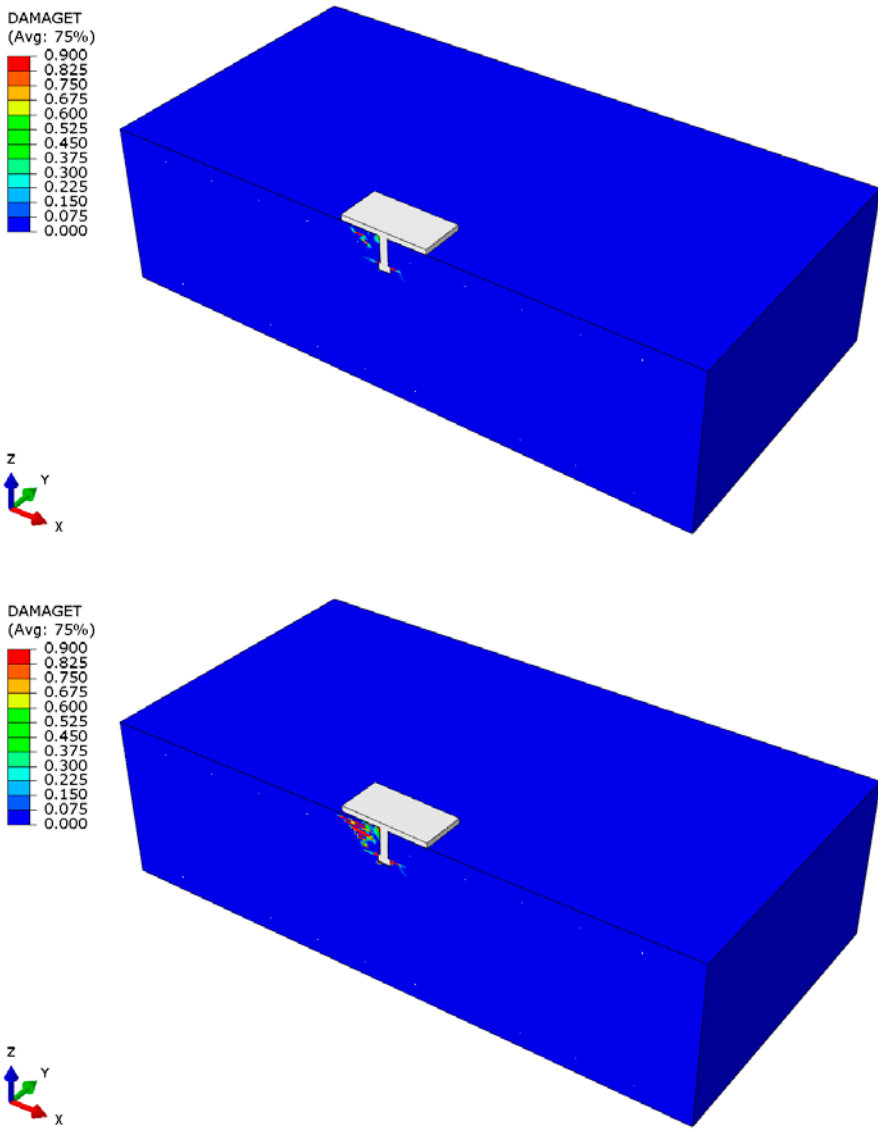

Figure A2-4 Damage tension parameter (DAMAGET) at failure load and at end of simulation for configuration 4 in Table A2-1 (ϕ16cc200). The X-Z plane is a symmetry plane.

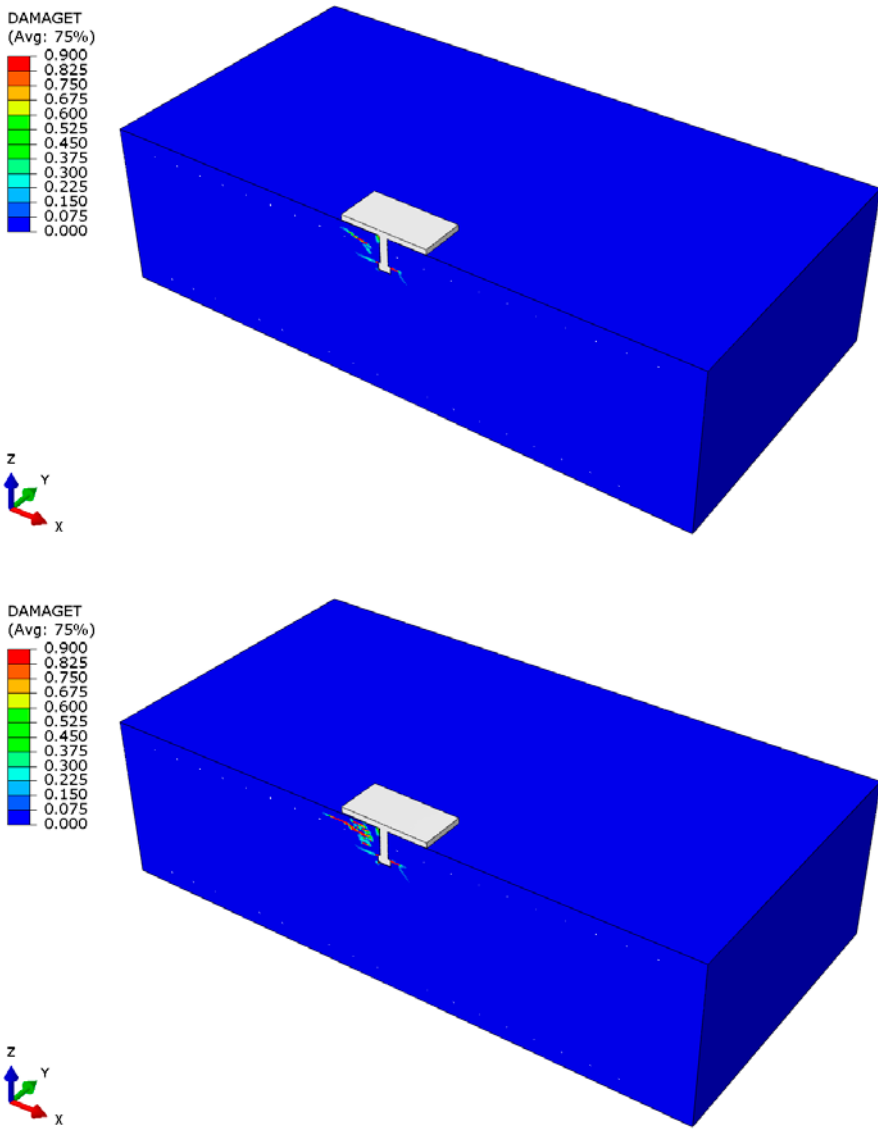

Figure A2-5 Damage tension parameter (DAMAGET) at failure load and at end of simulation for configuration 5 in Table A2-1 (ϕ16cc100). The X-Z plane is a symmetry plane.

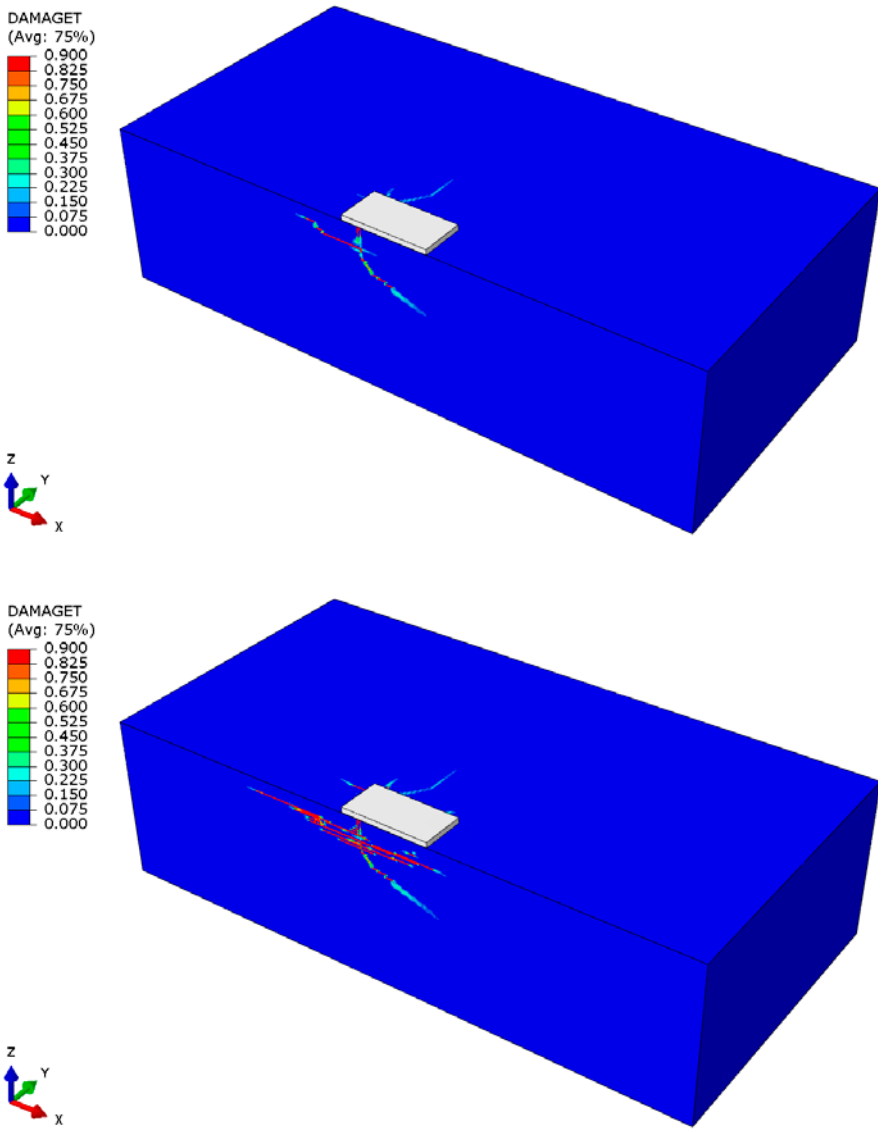

Figure A2-6 Damage tension parameter (DAMAGET) at failure load and at end of simulation for configuration 1 in Table A2-2 (no reinforcement). The X-Z plane is a symmetry plane.

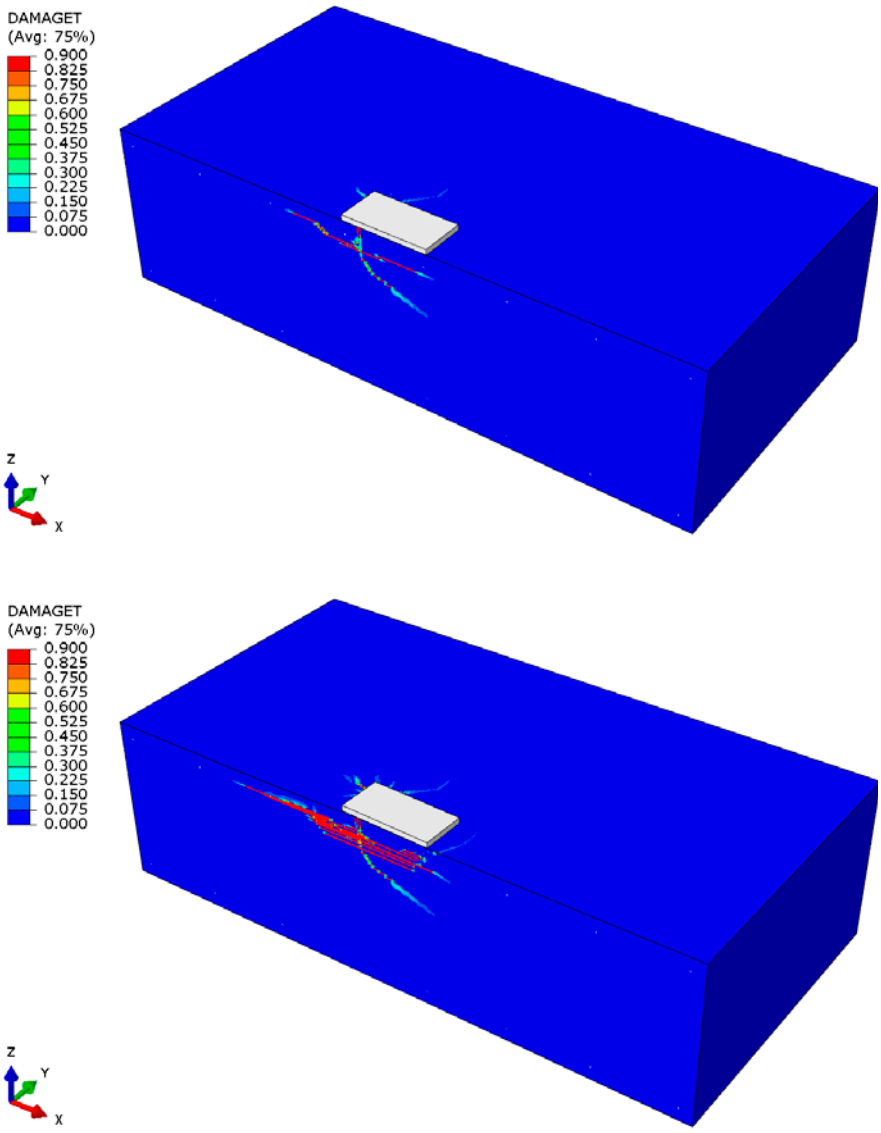

Figure A2-7 Damage tension parameter (DAMAGET) at failure load and at end of simulation for configuration 2 in Table A2-2 (ϕ12cc300). The X-Z plane is a symmetry plane.

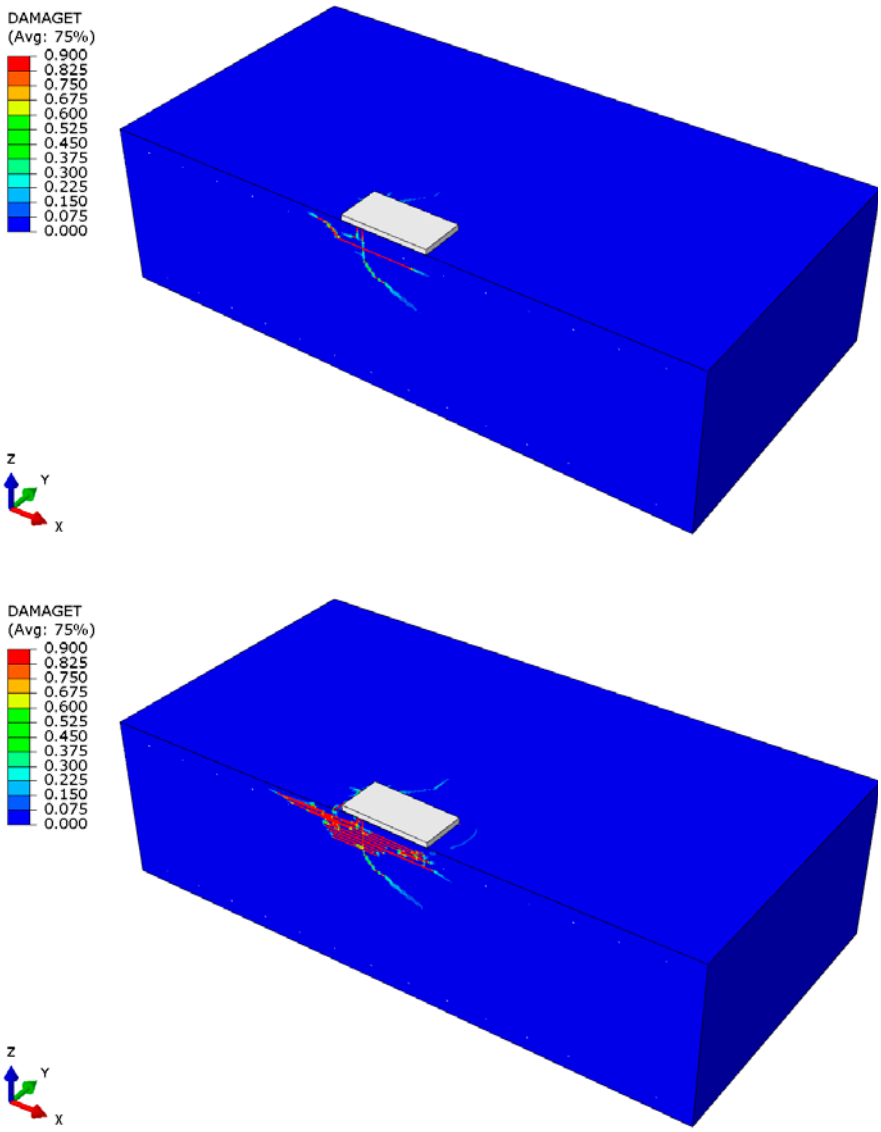

Figure A2-8 Damage tension parameter (DAMAGET) at failure load and at end of simulation for configuration 3 in Table A2-2 (ϕ12cc150). The X-Z plane is a symmetry plane.

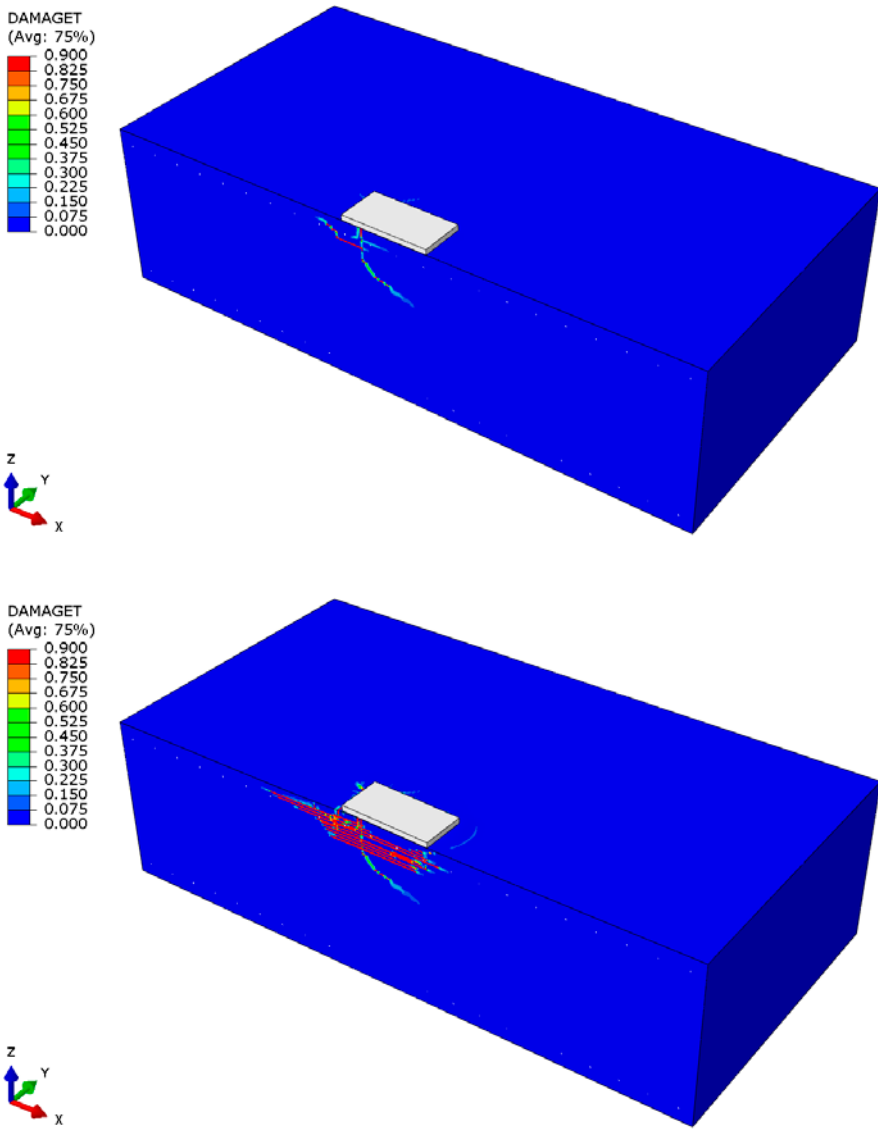

Figure A2-9 Damage tension parameter (DAMAGET) at failure load and at end of simulation for configuration 4 in Table A2-2 (ϕ12cc100). The X-Z plane is a symmetry plane.

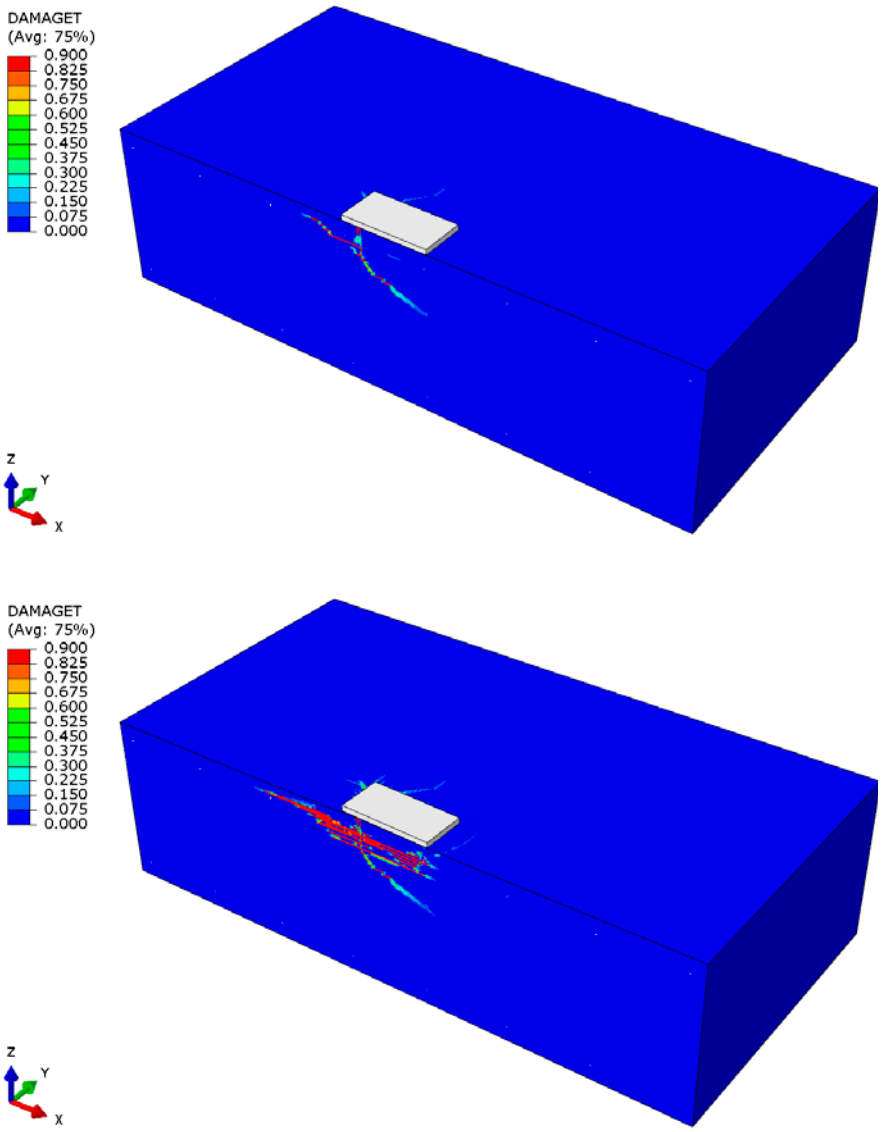

Figure A2-10 Damage tension parameter (DAMAGET) at failure load and at end of simulation for configuration 5 in Table A2-2 (ϕ16cc300). The X-Z plane is a symmetry plane.

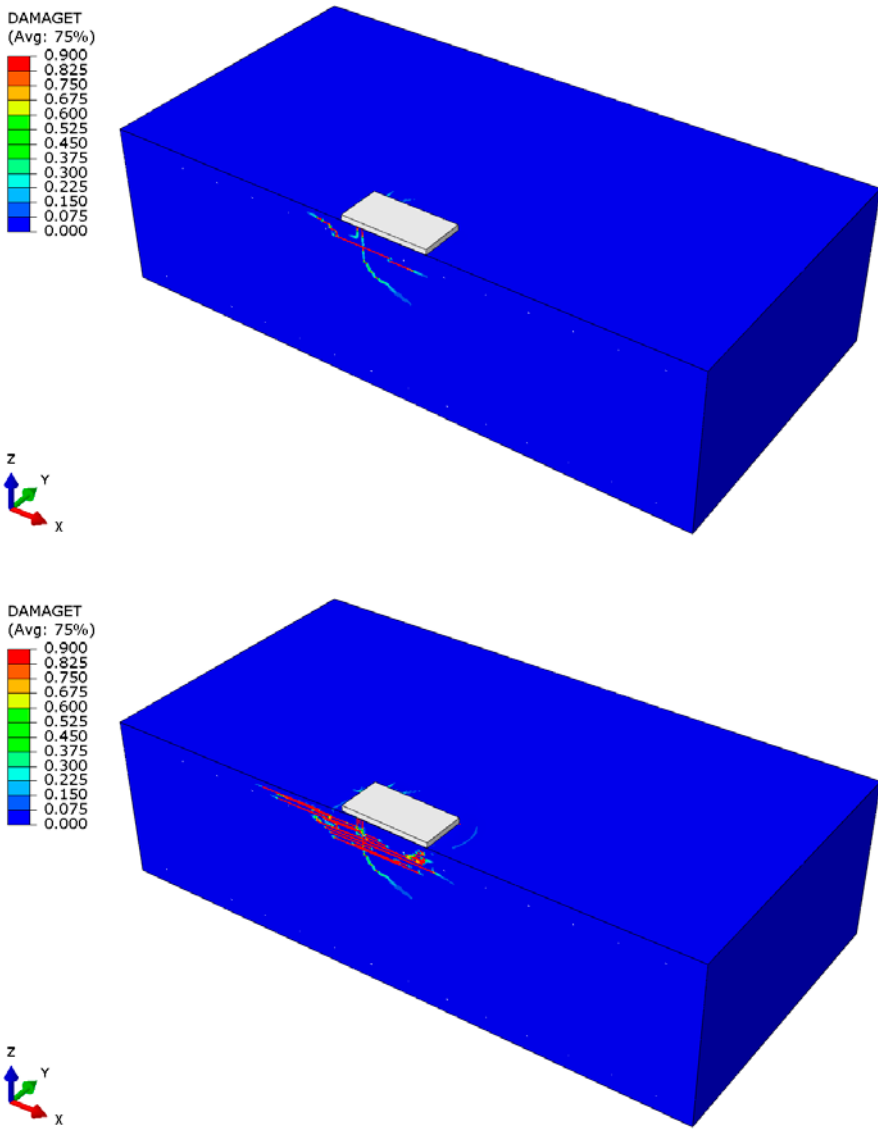

Figure A2-11 Damage tension parameter (DAMAGET) at failure load and at end of simulation for configuration 6 in Table A2-2 (ϕ16cc150). The X-Z plane is a symmetry plane.

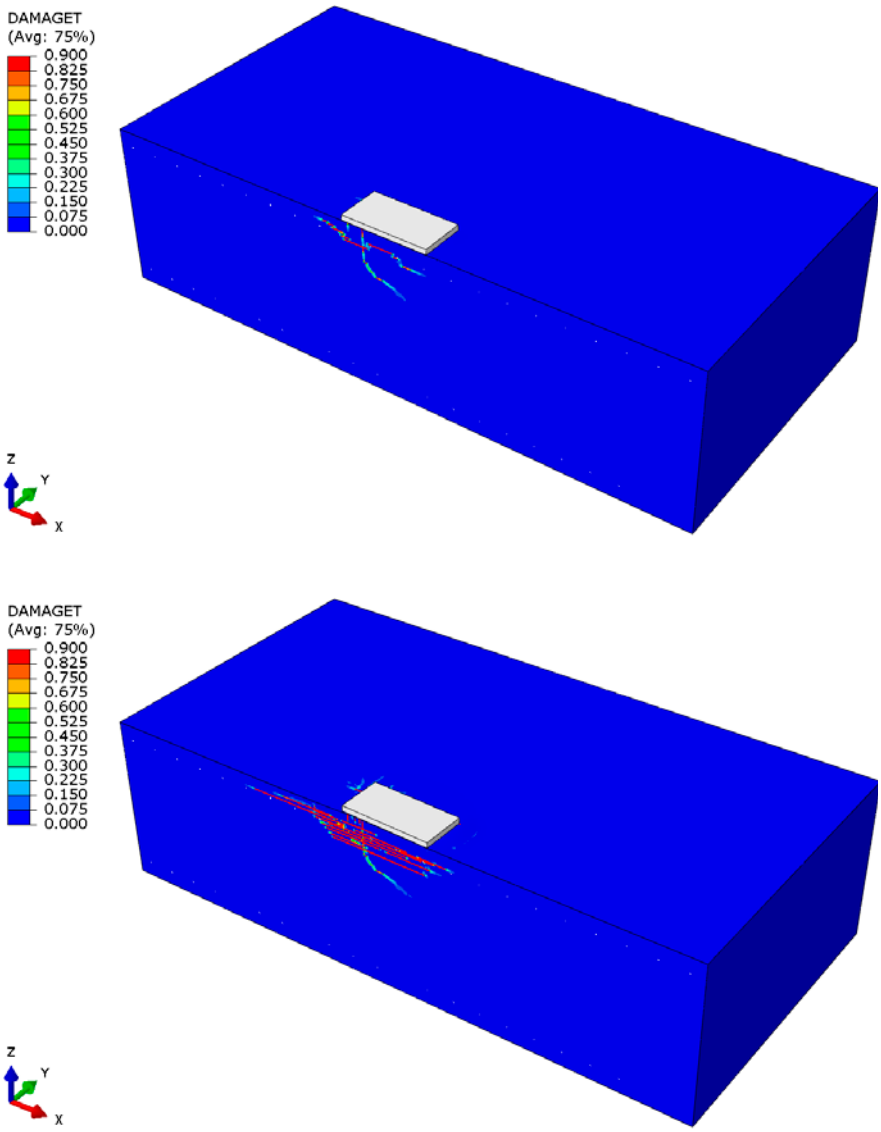

Figure A2-12 Damage tension parameter (DAMAGET) at failure load and at end of simulation for configuration 7 in Table A2-2 (ϕ16cc100). The X-Z plane is a symmetry plane.

APPENDIX 3

Extended result figures regarding numerical simulation of anchors loaded in tension and shear

In this Appendix, figures with the damage tension parameter (DAMAGET) are presented at time of maximum tension load and at time of maximum shear load for a group of four anchors loaded in tension and shear. The anchors embedment depth is h_{ef} = 100 mm. The configurations of centrically loaded anchor plates are summarised in table A3-1 and eccentrically loaded anchor plates in Table A3-2.

Table A3-1 Summary of results from numerical simulations of centrically loaded anchor plates.

No.	Model setup	$N_{u,simulation}$ [kN]	$V_{u,simulation}$ [kN]
1	u1=25 mm/s & u3=75 mm/s	193.2	312.9
2	u1=25 mm/s & u3=50 mm/s	156.5	400.5
3	u1=25 mm/s & u3=25 mm/s	100.5	563.3
4	u1=25 mm/s & u3=12.5 mm/s	37.7	680.1
5	u1=25 mm/s & u3=50 mm/s, ϕ16cc300	168.3	395.7
6	u1=25 mm/s & u3=50 mm/s, ϕ16cc150	164.8	356.2
7	u1=25 mm/s & u3=50 mm/s, ϕ16cc100	168.9	358.8

Table A3-2 Summary of results from numerical simulations of eccentrically loaded anchor plates.

No.	Model setup	$N_{u,simulation}$ [kN]	$V_{u,simulation}$ [kN]
1	e1, u1=25 mm/s & u3=50 mm/s	80.3	501.6
2	e1, u1=25 mm/s & u3=50 mm/s, ϕ16cc100	90.0	504.7
3	e2, u1=25 mm/s & u3=100 mm/s	82.1	374.2
4	e2, u1=25 mm/s & u3=100 mm/s, ϕ16cc100	77.3	365.8
5	e5, u1=25 mm/s & u3=250 mm/s	47.2	354.8
6	e5, u1=25 mm/s & u3=250 mm/s, ϕ16cc100	45.4	352.3

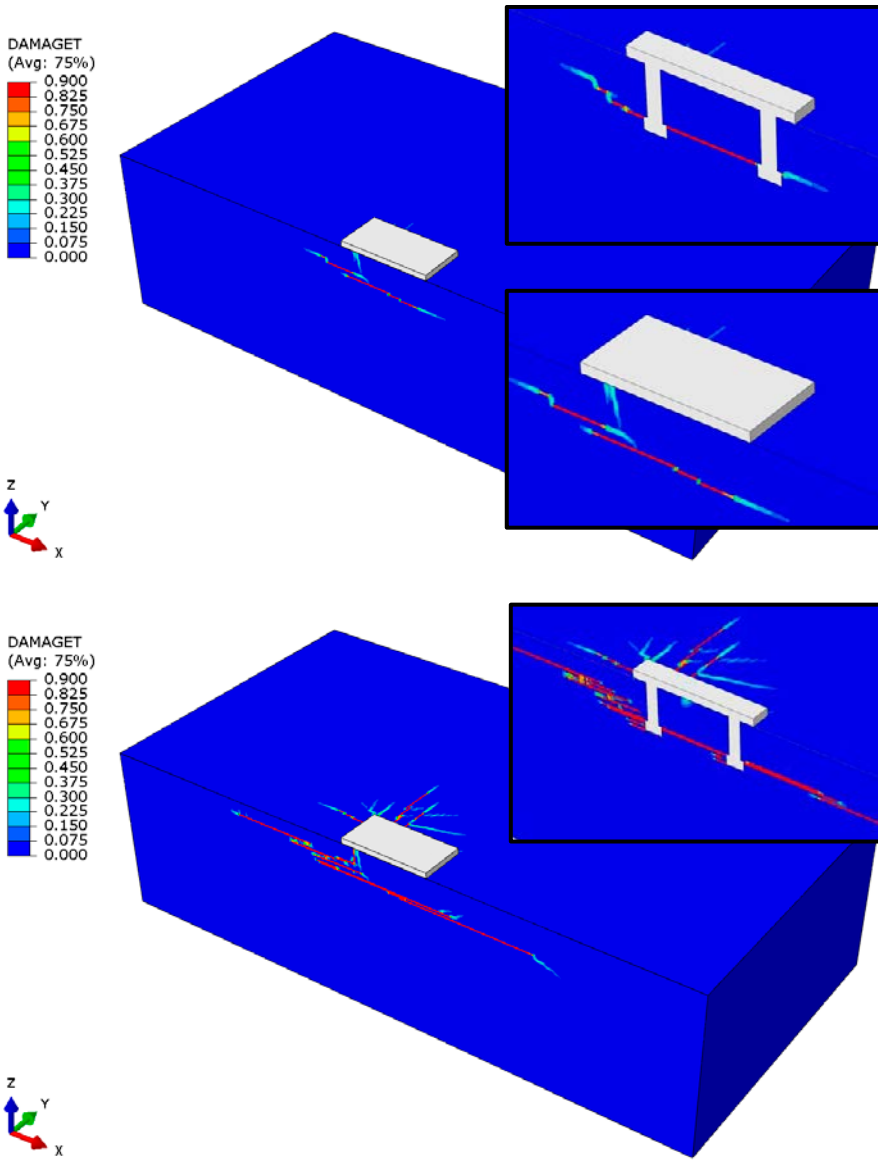

Figure A3-1 Damage tension parameter (DAMAGET) at time of maximum tension load and at time of maximum shear load for configuration 1 in Table A3-1. The X-Z plane is a symmetry plane.

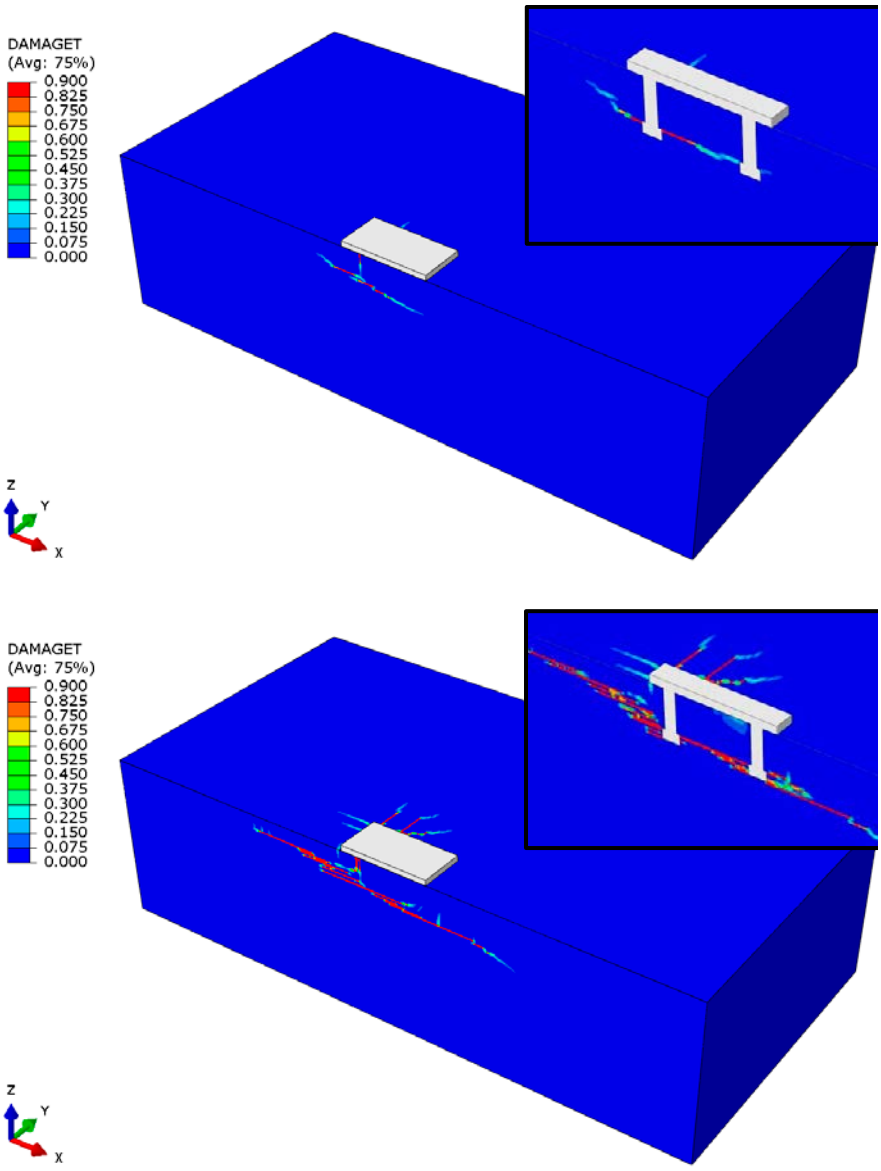

Figure A3-2 Damage tension parameter (DAMAGET) at time of maximum tension load and at time of maximum shear load for configuration 2 in Table A3-1. The X-Z plane is a symmetry plane.

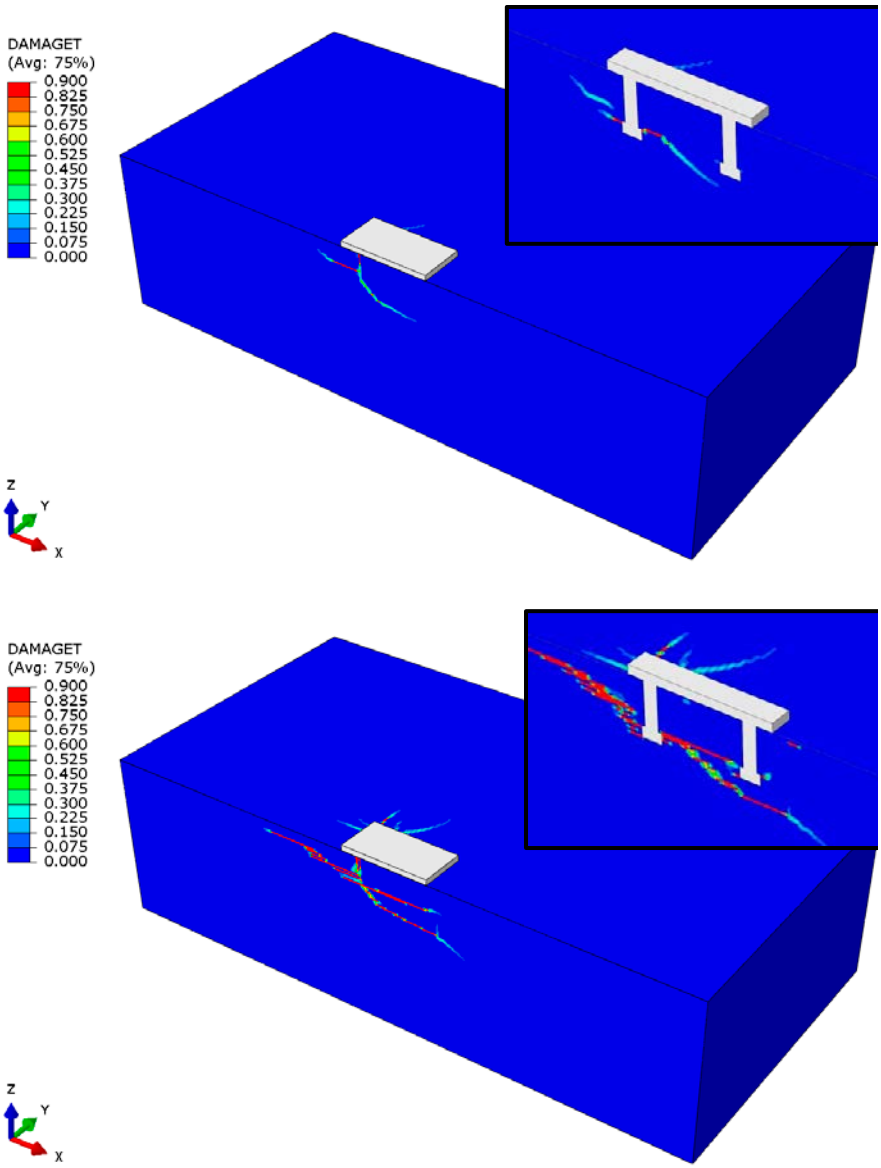

Figure A3-3 Damage tension parameter (DAMAGET) at time of maximum tension load and at time of maximum shear load for configuration 3 in Table A3-1. The X-Z plane is a symmetry plane.

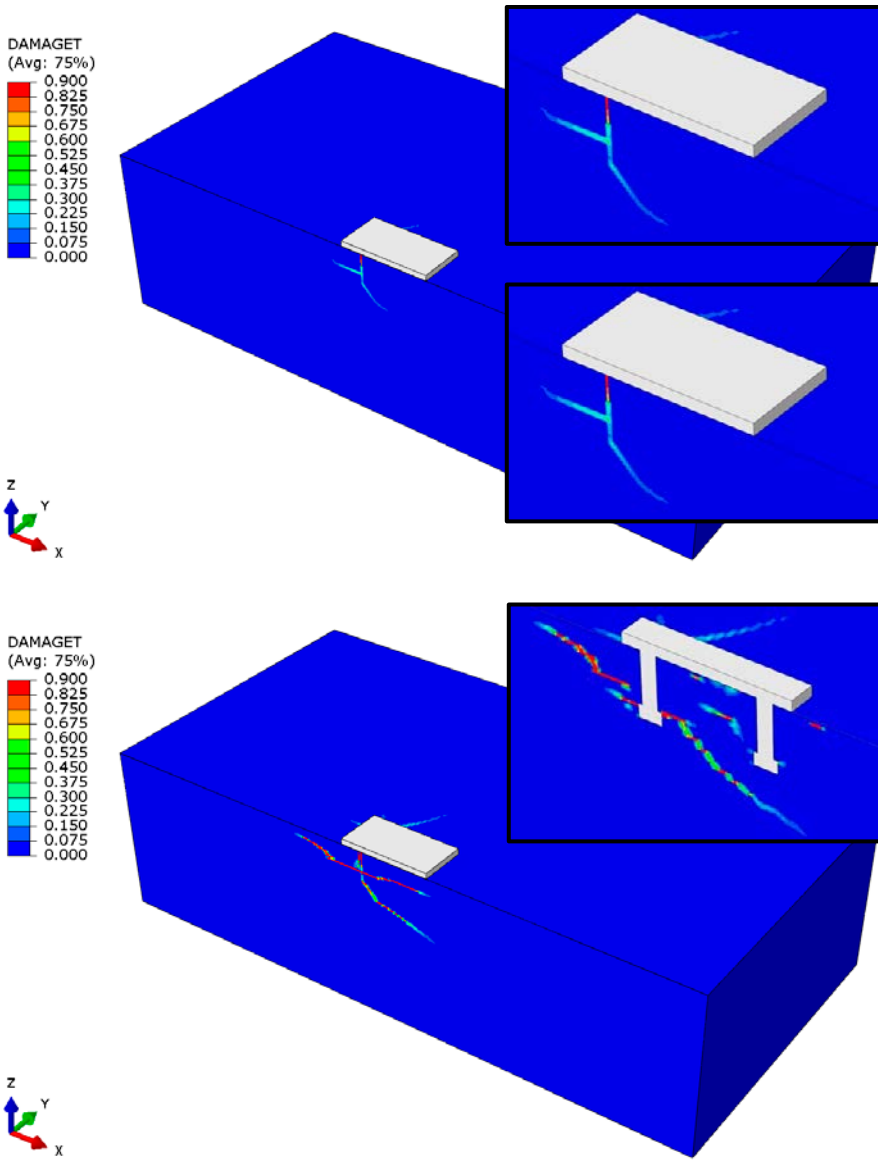

Figure A3-4 Damage tension parameter (DAMAGET) at time of maximum tension load and at time of maximum shear load for configuration 4 in Table A3-1. The X-Z plane is a symmetry plane.

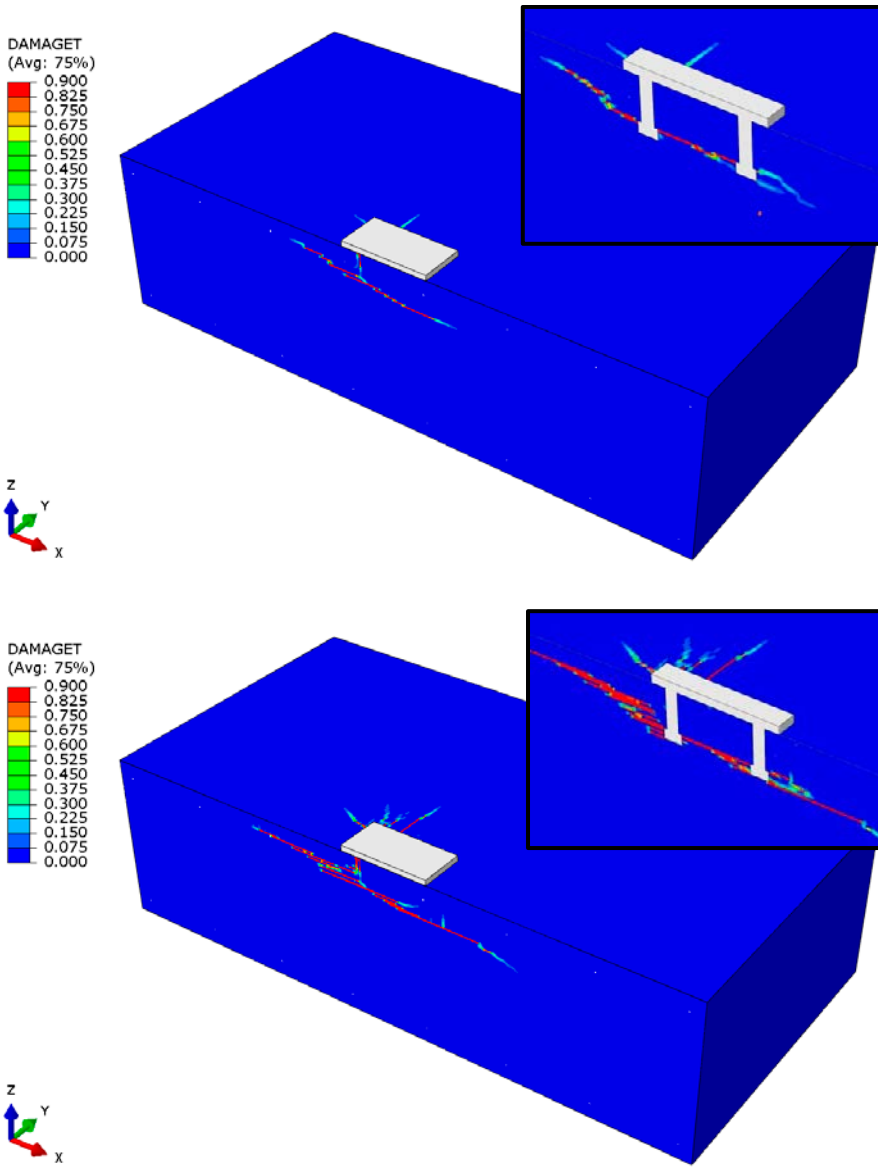

Figure A3-5 Damage tension parameter (DAMAGET) at time of maximum tension load and at time of maximum shear load for configuration 5 in Table A3-1. The X-Z plane is a symmetry plane.

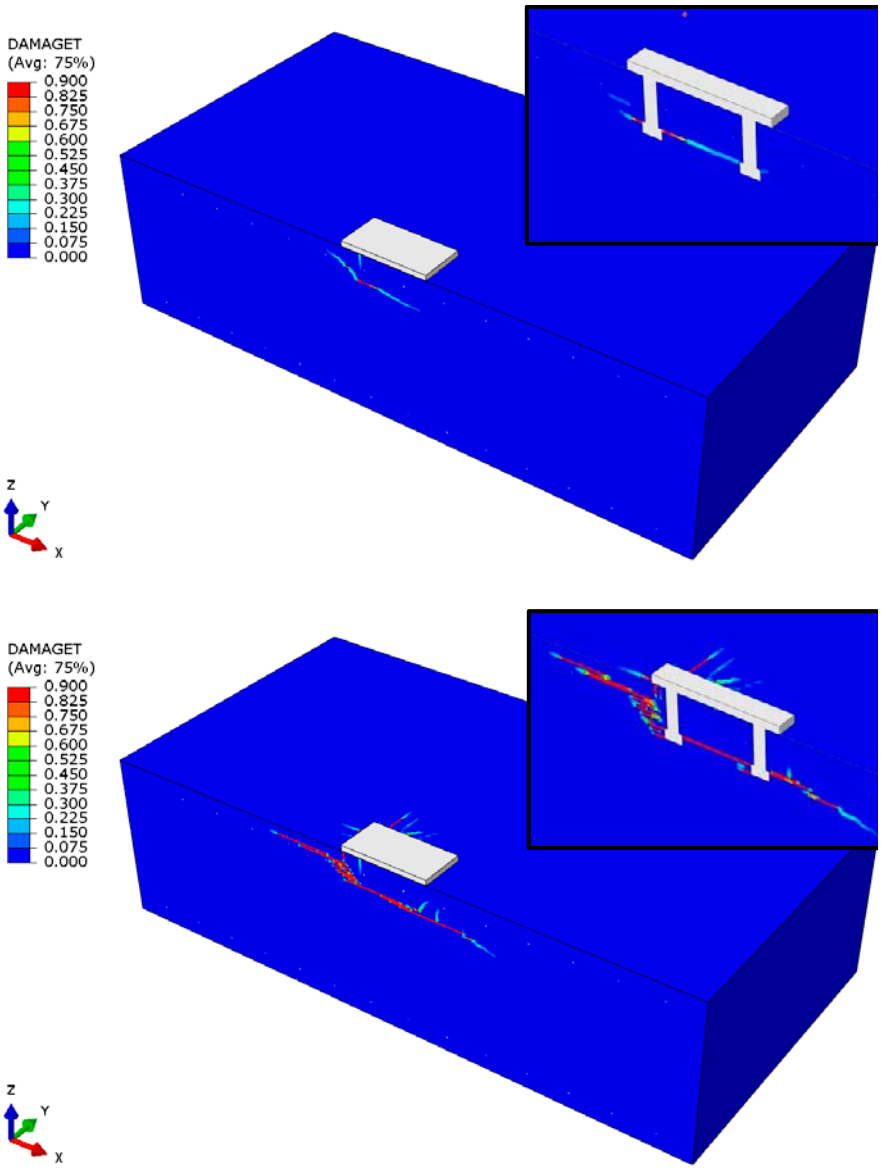

Figure A3-6 Damage tension parameter (DAMAGET) at time of maximum tension load and at time of maximum shear load for configuration 6 in Table A3-1. The X-Z plane is a symmetry plane.

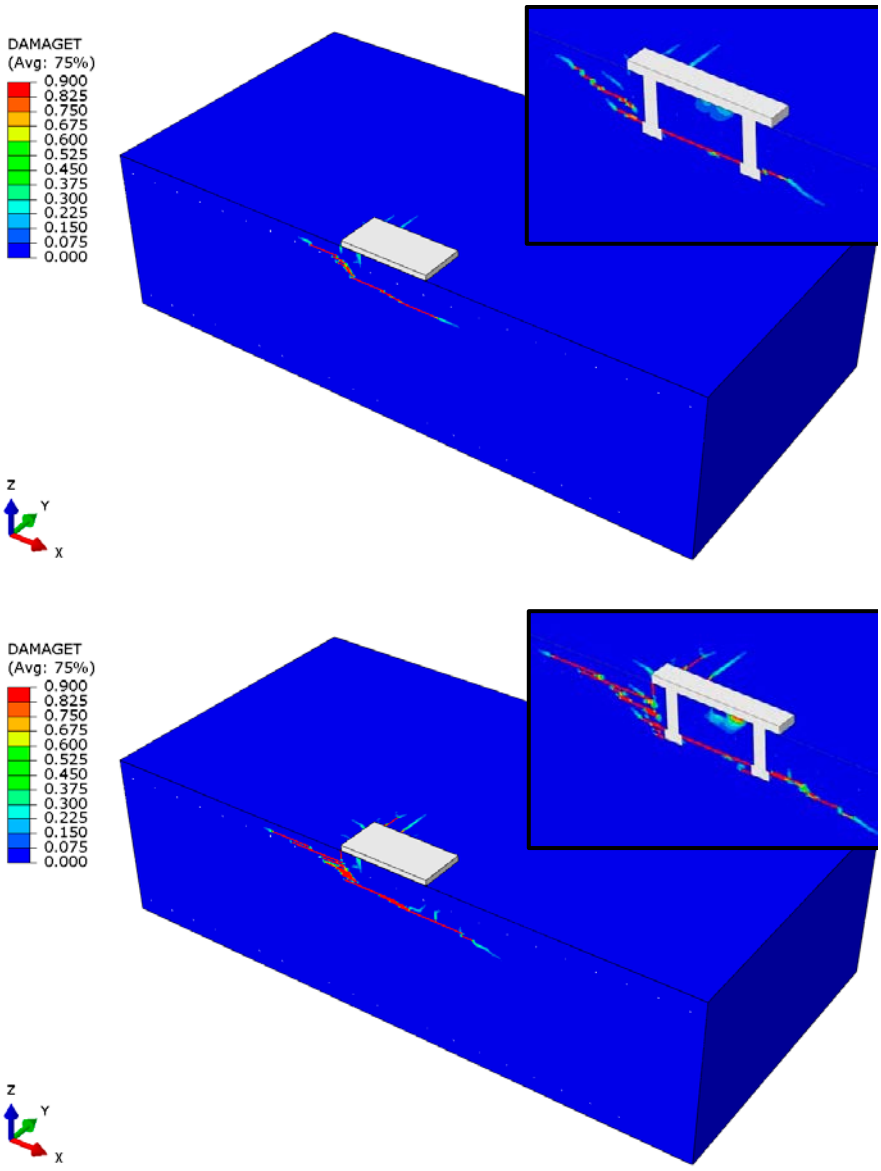

Figure A3-7 Damage tension parameter (DAMAGET) at time of maximum tension load and at time of maximum shear load for configuration 7 in Table A3-1. The X-Z plane is a symmetry plane.

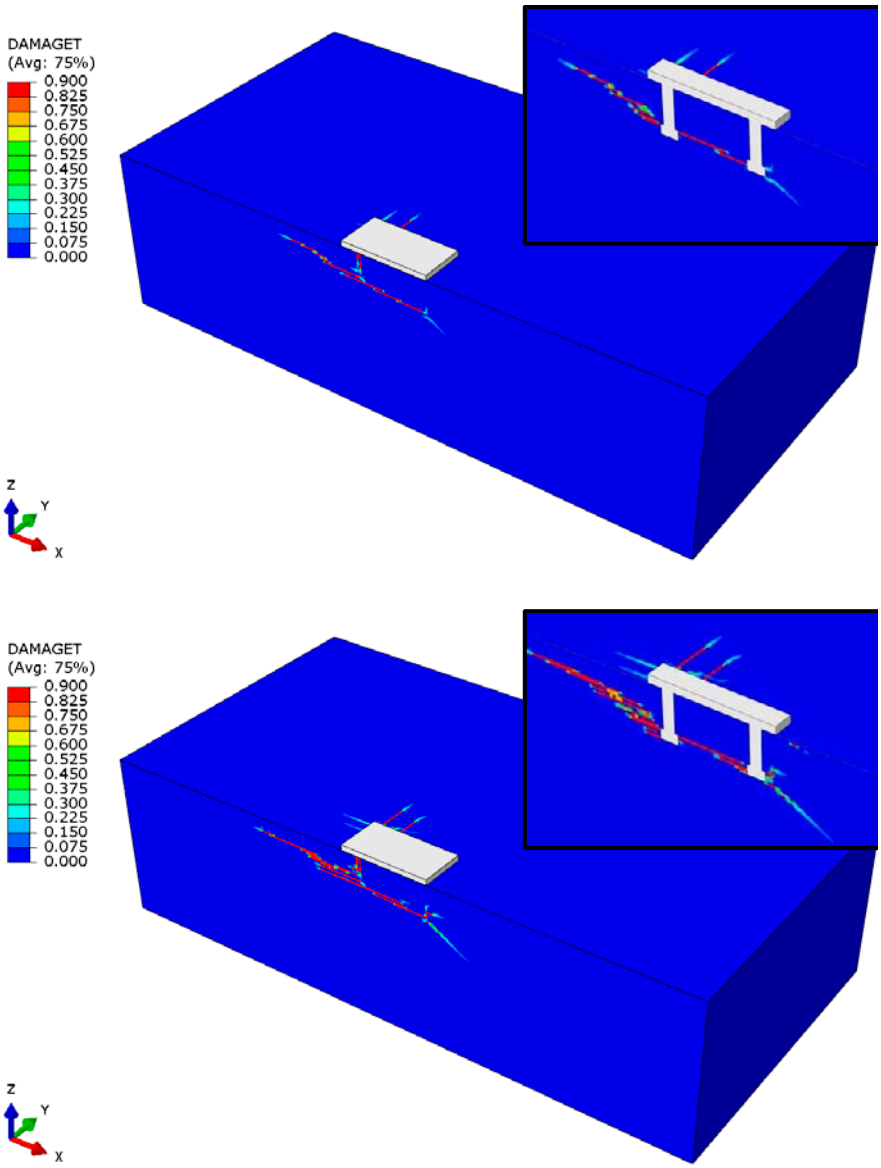

Figure A3-8 Damage tension parameter (DAMAGET) at time of maximum tension load and at time of maximum shear load for configuration 1 in Table A3-2. The X-Z plane is a symmetry plane.

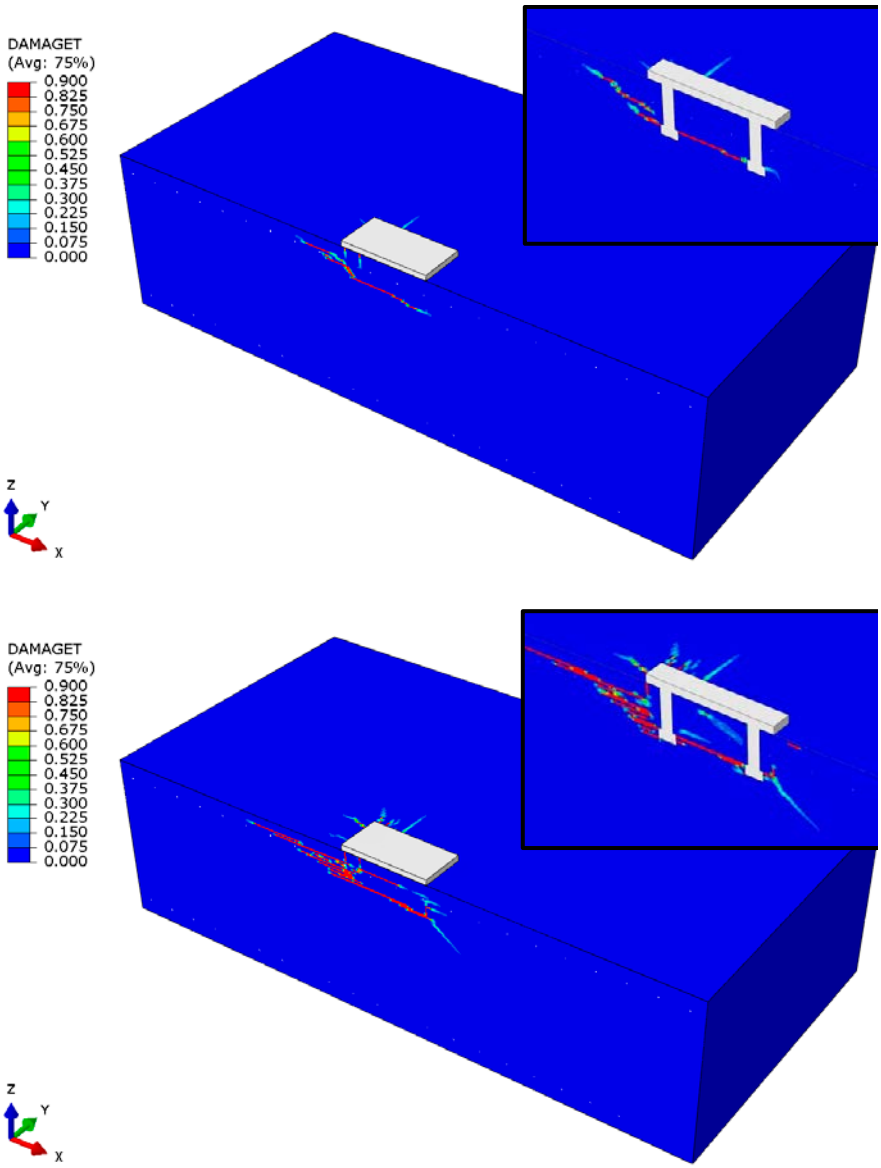

Figure A3-9 Damage tension parameter (DAMAGET) at time of maximum tension load and at time of maximum shear load for configuration 2 in Table A3-2. The X-Z plane is a symmetry plane.

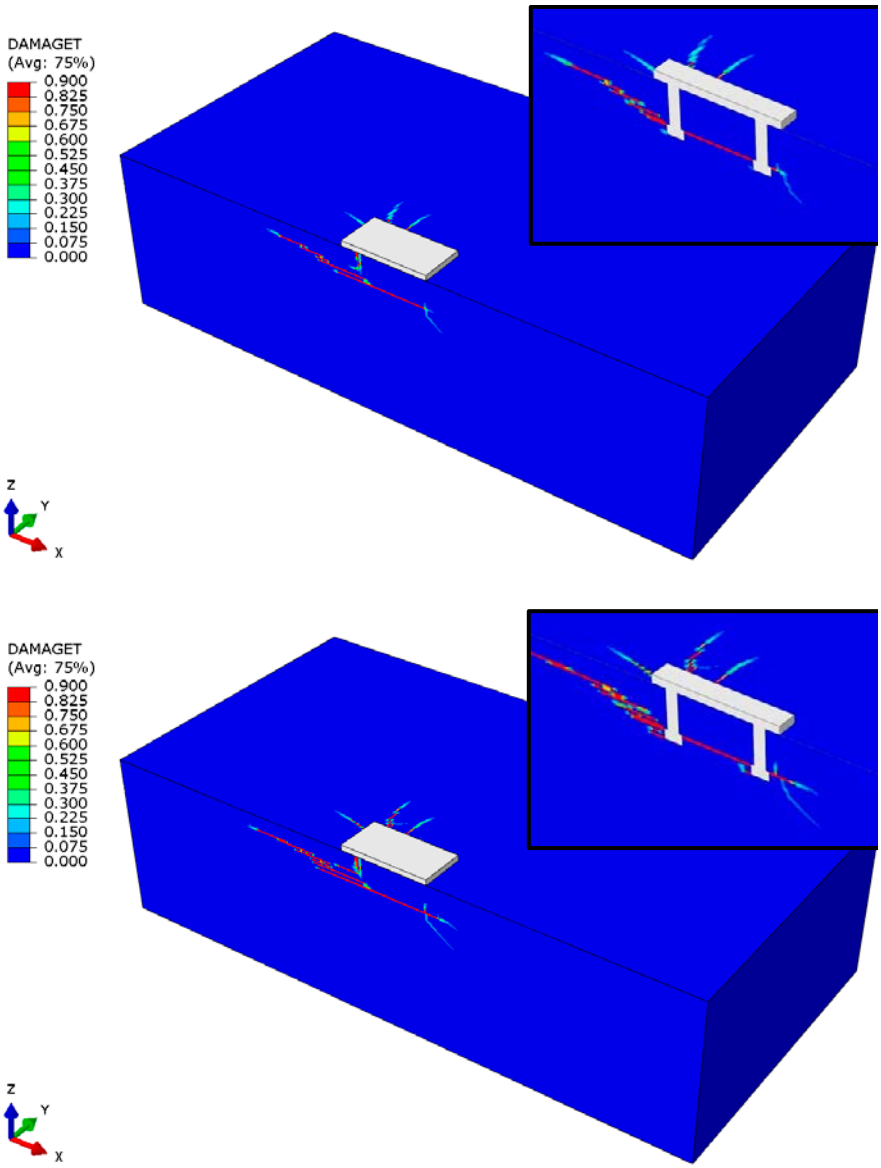

Figure A3-10 Damage tension parameter (DAMAGET) at time of maximum tension load and at time of maximum shear load for configuration 3 in Table A3-2. The X-Z plane is a symmetry plane.

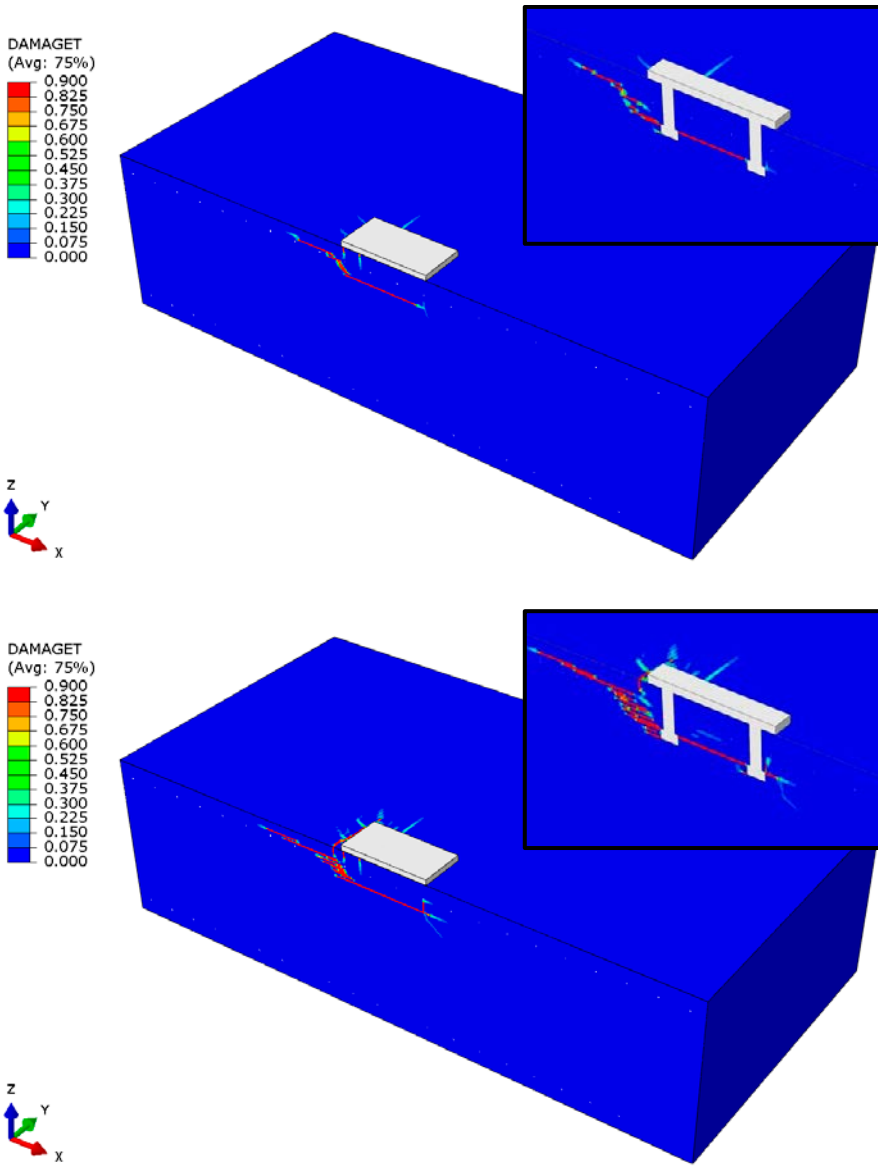

Figure A3-11 Damage tension parameter (DAMAGET) at time of maximum tension load and at time of maximum shear load for configuration 4 in Table A3-2. The X-Z plane is a symmetry plane.

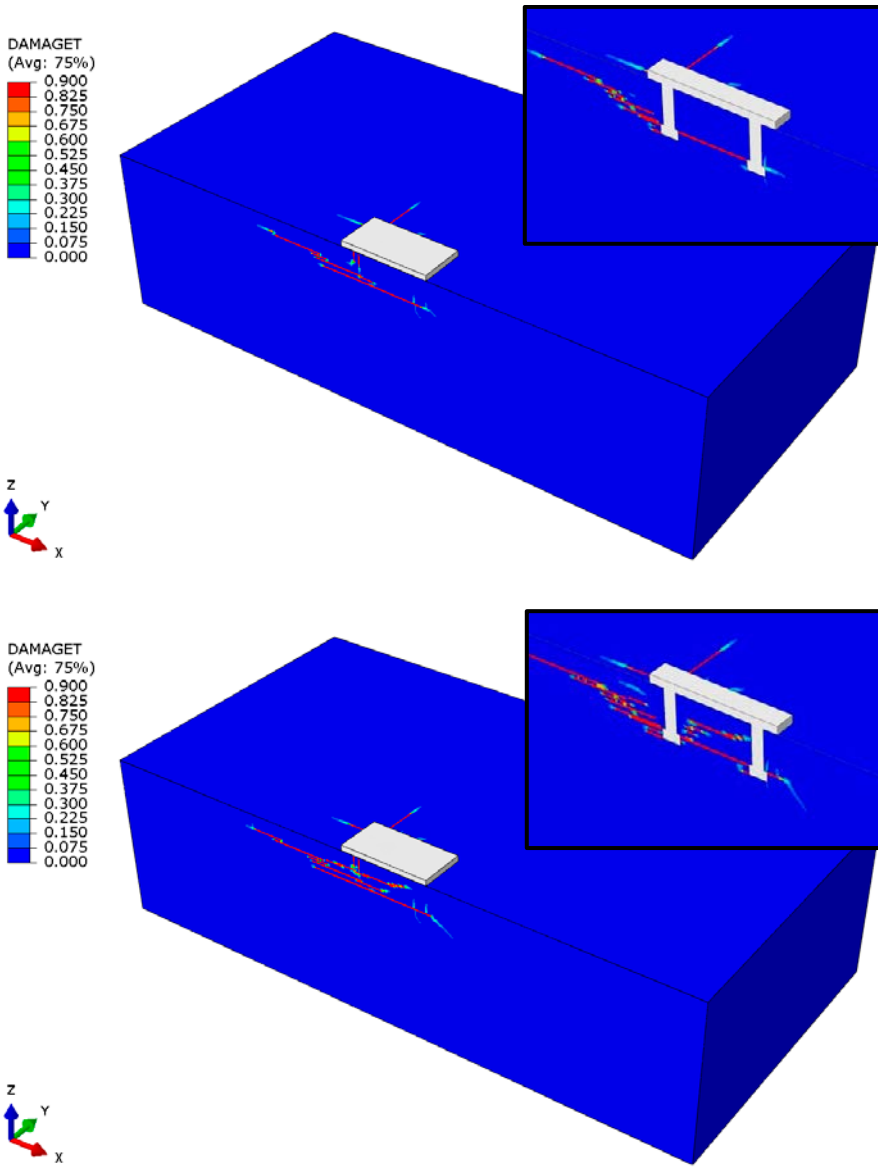

Figure A3-12 Damage tension parameter (DAMAGET) at time of maximum tension load and at time of maximum shear load for configuration 5 in Table A3-2. The X-Z plane is a symmetry plane.

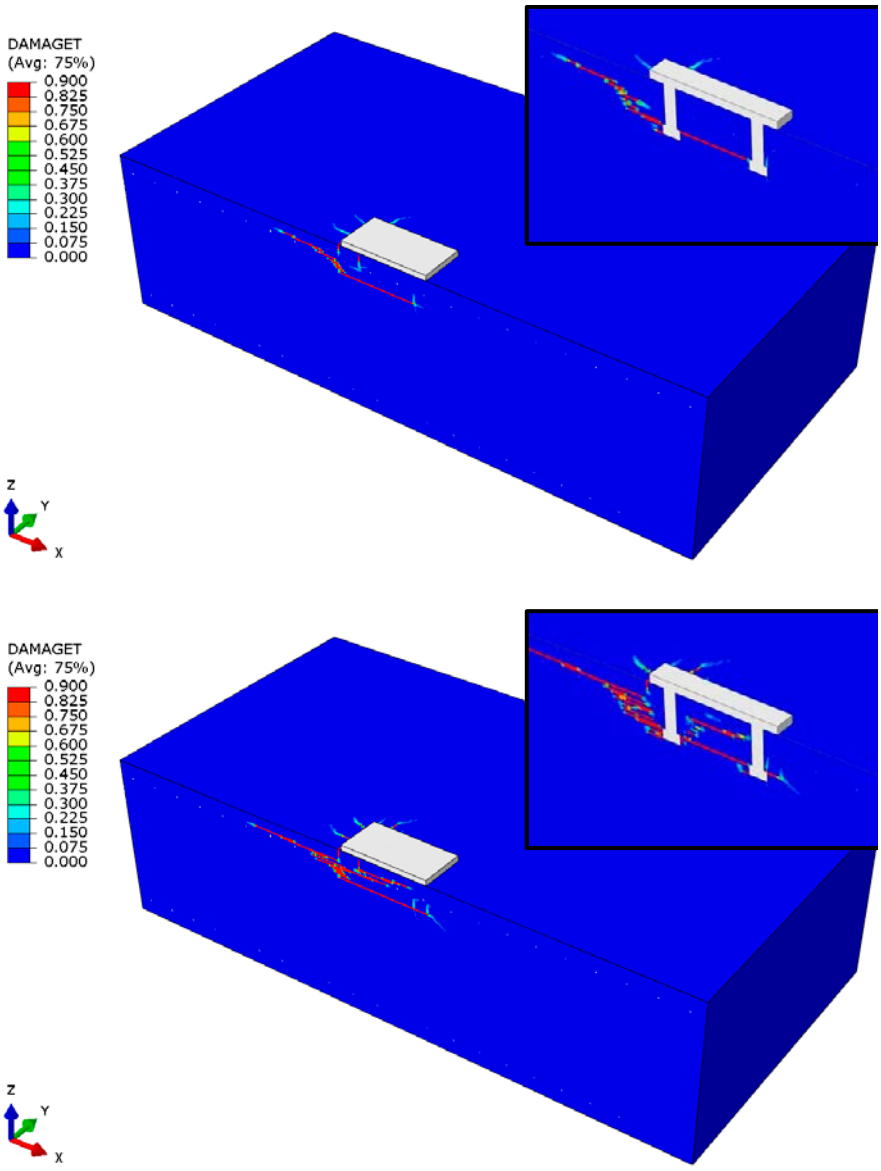

Figure A3-13 Damage tension parameter (DAMAGET) at time of maximum tension load and at time of maximum shear load for configuration 6 in Table A3-2. The X-Z plane is a symmetry plane.

2017:19

The Swedish Radiation Safety Authority has a comprehensive responsibility to ensure that society is safe from the effects of radiation. The Authority works to achieve radiation safety in a number of areas: nuclear power, medical care as well as commercial products and services. The Authority also works to achieve protection from natural radiation and to increase the level of radiation safety internationally.

The Swedish Radiation Safety Authority works proactively and preventively to protect people and the environment from the harmful effects of radiation, now and in the future. The Authority issues regulations and supervises compliance, while also supporting research, providing training and information, and issuing advice. Often, activities involving radiation require licences issued by the Authority. The Swedish Radiation Safety Authority maintains emergency preparedness around the clock with the aim of limiting the aftermath of radiation accidents and the unintentional spreading of radioactive substances. The Authority participates in international co-operation in order to promote radiation safety and finances projects aiming to raise the level of radiation safety in certain Eastern European countries.

The Authority reports to the Ministry of the Environment and has around 300 employees with competencies in the fields of engineering, natural and behavioural sciences, law, economics and communications. We have received quality, environmental and working environment certification.

Strålsäkerhetsmyndigheten
Swedish Radiation Safety Authority

SE-171 16 Stockholm
Solna strandväg 96

Tel: +46 8 799 40 00
Fax: +46 8 799 40 10

E-mail: registrator@ssm.se
Web: stralsakerhetsmyndigheten.se

Arkitektkopia AB, Bromma, 2017